

Identifying Activity and Selectivity Trends for
the Electro-synthesis of Hydrogen Peroxide via
Oxygen Reduction on Nickel-Nitrogen-Carbon
Catalysts

Identifying Activity and Selectivity Trends for the Electro-synthesis of Hydrogen Peroxide via Oxygen Reduction on Nickel-Nitrogen-Carbon Catalysts

By Ladan Shahcheraghi,

*A Thesis Submitted to the School of Graduate Studies in the Partial
Fulfillment of the Requirements for the Degree Master of Applied Science*

McMaster University © Copyright by Ladan Shahcheraghi

April, 2021

McMaster University

Master of Applied Science (2021)

Hamilton, Ontario (Department of Chemical Engineering)

TITLE: Identifying Activity and Selectivity Trends for the Electro-Synthesis of Hydrogen Peroxide via Oxygen Reduction on Nickel-Nitrogen-Carbon Catalysts

AUTHOR: Ladan Shahcheraghi (McMaster University)

SUPERVISOR: Dr. Drew Higgins

NUMBER OF PAGES: xix, 116

Abstract

Hydrogen peroxide (H_2O_2) is a valuable, environmentally friendly oxidizing agent with a wide range of applications. The on-site electrocatalytic production of H_2O_2 through the 2-electron ORR would bring the chemical to uses beyond its present reach, but relies upon the availability of cost-effective catalysts with high selectivity, activity, and stability. Herein we report the synthesis and electrocatalytic assessment of inexpensive and earth abundant nickel-nitrogen-carbon (Ni-N-C) electrocatalysts to gain insight into the activity and selectivity for the ORR towards H_2O_2 using the rotating ring disk electrode (RRDE) technique. We found that the activity and selectivity of the catalysts depended on the amount of nickel added during synthesis as well as the pH of the electrolyte.

Based on characterization by various microscopy and spectroscopy techniques, the materials were found to be heterogeneous in nature, and the presence of Ni during catalyst synthesis was identified as imperative for ORR performance in acidic electrolyte but had minimal impact on the performance in alkaline electrolyte. By correlating the results of electrochemical and material characterization, we postulate that atomically dispersed Ni- N_x/C sites are responsible for the ORR performance in acidic electrolytes, with an activity of -0.3 mA cm^{-2} and H_2O_2 selectivity of 43% measured for the best Ni-N-C catalyst at an electrode potential of 0.5 V vs RHE. In alkaline media, whereby the ORR is a more facile process, Ni-centered active sites, Ni_3S_2 particles formed during the catalyst synthesis, and nitrogen-doped carbon sites present in the carbon matrix of the catalyst structure were the likely active sites. This work highlights the potential and generates scientific insight into

the use of Ni-N-C catalysts for the electrochemical synthesis of H₂O₂, which will provide guidance towards the design of improved performance metal-nitrogen-carbon catalysts based on inexpensive precursors and simplistic synthesis techniques.

Acknowledgements

This work was financially supported by my supervisor and the department of Chemical Engineering at McMaster University.

First and foremost, I would like to greatly appreciate my supervisor, Dr. Drew Higgins for his continuous support and guidance.

Moreover, I would like to acknowledge the discussions and sharing of ideas that I have had from my colleagues at McMaster University. I am grateful of the things I have learnt and the great friends I have made during my time here.

Next, I would like to thank my M.A.Sc. examining committee, including Dr. Zeinab Hosseinidoust and Dr. Charles de Lannoy.

I wish to extend my appreciation to all the technical and nontechnical staff members of our department.

And above all, I would like to express my gratitude towards my parents and family who have always believed in me.

Contents

| | |
|---|-----|
| Abstract..... | iv |
| List of Figures..... | xi |
| List of Tables | xiv |
| Acronyms..... | xv |
| Declaration of Authorship | xix |
| 1 Introduction..... | 1 |
| 1.1 Hydrogen peroxide | 1 |
| 1.2 H ₂ O ₂ synthesis- History and State-of-the-art | 5 |
| 1.2.1 Large-scale processes..... | 7 |
| 1.2.1.1 Anthraquinone auto-oxidation (AQAQO) process..... | 7 |
| 1.2.1.2 Alcohol autoxidation | 10 |
| 1.2.1.3 Electrolytic methods (The Huron-Dow process) | 12 |
| 1.2.1.4 Comparison of large-scale production methods..... | 13 |
| 1.2.2 Emerging alternatives | 14 |
| 1.2.2.1 H ₂ O ₂ heterocatalytic synthesis | 16 |
| 1.2.2.1.1 Catalytic Reactors | 16 |
| 1.2.2.1.2 Direct Synthesis | 17 |
| 1.2.2.2 H ₂ O ₂ electrocatalytic synthesis..... | 20 |
| 1.2.2.2.1 Fuel-cells and electrolyzers..... | 21 |

| | |
|--|----|
| 1.2.2.2.2 Oxygen Reduction Reaction (ORR)..... | 24 |
| 1.3 Electrocatalysts for oxygen reduction reaction..... | 25 |
| 1.3.1 State-of-the-art electrocatalysts for ORR..... | 25 |
| 1.3.2 Metal-Nitrogen-Carbon catalysts | 26 |
| 1.4 Cell design and practical devices..... | 28 |
| 1.5 Essential electrochemistry fundamentals | 31 |
| 1.5.1 Sabatier analysis..... | 31 |
| 1.5.2 Thermodynamic concepts | 33 |
| 1.5.2.1 Oxygen reduction reaction (ORR)..... | 33 |
| 1.5.2.2 Hydrogen fuel cells electrode reactions..... | 35 |
| 1.5.2.3 Reaction rate, current density and Tafel analysis..... | 36 |
| 1.5.2.4 Mass transfer..... | 39 |
| 1.6 Thesis outline..... | 40 |
| 1.7 Thesis objectives and approach..... | 41 |
| 2 Methodology..... | 44 |
| 2.1 Materials | 44 |
| 2.1.1 Reagents | 44 |
| 2.1.2 Equipments | 46 |
| 2.2 Conventional 3-electrode electrochemical cell..... | 46 |
| 2.2.1 Preparation of electrode..... | 47 |
| 2.2.2 Set-up..... | 50 |
| 2.2.3 Cyclic voltammetry..... | 52 |

| | | |
|---------|---|----|
| 2.2.3.1 | Characterization of metal surfaces..... | 53 |
| 2.2.3.2 | Electrochemical active surface area (ECSA)..... | 54 |
| 2.2.4 | Rotating disk electrode (RDE)..... | 56 |
| 2.2.5 | Rotating ring disk electrode (RRDE)..... | 58 |
| 2.2.6 | Electrochemical measurements..... | 60 |
| 2.2.7 | Calibration of reference electrode..... | 61 |
| 2.3 | Catalyst Synthesis..... | 62 |
| 2.3.1 | Nickel-Nitrogen-Carbon catalyst | 63 |
| 2.3.2 | Nitrogen doped carbon catalyst..... | 64 |
| 2.3.3 | Commercial and pyrolyzed Ni ₃ S ₂ /Vulcan Carbon..... | 64 |
| 2.4 | Physicochemical characterization techniques | 64 |
| 2.4.1 | Scanning electron microscopy (SEM)..... | 65 |
| 2.4.2 | Transmission electron microscopy (TEM)..... | 65 |
| 2.4.3 | Energy-dispersive X-ray spectroscopy (EDX)..... | 66 |
| 2.4.4 | X-ray diffraction (XRD)..... | 67 |
| 2.4.5 | X-ray photoelectron spectroscopy (XPS)..... | 67 |
| 3 | Results and Discussion..... | 69 |
| 3.1 | Physical characterization | 69 |
| 3.2 | Electrochemical performance | 80 |
| 3.2.1 | Activity and selectivity of Ni-N-C catalysts in acidic electrolyte..... | 80 |
| 3.2.2 | Active sites of Ni-N-C catalysts in different pH electrolytes..... | 84 |
| 3.2.3 | Ni ₃ S ₂ contribution to the ORR activity | 86 |

| | | |
|---|--|----|
| 4 | Conclusions and suggested future work..... | 88 |
| 5 | Bibliography | 92 |

List of Figures

| | | |
|------|---|----|
| 1-1 | Representative schematic of the industrial and domestic applications of H ₂ O ₂ | 2 |
| 1-2 | Distribution of hydrogen peroxide consumption in Europe..... | 3 |
| 1-3 | Cyclic anthraquinone auto-oxidation process for H ₂ O ₂ production..... | 7 |
| 1-4 | The steps involved in the anthraquinone process for H ₂ O ₂ manufacture..... | 8 |
| 1-5 | Alkylanthraquinone hydrogenation..... | 9 |
| 1-6 | Ring hydrogenation..... | 9 |
| 1-7 | Hydrogen peroxide formation..... | 9 |
| 1-8 | Oxidation of a secondary alcohol for the synthesis of H ₂ O ₂ | 11 |
| 1-9 | H ₂ O ₂ synthesis by oxidation of MBA | 12 |
| 1-10 | Schematic representing several emerging alternative synthesis pathways to produce H ₂ O ₂ | 15 |
| 1-11 | Schematic setup of (a) batch autoclave reactor and (b) flow fixed-bed reactor.... | 17 |
| 1-12 | Direct synthesis of H ₂ O ₂ reaction scheme..... | 20 |
| 1-13 | Exemplified design of different electrocatalytic systems configuration for the H ₂ O ₂ production: (a) fuel cell, (b) electrolyzer..... | 22 |
| 1-14 | (a) RRDE set up for the quantitative measure of H ₂ O ₂ from ORR, (b) schematic of an H-cell configuration, and (c) schematic of a continuous flow cell with a catalyst deposited on a GDE..... | 29 |
| 1-15 | (a) Membrane-base flow reactor containing MEA with anode and cathode electrodes on each side of the membrane, and (b) microfluidic reactor consisting of a flow channel with liquid electrolytes..... | 31 |
| 1-16 | Exchange currents for electrolytic hydrogen evolution as a function of strength of intermediate metal-hydrogen bond formed during electrochemical reaction..... | 32 |
| 1-17 | Tafel plot | 39 |
| 1-18 | Schematic of the project workflow..... | 43 |

| | | |
|-----|--|----|
| 2-1 | Schematic representation of a conventional 3-electrode cell..... | 47 |
| 2-2 | Polishing glassy carbon disk electrode..... | 48 |
| 2-3 | Photos of (a) the experimental setup with the RRDE connected to Bio-Logic SP-300 bipotentiostat system, controlled by a computer and Pine rotator (b) RRDE with conventional three-electrode cell with a O ₂ /N ₂ gas inlet, Ag/AgCl reference electrode and graphite rod as the counter electrode, and (c) schematic diagram of the standard three electrode cell used for RRDE measurements..... | 51 |
| 2-4 | Potential–time excitation signal in a cyclic voltametric experiment..... | 52 |
| 2-5 | CV of a Pt electrode in 0.5 M H ₂ SO ₄ at 25 °C at 100 mV s ⁻¹ | 54 |
| 2-6 | Rotating disk electrode | 57 |
| 2-7 | Schematic of convective electrolyte flow induced by rotation of electrode..... | 57 |
| 2-8 | (a) Photo of RRDE and (b) schematic of the RRDE working principle for the measurement of H ₂ O ₂ . After reduction of O ₂ to H ₂ O ₂ at the disc, the H ₂ O ₂ is being collected and oxidized at the ring of the RRDE tip..... | 59 |
| 2-9 | CV of Ag/AgCl reference electrode calibration versus reversible hydrogen electrode (RHE) in (a) 0.1 M KOH and (b) 0.1 M HClO ₄ | 62 |
| 3-1 | SEM images of (a) N-C, (b) Ni-N-C-low, (c) Ni-N-C medium, and (d) Ni-N-C-high catalysts..... | 70 |
| 3-2 | Low and high magnification HRTEM results of (a,e) N-C, (b,f) Ni-N-C-low, (c,g) medium, and (d,h) high catalysts..... | 71 |
| 3-3 | Low and high magnification HRTEM results of N-C, Ni-N-C-low, medium, and high catalysts..... | 71 |
| 3-4 | STEM-HAADF and EDS maps for C, O, S, Ni..... | 73 |
| 3-5 | XRD of N-C, Ni-N-C-low, Ni-N-C-medium, and Ni-N-C-high catalysts..... | 74 |
| 3-6 | X-ray diffraction pattern of Ni-N-C-high catalyst, commercial Ni ₃ S ₂ , commercial Ni ₃ S ₂ mixed with Vulcan Carbon and pyrolyzed Ni ₃ S ₂ /VC nano-powders..... | 76 |
| 3-7 | (a) XPS spectrum of N-C, Ni-N-C-low, medium, high catalysts (b) deconvolution of the high-resolution XPS spectra of N 1s of N-C, Ni-N-C-low, medium, high catalysts..... | 77 |
| 3-8 | High-resolution XPS of N-C, Ni-N-C-low, medium, and high catalysts. (a) Ni 2p _{3/2} spectra, (b) the C 1s spectra, (c) N 1s spectra, (d) the O 1s spectra and (e) the S 2p spectra..... | 78 |

| | | |
|------|---|----|
| 3-9 | Cyclic voltammograms of N-C and Ni-N-C cast glassy carbon electrode in 0.1 M HClO ₄ saturated with N ₂ and O ₂ , respectively. Catalyst loading: 0.2 mg cm ⁻² , scan rates: 20 mV s ⁻¹ (a) N-C (b) Ni-N-C-low, (c) Ni-N-C-medium, (d) Ni-N-C-high catalyst..... | 80 |
| 3-10 | RRDE results for ORR on N-C and Ni-N-C catalysts containing different Ni concentrations. (a) O ₂ reduction current densities obtained from the disk electrode, (b) ring currents collected on the Pt ring at a constant potential of 1.2 V _{RHE} (c) calculated selectivity of catalysts for reduction of O ₂ to H ₂ O ₂ | 83 |
| 3-11 | Number of transferred electrons (n) as a function of electrode potential in ORR performed in 0.1 M HClO ₄ using a catalyst loading of 0.2 mg cm ⁻² on the RRDE tip, at room temperature and ambient pressure..... | 83 |
| 3-12 | RRDE results for ORR on N-C and Ni-N-C-medium catalysts in two different electrolytes of 0.1 M HClO ₄ and 0.1 M KOH (a) O ₂ reduction current densities obtained from the disk electrode, (b) ring currents collected on the Pt ring at a constant potential of 1.2 V _{RHE} (c) calculated selectivity of catalysts for reduction of O ₂ to H ₂ O ₂ | 85 |
| 3-13 | RRDE results for ORR on N-C and Ni-N-C catalysts containing different Ni concentrations in 0.1 M KOH electrolyte, (a) O ₂ reduction current densities obtained from the disk electrode, (b) ring currents collected on the Pt ring at a constant potential of 1.2 V _{RHE} (c) calculated selectivity of catalysts for reduction of O ₂ to H ₂ O ₂ | 86 |
| 3-14 | RRDE results for ORR on Vulcan Carbon (VC), pyrolyzed Ni ₃ S ₂ /VC and commercial Ni ₃ S ₂ /VC nano-powders in two different electrolytes of 0.1 M HClO ₄ (a-c) and 0.1 M KOH (d-f) (a,d) O ₂ reduction current densities obtained from the disk electrode, (b,e) ring currents collected on the Pt ring at a constant potential of 1.2 V _{RHE} (c,f) calculated selectivity of catalysts for reduction of O ₂ to H ₂ O ₂ | 87 |

List of Tables

| | | |
|-----|---|----|
| 1-1 | Mechanisms for electrocatalytic Oxygen Reduction Reaction..... | 35 |
| 2-1 | Reagents..... | 45 |
| 2-2 | Principle equipments..... | 46 |
| 2-3 | Dimensions of RDE and RRDE..... | 49 |
| 3-1 | Elemental compositions of Ni-N-C-low, Ni-N-C-medium, Ni-N-C-high, and metal-free N-C catalyst samples from STEM-HAADF and EDS analysis..... | 73 |
| 3-2 | Elemental compositions of Ni-N-C-low, Ni-N-C-medium, Ni-N-C-high, and metal-free N-C catalyst samples from XPS analysis..... | 77 |
| 3-3 | Detail breakdown of N 1s signal showing the peak position and relative composition of different near-surface nitrogen groups..... | 79 |

Acronyms

Abbreviations

| | |
|------|--|
| ACS | American chemical society |
| AFC | Alkaline fuel cell |
| AHQ | 2-alkyl 9,10- dihydroanthraquinone |
| AQ | Alkylanthraquinone |
| AQAO | Anthraquinone auto-oxidation |
| BVE | Butler-Volmer equation |
| CCEM | Canadian centre of electron microscopy |
| CM | Cyanamide |
| CV | Cyclic voltammetry |
| DFT | Density functional theory |
| ECSA | Electrochemically active surface area |
| EDX | Energy dispersive x-ray |
| GC | Glassy carbon |
| GDE | Gas diffusion electrode |

| | |
|------------|---|
| HAADF-STEM | High-angle annular dark-field scanning transmission electron microscopy |
| HRTEM | High-resolution image-corrected transmission electron microscopy |
| HER | Hydrogen evolution reaction |
| HOR | Hydrogen oxidation reaction |
| IPA | Isopropanol |
| MAX | McMaster analytical x-ray diffraction facility |
| MBA | Methylbenzyl-alcohol |
| MEA | Membrane electrode assembly |
| M-N-C | Metal-nitrogen-carbon |
| N-C | Nitrogen-carbon |
| Ni-N-C | Nickel-nitrogen-carbon |
| ORR | Oxygen reduction reaction |
| PEM | Proton exchange membrane |
| PEMFC | proton exchange membrane fuel cell |
| PANI | Polyaniline |
| RDE | Rotating disk electrode |
| RRDE | Rotating ring disk electrode |

| | |
|------|--|
| RHE | Reversible or reference hydrogen electrode |
| SA | Surface area |
| SEM | Scanning electron microscopy |
| STEM | Scanning transmission electron microscopy |
| TEM | Transmission electron microscopy |
| VC | Vulcan carbon |
| WOR | Water oxidation reaction |
| XPS | X-ray photoelectron spectroscopy |
| XRD | X-ray diffraction |

Symbols

| | |
|-----------|-------------------------------------|
| C_d | capacitance of the double layer |
| C_s | specific capacitance |
| e^- | electron |
| E | potential |
| E° | standard reversible redox potential |
| i_d | disk current density |
| I_d | disk current |

| | |
|----------|---------------------------------|
| I_r | ring current |
| n | number of electrons transferred |
| N | collection efficiency |
| v | scan rate |
| ω | electrode rotation rate |

Declaration of Authorship

I, Ladan Shahcheraghi, declare that this thesis titled, “Identifying Activity and Selectivity Trends for the Electro-Synthesis of Hydrogen Peroxide via Oxygen Reduction on Nickel-Nitrogen-Carbon Catalysts” and the work presented in it are my own.

Chapter 1

This chapter includes content that has been adapted from:

“Identifying Activity and Selectivity Trends for the Electro-synthesis of Hydrogen Peroxide via Oxygen Reduction on Nickel-Nitrogen-Carbon Catalysts.”

Ladan Shahcheraghi, Chunyang Zhang, Hye-Jin Lee, Melissa Cusack-Striepe, Fatma Ismail, Ahmed Abdellah and Drew C. Higgins, 2021 (Submitted).

Introduction

1.1 Hydrogen peroxide

Hydrogen peroxide, H_2O_2 , is a valuable, environmentally friendly, and strong oxidizing agent that can be found in a form of an aqueous solution with different concentrations. It is a colorless solution with a low pH and miscible with water in every proportion^{1,2} that has been ranked as the top 100 most important chemicals in the world that has a large number of domestic and industrial applications (**Figure 1-1**), usually related to green and sustainable chemistry^{3,4}. Its uses cover a many diverse fields from the environmental protection where it is used as an detoxifying, disinfecting agent to wastewater treatment where it is mostly applied for colour removal.

Other industries include the pulp and paper industry, where H_2O_2 plays a bleaching agent role as well as deinking agent in the wastepaper recycling, textile industry that makes use of the bleaching, oxidizing properties of this chemical, cosmetic and pharmaceutical

industry where disinfection and bleaching processes are only done with the use of H_2O_2 , packaging and food industry which uses H_2O_2 for disinfection of the packages in order to control the bacteria and make them aseptic, detergent and cleanser industry which again uses H_2O_2 as a disinfectant and antiseptic chemical and finally chemical industries that involve reactions such as epoxidation, hydroxylation and oxidation. Furthermore, its vast uses covers even applications such as being used as a propellant as well as for the cleaning of silicon discs for producing printed circuit boards in the electronics ^{1,5-8}.



Figure 1-1: Representative schematic of the industrial and domestic applications of H_2O_2 , reprinted with permission from [9], Copyright (2021).

The distribution and various industrial uses of H_2O_2 in Europe is shown in **Figure 1-2**². The most outstanding factor about this green chemical is the fact that its oxidation reaction produces only two products: water and oxygen¹⁰. It is also a versatile oxidant with high oxidation power and can be staying effective in the entire pH scale ($E^\circ = 1.763$ V at pH 0, $E^\circ = 0.878$ V at pH 14) with water being the only co-product⁷. Increased attempts to

prevent environmental damage as well as the diverse applications of H₂O₂ derived an upswing in demand for this chemical¹¹ such that the global capacity of H₂O₂ reached 5.5 million metric tons in 2015, which has significantly gone beyond the forecast of 4.3 and 4 million tons that were estimated 2011 and 2012 respectively¹¹⁻¹³. The cost of transportation for this chemical was estimated to be about ten times greater than its production cost, arising due to this compound being corrosive, releasing explosive vapors, causing health hazards and hence being extremely hazardous in nature¹⁰.

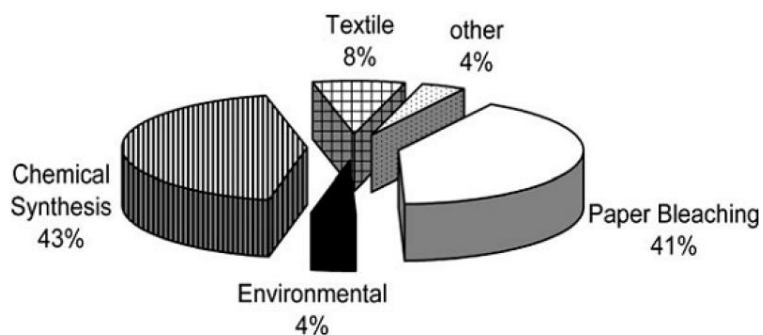
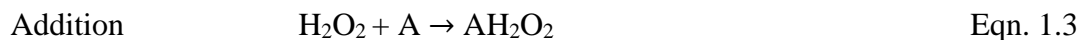
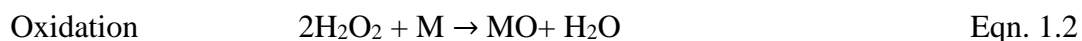
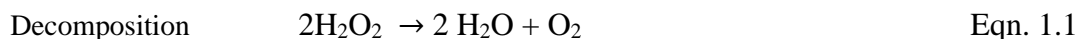


Figure 1-2: Distribution of hydrogen peroxide consumption in Europe, with permission from [2], Copyright 2006, Wiley and Sons.

Hydrogen peroxide goes under different reactions based on the type of the substrate. These reactions are summarized into decomposition, oxidation, molecular addition, reduction, and substitution and are presented in **equations 1.1 - 1.5** below.





Equation 1.1 represents the H_2O_2 decomposition reaction which is important to be controlled as it is exothermic ($100.4 \text{ kJ mol}^{-1}$) and produces oxygen. The rate of this reaction is governed by three different factors including the temperature, peroxide concentration as well as the concentration of the impurities and stabilizers present in the reaction which if reduced can minimize the rate of decomposition. The presence of substances such as transition metals and their compounds trigger the decomposition of peroxide and the enzyme catalase in our body which mainly functions for the removal of metabolism toxic by-products as well as reducing the oxidative stress, catalyzes this reaction. In the oxidation reaction shown in **equation 1.2**, H_2O_2 acts as a strong oxidizing agent in acidic media where M can be compounds such as lead sulphide (**equation 1.6**) potassium ferrocyanide, sodium arsenite, potassium iodide, ferrous sulphate and others.

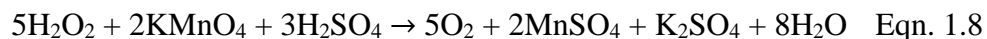


In the addition reaction shown in **equation 1.3**, H_2O_2 can add itself to double bonds such as the addition of H_2O_2 to CH_2CH_2 (ethene) to produce ethylene glycol according to **equation 1.7**.



Hydrogen peroxide is capable of acting as a strong reducing agent too and reduce other oxidizing compounds that are stronger such as potassium permanganate (KMnO_4) (**equation 1.8**), cerium (IV) sulfate ($\text{Ce}(\text{SO}_4)_2$), sodium hypochlorite (NaOCl), and chlorine (Cl_2) that can be the R in **equation 1.4**. Potassium permanganate and cerium (IV)

sulfate are two of the famous compounds that are used as standard chemicals in the volumetric determination of H_2O_2 ⁸.



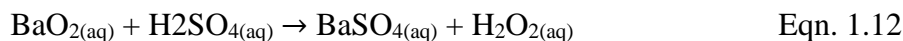
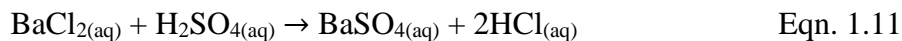
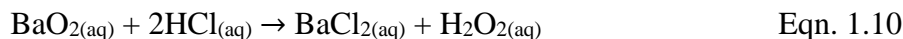
In the substitution reaction (**equation 1.5**), RX represents carboxylic acids which in the substitution reaction with H_2O_2 produces peroxy acid such as the preparation of peracetic acid that is used as a disinfectant from acetic acid and H_2O_2 as represented by **equation 1.9** ².



1.2 H_2O_2 synthesis - history and state-of-the-art

The discover of hydrogen peroxide first happened in 1818 by the French chemist named Louise-Jaques Thenard and the first record of its commercialization revealed in the period of 1865 to 1875. The process that was introduced by Thenard continued to be used to produce H_2O_2 and did not change until the middle of twentieth century ¹. This process involves the reaction of barium peroxide with nitric acid that results in the production of H_2O_2 and barium nitrate. The concentration of the H_2O_2 produced by this method is quite low, however it could be increased if nitric acid is replaced by hydrochloric acid in the reaction (**equation 1.10**). The maximum H_2O_2 production achieved by this method at its time was equal to 2000 metric tonnes of H_2O_2 per year^{10,14}. Two major challenges were faced by the Thenard in this process including the yield as low as 3% as well as the low stability of H_2O_2 . From the disadvantages, the high production costs as well as the high

decomposition rate of the H₂O₂ that were due to its high level of impurity, can be named too¹⁴.



Nowadays, H₂O₂ can be produced either chemically or electrochemically. Its industrial production is mainly based on either: the anthraquinone auto-oxidation (AQAO) process which is a thermal-chemical process or the Huron-Dow process that is considered as an electrochemical process ^{6,15,16}. Currently, it is industrially produced almost extensively by the conventional batch multi-step AQAO process that was first commercialized by Riedl and Pfeleiderer in 1939 at I. G. Farbenindustrie Corporation (German) (1 metric ton H₂O₂ per day) ^{17,18}.

This is an effective process conducted in large-scale facilities and it is still the most broadly used process that represents more than 95% of H₂O₂ production today ¹². However, this process has number of drawbacks including the complex extraction and separation steps, high energy consumption and waste generation (process not sustainable), need for large-scale equipment, organic solvents, stabilizers, as well as the storage, transportation, and handling of bulk H₂O₂ that involves safety hazards and increases the expenses and costs due to the high reactivity of H₂O₂, affecting the sustainability of this process negatively. These deficiencies made it imperative to search and develop novel cleaner alternative methods with lower costs for H₂O₂ synthesis, storage, and transportation for the

decentralized production of H_2O_2 ^{19,20}. In the subsequent sections, large-scale processes that includes the including the actual AO process will be discussed followed by the comparison of the methods with the AO process, and ultimately, emerging alternatives such as the direct synthesis and electrochemical methods.

1.2.1 Large-scale processes

In this section the three types of large-scale processes namely the auto-oxidation, alcohols oxidation as well as the electrochemical synthesis will be discussed.

1.2.1.1 Anthraquinone auto-oxidation (AQAO) process

Figure 1-3 demonstrates a cyclic auto-oxidation process that is known as anthraquinone process ¹⁰. In this process, H_2O_2 is produced via the indirect oxidation of hydrogen via four major steps: 1) hydrogenation, 2) oxidation, 3) H_2O_2 extraction, and 4) treatment of the working solution. **Figure 1-4** resembles a simplified flow diagram of the steps involved in this process ⁷.

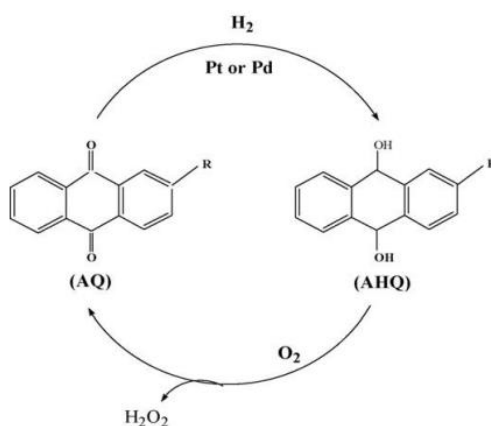


Figure 1-3: Cyclic anthraquinone auto-oxidation process for H_2O_2 production, with permission from [2], Copyright 2006, Wiley and Sons.

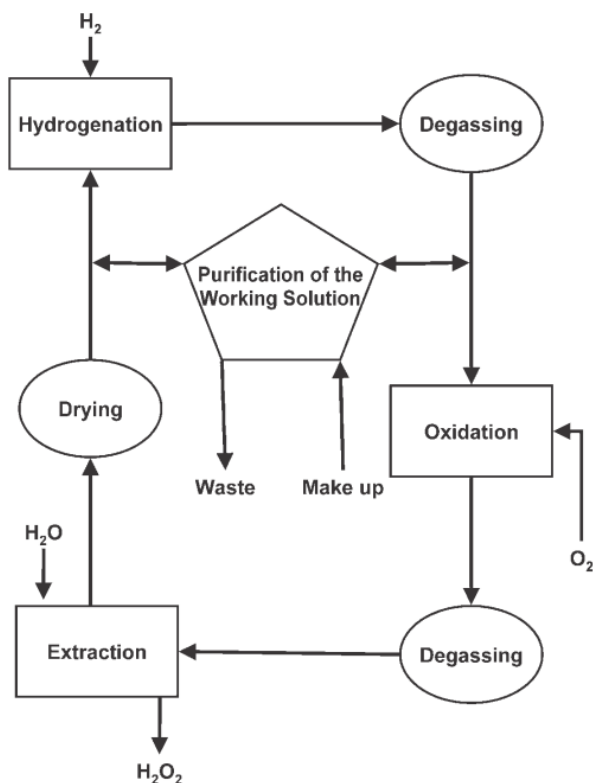


Figure 1-4: The steps involved in the anthraquinone process for H₂O₂ manufacture, with permission from [2], Copyright 2006, Wiley and Sons.

The mechanism of the AO process was developed by Riedl–Pfleiderer which basically follows two main steps. The first step involves the reduction of alkylanthraquinone (AQ) (usually 2-ethylanthraquinone) to the corresponding anthraquinol or 2-alkyl 9,10- dihydroanthraquinone (AHQ) (**Figure1-5**) with hydrogen under pressure using a hydrogenation catalyst (e.g., Pt or Pd) and the hydrogenation of the unsubstituted aromatic ring to 5,6,7,8-tetrahydroanthrahydroquinone as the side reaction (**Figure1-6**).

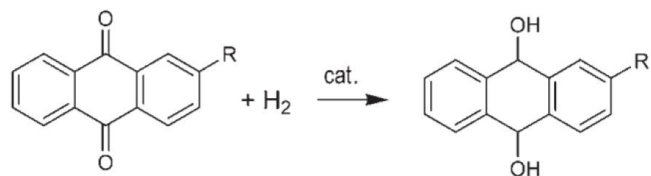


Figure 1-5: Alkyanthraquinone hydrogenation, with permission from [2], Copyright 2006, Wiley and Sons.

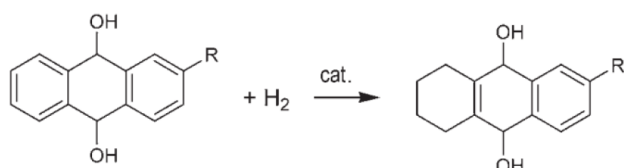


Figure 1-6: Ring hydrogenation, with permission from [2], Copyright 2006, Wiley and Sons.

Subsequently in the second step involves the separation of the solution that contains the AHQ from the hydrogenation catalyst followed by its oxidization back to the original alkyanthraquinone (AQ) in oxygen or air medium while simultaneously producing H_2O_2 (Figure 1-7) ^{7,18,19}.

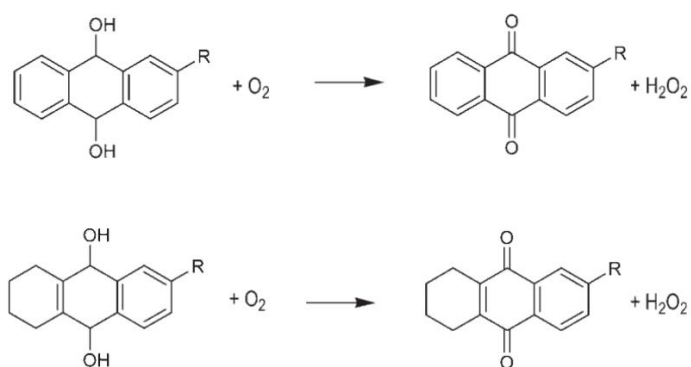


Figure 1-7: Hydrogen peroxide formation, with permission from [2], Copyright 2006, Wiley and Sons.

The resulting alkyanthraquinone (AQ) results in the generation of more H_2O_2 when it is entered the cyclic process. The distillation of the aqueous H_2O_2 (around 30% wt) is

then carried out under reduced pressure in order to eliminate any sort of impurities present and also to increase the concentration of H₂O₂ to as high as 70%, followed by the recycling of the mixture of solvent/anthraquinone. High yields of the peroxide can be achieved by maximizing the solubility of the working compound – anthraquinone in the solvent which in this process is a non-aqueous media. This can be accomplished by using a mixture of organic solvents, including esters/hydrocarbons or octanol/methyl-naphthalene^{6,7,10}.

The AQAO process is hardly considered as a “green” method.^{19,21} Even though it produces majority of the supply of H₂O₂ in the world, it is not without remarkable disadvantages. Contamination of the peroxide, generation of the unwanted side products such as acetone as well as the safety concerns raised from potential explosive reactions arise from the same complex organic solvent that is used to maximize the yield of H₂O₂^{10,15}. Moreover, AQAO process is an extremely expensive process; the operational costs involved with the removal of the organic impurities that is a very energy intensive process, is high. Also, the capital costs are high due to the non-selectiveness of the hydrogenation step and the deactivation of the hydrogenation catalyst by the H₂O₂ product. These high operating and capital costs would therefore mean that the quantity of the H₂O₂ produced by this process must be large, thus making AQAO process suitable only for large scale operations^{10,22}.

1.2.1.2 Alcohol autoxidation

An alternative approach towards the large-scale production of H₂O₂ is the partial oxidation of primary or secondary alcohols. From the auto-oxidation of 2-propanol which

is a liquid-phase process, the main product H_2O_2 is produced along with two co-products of aldehyde or ketone shown in **Figure 1-8**. This process was used by Shell Chemical from 1957 to 1980. It involves the oxidation of the 2-propanol/water azeotrope by an oxygen-enriched gas stream that contains 80-90% O_2 at 90-140°C under 10-15 bar. The quality of H_2O_2 obtained from this method is lower than those from the AO process since it is difficult to obtain a high purity of H_2O_2 due to the solubility of the alcohol in the peroxide phase^{7,21,23}.



Figure 1-8: Oxidation of a secondary alcohol for the Synthesis of H_2O_2 , with permission from [2], Copyright 2006, Wiley and Sons.

A parallel process for a large-scale production of H_2O_2 was developed by Repsol and Lyondell Chemical which was formerly known as Arco Chemical and was based on oxidation of a methylbenzyl-alcohol (MBA) (**Figure 1-9**) in a liquid phase in the absence of catalyst at temperature and pressure range of 120-180 C and 3-10 bar respectively where MBA is known to be the coproduct of propylene/oxide/styrene process. The conversion rate and H_2O_2 selectivity claimed by the patent for this process is claimed by the patent to be 32 and 97% respectively. The H_2O_2 content achieved in the liquid phase with concentration of 7.5% is much greater than the one attained in the conventional anthraquinone-based process^{8,21}.

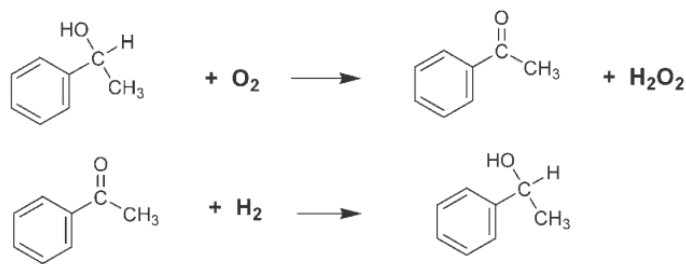
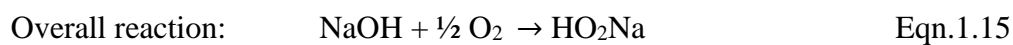
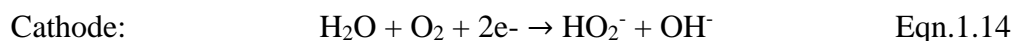
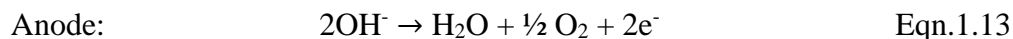


Figure 1-9: H₂O₂ synthesis by oxidation of MBA, with permission from [2], Copyright 2006, Wiley and Sons.

1.2.1.3 Electrolytic methods (The Huron-Dow Process)

Peroxide solutions production by electrolytic means, specifically the production of alkaline peroxide solutions was developed as a patent in 1984 by the Dow Chemical Company as an another alternative for the industrial large-scale production of H₂O₂²⁴. In 1994, they introduced an application of the patent about the composite membrane for chemical synthesis as well as the method of using them along with the type of chemical reactor used for their incorporation. Later in 1996, they created their second application of the patent for a composite membrane to be used in chemical synthesis of H₂O₂ from H₂ and O₂²¹. The H₂O₂ in the Dow process is produced by electrolysis method using a dilute solution of NaOH inside an electrochemical cell where the following anodic and cathodic reactions occur (**equations 1.13-1.15**)⁷.



The commercial application of reducing oxygen electrochemically at the cathode to produce H_2O_2 in alkaline media is very similar to the one first developed by Oloman and Watkinson in 1979^{10,25}. The same basic principle of Oloman's design was followed in the Dow process where oxygen is reduced to H_2O_2 at an $\text{H}_2\text{O}_2/\text{NaOH}$ weigh ratio of 1:1:7 on the graphite made cathode of a trickle bed cell with an electrolyte made up of an alkaline solution^{10,16,25,26}. However, Oloman faced the challenge of low oxygen solubility which resulted in mass transfer limitations which was ultimately overcome by applying high pressure (800 kPa) to the cathode. Dow enhanced this design by using graphite chips that were coated with Teflon as packed bed material which resulted in the improvement of the mass transfer of oxygen without pressurization of the system. This led to the successful commercialization of the application of this process in the pulp and paper industry. Other industry such as the pulp bleaching industry made use of the alkali peroxide technology as this industry does not require the peroxide to be separated from the caustic soda in the product^{19,21}. The Dow-Huron process is better suited for on-site and in-situ synthesis of H_2O_2 as compared to the AQAQO process, owing it to its better portability. However, since H_2O_2 is in alkaline media, long terms stability of the H_2O_2 is limited- leading to potential problems in long term storage as well as transportation. Moreover, the alkalinity needs to be reduced by execution of extra steps before it can be used for neutral and acidic processes^{10,15}.

1.2.1.4 Comparison of large-scale production methods

The AO process is on top of the list of methods of production of H_2O_2 (primary and secondary alcohol oxidation, electrochemical) and produces more than 95% of H_2O_2 in the

world. This is mainly because of the continuous production of H_2O_2 at mild temperatures without any direct contact between the two gases of O_2 and H_2 . The limitations of this process are however remarkable. Heavy and expensive equipments are required as the mass transport limitations in the hydrogenation and oxidation reactions causes inefficiencies in the process and the recovery of the product by liquid-liquid extraction involves organic contamination that needs to be separated. Moreover, the by-products namely overhydrogenated AQ and solvent that are formed as a result of the uncontrollable H_2/AQ ratio and AQ residence time during the hydrogenation step need to be continuously removed which further limits this process. In addition, the working solution and the water come in contact to each other inside the stripping column which results in the cross-contamination of the phases which is an important limiting factor. Furthermore, both the concentrated as well as the purified form of the product H_2O_2 requires the energy intensive distillation process as the H_2O_2 between the water and organic phase do not have the optimum partition coefficient which further adds on to the inefficiency of this process^{7,20,21}.

1.2.2 Emerging alternatives

Considering the drawbacks of the large-scale production methods, the efficiency of these processes is questioned, and researchers are focusing on alternative green and efficient synthesis methods that can be executed at the point of use based on a clean technology that generates this environmentally friendly oxidant in a delocalized manner and takes advantage of its full potential. The Emerging alternative synthesis methods suggested in the literature for the production of H_2O_2 are summarized in **Figure 1-10**²⁷.

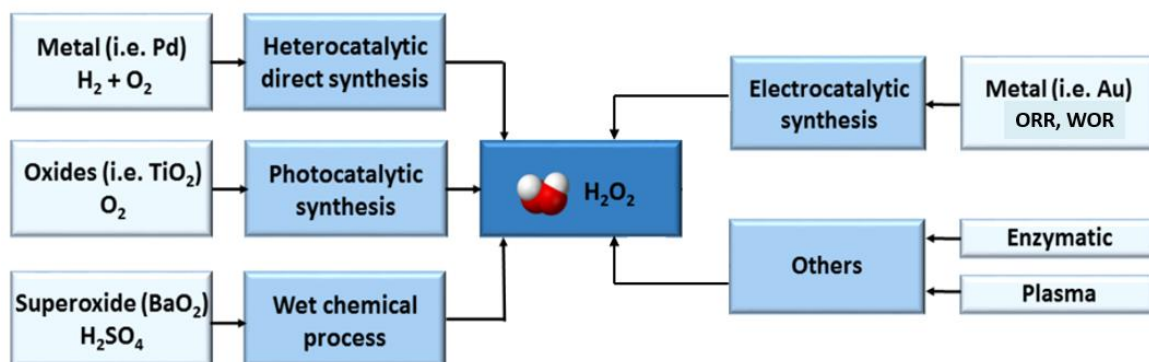
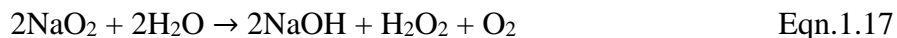


Figure 1-10: Schematic representing several emerging alternative synthesis pathways to produce H_2O_2 .

The heterocatalytic direct synthesis and electrocatalytic synthesis methods are described in detail. The other methods, however, are briefly mentioned here. The comprehensive review on the peroxide synthesis beyond the anthraquinone process by Campos-Martin et al ⁷ provides further information for readers that require a more detailed study on these methods.

The photocatalytic synthesis of H_2O_2 over semiconductor oxides such as TiO_2 and SnO_2 have been investigated by researchers in detail recently ^{7,28}. This reaction is primarily relying on the oxidative oxygen containing species, named as OH , O_2^- and H_2O_2 that are formed at the surface of semiconductor oxides irradiated by UV ²⁹⁻³⁴. The other synthesis route known as the wet-chemical process uses superoxide compounds such as BaO_2 and NaO_2 to produce H_2O_2 in a reaction with a liquid solvent shown in **equations 1.16-1.17** ^{9,35}. Other processes include the enzymatic and plasma process. Enzymatic process is associated with the production of H_2O_2 by living organisms either as by-product of an

autoxidation reaction or through $1-e^-$ reaction of oxygen ^{7,36}. In a plasma process, H_2O_2 is produced from H_2 and O_2 by electric discharges at atmospheric pressure ³⁷.



These synthesis routes have a lower productivity and efficiency than the anthraquinone process in the large scale ⁷. However, the two other alternatives of heterocatalytic as well as the electrocatalytic synthesis methods have caught many researcher's attention due to their flexibility in small-scale widespread applications productivities matching the demand of typical application ³⁸⁻⁴⁰.

1.2.2.1 H_2O_2 heterocatalytic synthesis

Hydrogen peroxide can be produced via a heterocatalytic reaction starting from O_2 and H_2 . This synthesis route which is also known as the direct synthesis, is an elegant, efficient, and much greener alternative to the classical anthraquinone method since it does not involve the intermediate species (i.e., anthraquinone) in the reaction, hence it would have 100% atomic efficiency. In addition, the relatively small size of the reactors in this system makes the decentralized production of H_2O_2 viable wherever low peroxide concentrations are required ⁴¹.

1.2.2.1.1 Catalytic reactors

There are two main reactor designs in heterogenous catalysis known as the batch and the flow reactor shown in **Figure 1-11**. They vary in terms of the way of production

and collection of products ⁹. The synthesis of H₂O₂ is most commonly done in a batch autoclave reactor shown in **Figure 1-11** where H₂O₂ remains in the closed pressurized system for the whole duration of the reaction. However, the challenge comes with the measurement of the absolute synthesis rate in this type of reactor since the formed peroxide is in contact with the catalyst and hence can further react. On the other hand, the residence time as well as the catalyst reactant contact can be controlled in the other type of the reactor known as the flow fixed-bed reactor demonstrated in **Figure 1-11 b** which makes the study of the reaction rates possible. A new alternative to these reactors that is recently developed is the so-called “catalytic membrane” type of reactor which has the advantage of avoiding contact between the reactant gases O₂ and H₂ and hence resulting in high concentration of H₂O₂ ^{42,43}.

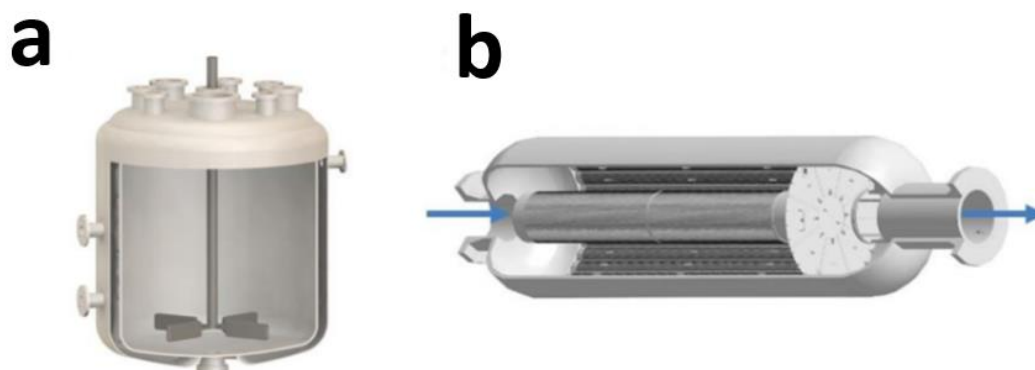


Figure 1-11: Schematic setup of a) batch autoclave reactor and b) flow fixed-bed reactor, taken from [9].

1.2.2.1.2 Direct synthesis

An alternative route to H₂O₂ synthesis was introduced by the combination of molecular O₂ and H₂ in order to avoid the use of AQ. This process was first reported as a

patent in 1914 by H. Henkel and W⁴⁴. Later on, in 1939 another patent on a small-scale production of H₂O₂ that involved usage of noble metals catalysts that were capable of fixing hydrogen through heterogeneous catalysis¹⁷, such as palladium (Pd), platinum (Pt), nickel (Ni), lead to the field of “direct synthesis” in a catalytic reactor^{7,45-47}. The reaction $H_2 + O_2 \rightarrow H_2O_2$ is in principle the simplest method by which H₂O₂ is produced from its elements in a one-pot process with a much lower capital and operating costs and a real breakthrough in H₂O₂ chemistry. However, as shown in **Figure 1-12**, it involves a complex reaction scheme as many reactions simultaneously or consecutively occur that are all highly exothermic and thermodynamically favourable depending on the catalyst used, reaction conditions as well as the type of promoters or additives that are present in the reaction medium. Among these reactions, the three reactions of 1. water formation 2. H₂O₂ decomposition and 3. H₂O₂ reduction are the unwanted reactions⁷.

The direct synthesis process poses some serious drawbacks. The highly explosive nature of the mixtures of hydrogen/oxygen over different ranges of concentration makes this process extremely dangerous. The process can happen safely by two ways of 1. carefully controlling the ratio of the hydrogen to oxygen and 2. adding large quantities of a dilutant such as gases like nitrogen, argon or carbon dioxide which results in a great reduction in productivity as the high selectivity towards H₂O₂ is only achieved within the explosive range of O₂/H₂ mixtures (5:1 to 20:1). In addition, the catalysts used in this process are the other major problem in achieving a high selectivity of the H₂O₂ since they actively catalyze the undesirable side reactions such as the combustion reaction where

hydrogen is turned to water and the decomposition reaction where unstable H_2O_2 is broken down into water and oxygen which reduces the yield H_2O_2 over water⁴⁸⁻⁵¹.

Effective strategies to overcome these problems include use of catalytic membrane reactors, in which the two gaseous reactants (i.e. O_2 and H_2) can be used in a pure form and kept separate, preventing their direct contact as well as the major safety issues related to the hydrogen/oxygen mixtures^{28,52-55}. Dense palladium membranes are particularly used for the liquid-phase synthesis of hydrogen peroxide from the two gases H_2 and O_2 . This strategy has its own limitation too including the limited mass transport that results in the reduced rate of production of H_2O_2 that is too low for industrial applications⁴³. Other strategies include the addition of acids and heterogenous catalysts into the reaction medium to prevent the undesired decomposition reaction of H_2O_2 , which would otherwise occur in alkaline medium⁴⁸. Also, catalyst poisons (i.e. halides such as chlorides and bromides) can be added to delay the unwanted water production reaction in order to increase the selectivity of H_2O_2 ⁵⁶. These drawbacks appeared to be controllable once the first plant for the H_2O_2 production through direct synthesis was announced by Degussa-Headwaters to be constructed in 2007 with patents revealing the use of palladium nanoparticles deposited on carbon as the active catalyst, alcohol a solvent and hydrogen in concentrations outside the flammability limits^{1,7}.

In the same year, direct synthesis of H_2O_2 using a fuel cell system with gas-diffusion cathode was introduced by Yamanaka et al. that resulted in the maximum product concentration of 1.2 wt%. under desirable reaction conditions such as the current density

of 12.7 mA cm^{-2} , and a reaction time of 6h. His group also managed to achieve production of 7 wt% $\text{H}_2\text{O}_2/\text{NaOH}$ solutions ⁵⁷.

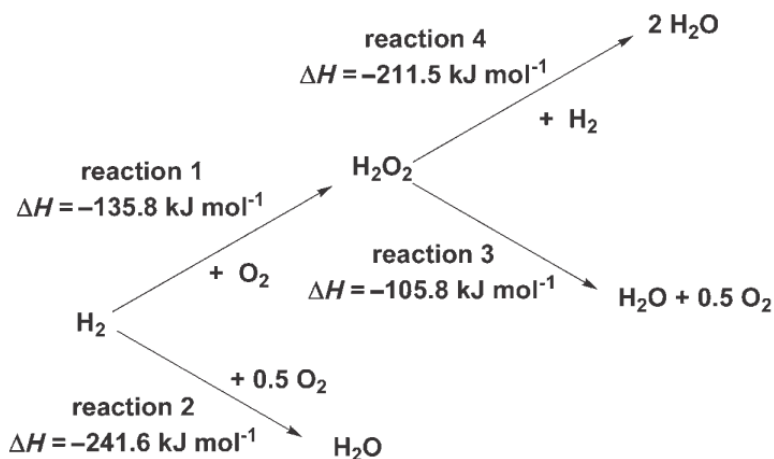


Figure 1-12: Direct synthesis of H_2O_2 reaction scheme, taken from [5].

1.2.2.2 H_2O_2 electrocatalytic synthesis

Hydrogen peroxide can be produced through electrochemical synthesis method via a 2e Oxygen Reduction Reaction (ORR) and/or as an intermediate of the full 4e ORR in three different electrolytic conditions (i.e., alkaline, acidic an even neutral). Electrochemical reactors offer an attractive alternative, where H_2 and O_2 gases are feed to the electrodes separately- playing a key role in energy conversion together with the decentralized chemical synthesis of H_2O_2 . H_2O_2 can be synthesized through different configurations of electrocatalytic reactors (i.e. fuel cells and electrolyzers) which is introduced here together with the fundamental information on the ORR ⁴¹.

1.2.2.2.1 Fuel-cells and electrolyzers

Fuel cells and electrolyzers are two different configurations of open electrochemical devices where the redox couple half-reactions namely the oxidation ($\text{Red1} \rightarrow \text{Ox1} + n\text{e}^-$) and reduction ($\text{Ox2} + n\text{e}^- \rightarrow \text{Red2}$) take place at each electrode separately (i.e., anode (A) and cathode (C) respectively). Standard potential (E°) is used to describe each of these half reactions with the reversible electrode potential (measured under standard conditions) known as the standard hydrogen electrode (SHE, $2\text{H}^+ + 2\text{e}^- \rightarrow \text{H}_2$) whose E° is conventionally 0. The standard potential of the half-reaction is used for the determination of 1. Spontaneity of the redox reaction and 2. the cell voltage in case of half-reactions at the electrode. The main difference between the fuel cell and the electrolyzer is that in the former, energy produced by the spontaneous process is harvested, however in the latter case, the energy must be provided to the system from a power supply for the nonspontaneous redox reaction to take place. **Figure 1-13** shows the different types of electrochemical devices that can be designed for the production of H_2O_2 through ORR ($\text{O}_2 \rightarrow \text{H}_2\text{O} / \text{H}_2\text{O}_2$, $E^\circ = 1.229/0.69 \text{ V}$) based on the anodic oxidation reaction chosen.

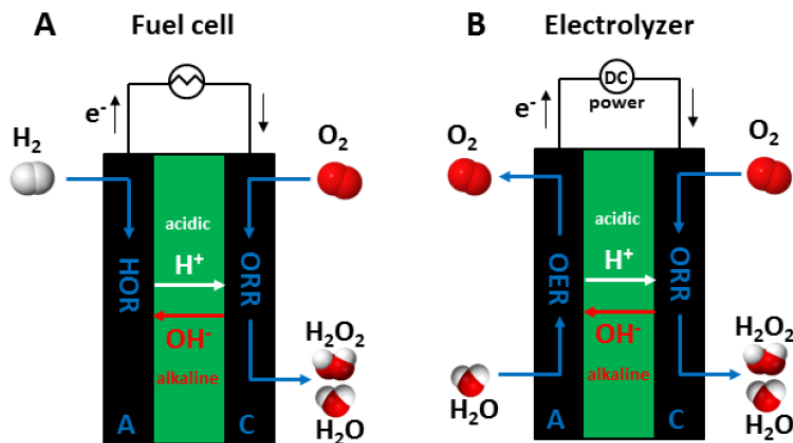


Figure 1-13: Exemplified design of different electrocatalytic systems configuration for the H_2O_2 production: (a) fuel cell, (b) electrolyzer, taken from [9].

The synthesis of H_2O_2 vis electrolysis was first introduced by Consortium für elektrochemische Industrie⁷ in 1895 with the proposal of various cell designs coming after 25,40,58–66,66–71. In a more recent years, fuel cell configurations have also been investigated 72–82.

The synthesis of H_2O_2 through fuel cell technology has provided many benefits over the conventional methods discussed earlier. These advantages include the zero-emission process, the cell does not require electricity to operate, electricity is being generated and can be used to decrease the energy costs, the modular unit being small, as well as zero transportation costs since H_2O_2 is synthesized in a decentralized manner at the point of use⁸³. In a techno-economics point of view, the overall cost for the H_2O_2 production using a fuel cell that uses a PGM-free catalyst such as the Ni-N-C catalyst proposed in this project, is much lower as compared to the conventional anthraquinone process that involves a large capital and operational costs along with the high cost associated with the expensive

palladium catalyst. The price of every gram of the Ni-N-C catalyst we synthesized here is around 1200 times less than the state-of-the-art noble metal platinum catalyst that is used in PEM fuel cells.

Most fuel cells require acid environment instead of alkaline to produce H_2O_2 since there are few drawbacks associated with the use of alkaline media. For example, H_2O_2 is less stable in alkaline environment and can go through the unwanted decomposition reaction especially at pH greater than 9. Moreover, H_2O_2 has a broader application in acidic media due to its stronger oxidation power in acid media as compared to the basic media. Also, proton exchange membrane (PEM) stands above all type of fuel cells in terms of stability and conductivity and there is no commercially competitive anion exchange membrane that can compete with that in device development. These drawbacks have shifted the industrial motivation towards the improvement of H_2O_2 catalysis in acid media, particularly using PEM fuel cells ¹³.

The electrolyzer and the fuel cell have different anodic oxidation reactions. In the former, O_2 is produced at the anode via the oxidation of H_2O or OH^- in acidic and alkaline media respectively which is known as the oxygen evolution reaction (OER) (**Figure 1-13b**). However, in the fuel cell, the anodic reaction is the hydrogen oxidation reaction (HOR) (**Figure 1-13a**) which has a standard potential ($E^\circ = 0 \text{ V}$) lower than the cathodic ORR standard potential, making the reactions in the fuel cell spontaneous. Fuel cells are more efficient as compared to electrolyzers since both electricity and chemical production can be harvested from a single system, However, electrolyzers are simpler to operate as they do not need a supply of H_2 . With the electricity as their only requirement and O_2 supply

at the cathode side that can be supplied by air or even better recycled directly from the anode, they can easily be commercialized as table-top systems in hospital and home-based applications ⁷⁰. The unwanted hydrogen evolution reaction (HER) reaction that occurs concurrently at low potentials, however, needs to be prevented in these systems.

1.2.2.2.2 Oxygen reduction reaction (ORR)

The ORR is a complex multi-reaction process in which oxygen is reduced either via the 4e or the 2e pathway. It occurs on a catalyst surface and is a fundamental process in electrocatalysis. The complete 4e ORR that produces water as the product, is rather sluggish and limits the commercialization of fuel cell systems on a large scale ^{84,85}. The mechanism of such complex multi-e reaction is still controversially discussed, especially the elementary steps and the reaction intermediates ^{84,85}. However, it is commonly accepted that the reduction of oxygen to water can take place via the direct 4e reduction pathway shown in **equation 1.18** where the strong O=O is broken early, resulting in the maximization of the electrical efficiency of the PEM fuel cell in which the 4e pathway is favoured ⁸⁶. Oxygen can also be reduced via the 2e reduction pathway to produce H₂O₂ under acidic and alkaline conditions showed in **equations 1.19-1.20** where the hydroperoxyl radical (HO₂[·]), represents the radical form of H₂O₂ in a basic solution. There have been many investigations done for the H₂O₂ production in alkaline medium with metal-free carbon used as the common electrocatalyst which results in a great reduction in costs ^{72,73,78,80,87}.

However, the synthesis in alkaline media has the disadvantage of degradation of H₂O₂ caused by the presence of hydroxyl ions. In addition, the low membrane efficiency of an alkaline fuel cell (AFC) is also limiting the technology. The low stability of the H₂O₂ in alkaline media has shifted the direction of research more towards the electrochemical synthesis in acidic media such as proton exchange membrane fuel cell (PEMFC)⁸⁸ which appears to be a more promising route for the production of H₂O₂⁸⁹.



1.3 Electrocatalysts for oxygen reduction reaction

1.3.1 State-of-the-art electrocatalysts for ORR

The activity and selectivity of a catalyst towards the production of H₂O₂ is dictated by the surface binding energy with the single intermediate species (OOH*, where * indicates an adsorbed species) involved in the 2e⁻ ORR. For a catalyst to be selective towards H₂O₂, the catalyst must undergo associative adsorption of O₂ and retain the O-O bond during the ORR⁹⁰⁻⁹². Electrocatalysts for the electrochemical production of H₂O₂ from the 2e⁻ ORR are conventionally based on noble metal alloys. Particularly, Pt or Pd alloys with metals such as Hg or Au have been demonstrated as promising catalysts with high activity and selectivity towards H₂O₂ by tuning the catalyst binding energies with the

reactive intermediate OOH* (electronic effect) or by providing ensemble effects that enable preservation of the O-O bond ⁹³⁻⁹⁵.

By computationally screening a variety of Pt- and Pd-alloys, Siahrostami et al. discovered Pt-Hg alloys that were verified experimentally to provide a selectivity of 96% and activity over 25 A/g_{pt} towards H₂O₂ in an acidic electrolyte. This excellent activity was brought up by the presence of single atom active sites (Pt) isolated by the alloying element (Hg) that could tune reactant binding energies and preserve the O-O bond ⁹⁶. Moving forward, it is desirable to avoid the use of Hg due to its toxicity and to minimize the use of platinum group metals due to their high cost and intrinsic selectivity towards the 4e⁻ ORR if the formation of Pt (or Pd) clusters cannot be avoided ⁹⁷⁻¹⁰¹. These challenges have shifted the direction of research towards platinum group metal-free ORR catalyst.

1.3.2 Metal-nitrogen-carbon catalysts

Nitrogen-doped carbon materials have been investigated as low-cost ORR catalyst alternatives that are straightforward to prepare from inexpensive precursors ^{98,99,102-105}. However, nitrogen-doped carbons conventionally show low activity in acidic medium, which can be overcome by the addition of a small amount of transition metal species (*i.e.*, ~1 wt. % of Ni, Co, Mn, Fe, etc.) during synthesis to enable the formation of atomically dispersed M-N_x/C moieties that can be active for the ORR ¹⁰⁶⁻¹¹². This class of catalyst are typically denoted as M-N-C and are prepared via the pyrolysis of a wide variety of inexpensive catalyst precursors containing carbon, nitrogen and one (or more) active transition metals ^{93,112}. Research on M-N-C catalysts has previously largely focused on Fe-

^{113–117}, Co-^{118–121} or Mn-N-C^{122–128} materials as inexpensive replacements to platinum group metal catalysts for the 4e⁻ ORR in fuel cell applications^{92,118,129–134}.

However, more recently interest has been sparked towards the development of M-N-C catalysts for the 2e⁻ electrochemical ORR for the production of H₂O₂. In particular, with the hypothesis being that the active site in M-N-C catalysts is a single, atomically dispersed transition metal ion coordinated by N/C containing ligands, this is an isolated active site structure with possibility to associatively adsorb O₂ molecules and preserve the O-O bond during the ORR. Furthermore, the appropriate choice and transition metal type and synthesis method provides opportunity to tune the binding energies between the active site structures and reactive intermediates and to maximize the surface concentration of the catalytically active sites (*e.g.*, M-N_x)^{26,135–137}.

In a recent study by Gao et al¹³⁷, various M-N-C (M = Mn, Fe, Co, Ni, and Cu) catalysts were systematically studied theoretically and experimentally for their electrocatalytic activity towards H₂O₂ synthesis in acidic media¹³⁸. Co-N-C revealed the highest activity and selectivity towards H₂O₂, with CoN₄ postulated computationally, and supported by operando XAS characterization, as the active site structure. This catalyst outperformed the expensive state-of-the-art noble-metal-based electrocatalysts in 0.1 M HClO₄ with a stable (10 hours) kinetic current density of 1 mA/cm²_{disk} at 0.6 V vs RHE and a H₂O₂ Faradaic efficiency > 90%. The high selectivity and activity of Co-N-C electrocatalyst as compared to other screened metals was also supported by Sun et al⁹⁸ while studying a series of M-N-C materials (M= Mn, Fe, Co, Ni, and Cu) consisting of

atomically dispersed catalytically active M-N_x moieties. The results revealed that Co-N-C achieved H₂O₂ selectivity of as high as 80 % (at 0.1 V RHE).

Although Co-N-C has been identified as the most active candidate for the electrochemical production H₂O₂ in these studies; however this contradicts previous literature that has identified Co-N-C catalysts as very active for the 4e⁻ ORR in fuel cells¹¹⁸, indicating there may be challenges maintaining high 2e⁻ selectivity when integrating these catalysts into high loading 3-dimensional electrodes. In addition, considering the trend shown in the study by Sun et al⁹⁸, Ni-N-C was found to be the second most active M-N-C catalyst for the production of H₂O₂. Ni has the additional advantage of being 3 times less expensive than Co, and Ni-N-C catalyst have been widely reported for other electrochemical reactions such as CO₂ reduction to CO^{139,140}. However, systematic investigations into their preparation and use as ORR catalysts in varying pH electrolytes for the production of H₂O₂ remain largely uninvestigated.

1.4 Cell design and practical devices

Even though we have several promising electrocatalysts that are reported in the literature for the electrochemical production of H₂O₂, it is a challenge to achieve a high activity and selectivity in real industrial systems. A successful translation of the results from a bench laboratory scale to practical devices such as flow cell is dependant upon the right cell design¹⁴¹⁻¹⁴³. Rotating-ring-disk electrode (RRDE) technique (**Figure 1-14a**) that is used in our study (section), is the most common facile method used for the assessment of the electrocatalytic performance of the catalysts and the quantitative measurement of the

H_2O_2 production in a laboratory scale ¹³. Its commercialization for the bulk electroynthesis of H_2O_2 is hindered due to the small area of the electrode that makes it impractical to desorb the product rapidly and prevent its further reduction to water ⁹³.

H-cells are one type of setup analogous to a one pot batch reactor that is used for the bulk synthesis of H_2O_2 . It consists of porous electrodes placed in a liquid electrolyte (**Figure 1-14b**). However, the challenge faced by these cells comes with the quick deterioration of the performance that results in the lower rate of reaction, H_2O_2 concentration, selectivity as well as the current density that is brought by the lower solubility of the O_2 in liquid phase electrolyte ^{144–146}. This has shifted the industry to focus on pressured electrolytes and gas-diffusion electrodes (GDEs) (**Figure 1-14c**) that acts as a membrane separating the O_2 and liquid electrolyte. The mass transport of O_2 is much higher in the gas phase in this type of cell as compared to the liquid phase which meets the challenge faced by the H-cells ¹⁴⁷.

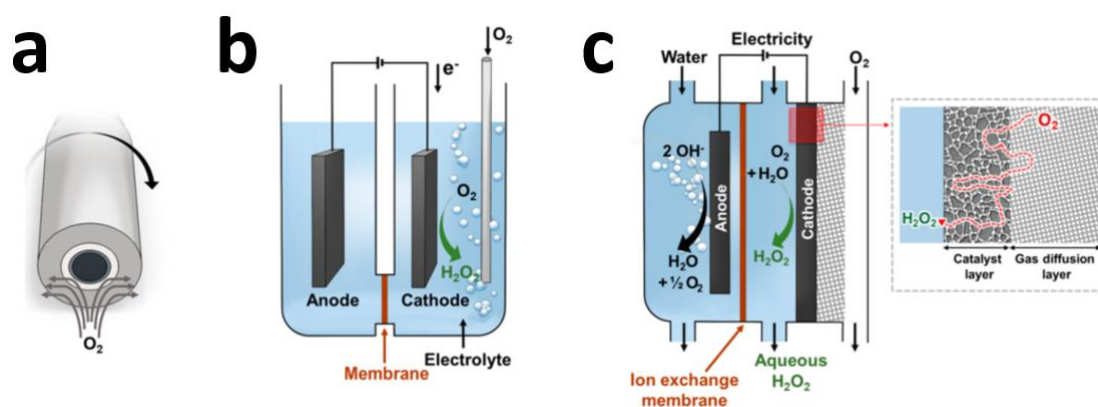


Figure 1-14: (a) RRDE set up for the quantitative measure of H_2O_2 from ORR, reprinted with permission from [93], Copyright 2020 American Chemical Society, (b) schematic of an H-cell configuration, reprinted with permission from [13], Copyright 2018 American Chemical Society, and (c) schematic of a continuous flow cell with a catalyst deposited on a GDE, reprinted with permission from [93], Copyright 2020 American Chemical Society.

The mass transport is another important factor on top of the catalyst performance that determines the selectivity and faradaic efficiency of a particular cell. This is because, high local concentration of the product close to the surface of the electrode needs to be prevented in the practical applications to prevent the undesirable reduction reaction of H_2O_2 to water. That is why the flow of the mass transport of the reactants and products to and from the electrodes are controlled in the flow cell reactors by controlling reactor's inflow and outflow. These flow cell reactors exist as either membrane-based or microfluidic cells^{13,93,148}.

Membrane-based flow cells consist of a polymer electrolyte membrane that separates the cathode and anode. The oxygen reduction reaction (ORR) takes place at the cathode and the water oxidations occurs at the anode. This type of flow cell however has a limitation of using a minimum catholyte flow rate. This is overcome by using "catholyte-free" flow reactors in order to obtain highly concentrated H_2O_2 solutions. The best type of reactor is the membrane electrode assembly (MEA) where a GDE is combined with an ion exchange polymer membrane in one unit as shown in **Figure 1-15a**. However, it has a disadvantage of large internal resistance a result of having proton and anion as the membrane components, which will in turn decrease the efficiency of electrical power consumption and can result in a significant loss in performance^{93,147,149}.

The second type of flow cell known as the microfluidic cell was first invented by Kenis (**Figure 1-15b**)^{150,151}. Most recent research configuration from Xia et al, showed that H_2O_2 could be generated in this membrane free cells at both the cathode and anode electrodes at a high rate and with a great efficiency by combining active electrode materials

for the 2e WOR at the anode and a 2e ORR catalyst at the cathode ¹⁵². The scale up from RRDE measurements to these actual real systems has always been a challenge as the measurements obtained using RRDE and H-cell are not an accurate representative of the flow cells necessary for large-scale production ⁹³.

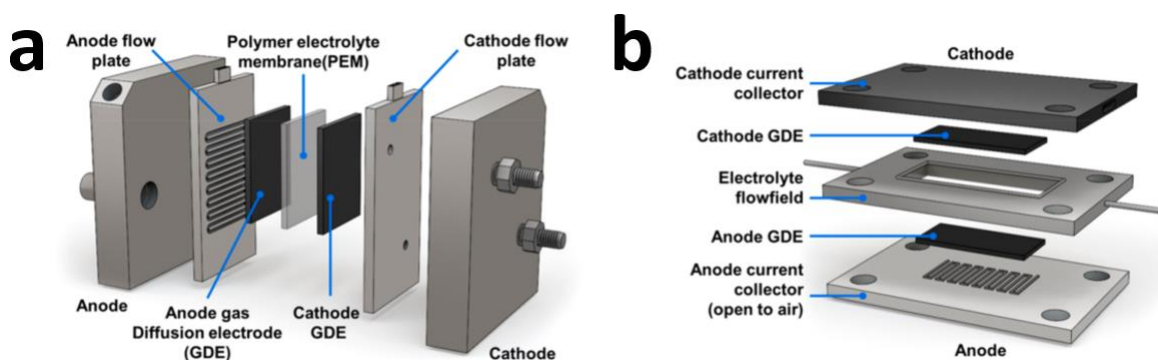


Figure 1-15: (a) Membrane-base flow reactor containing MEA with anode and cathode electrodes on each side of the membrane, reprinted with permission from [93], Copyright 2020 American Chemical Society, and (b) microfluidic reactor consisting of a flow channel with liquid electrolytes, reprinted with permission from [141], Copyright 2018 American Chemical Society.

1.5 Essential electrochemistry fundamentals

1.5.1 Sabatier analysis

The main goal of electrocatalysis method is providing electrochemical alternative reaction pathways that can enhance the reaction kinetics, increase the current density of the reaction and making them happen potentials close to the thermodynamically reversion potential. The catalyst in these reactions can be either absorbed or a solution-free species.

Earth's crust primarily consists of the element oxygen with oxygen reduction reaction (ORR) considered as the most important reaction in life processes and energy

conversion systems (e.g., fuel cells). The correlation between the metal catalysts and their peak catalytic activity is an important concept in electrochemistry that was established by Sabatier Analysis which was used to study the ORR reaction. The results of this analysis were presented in a form of a volcano plot demonstrated in **Figure 1-16**, showing that the catalyst activity is dependant on the oxygen adsorption energies on a pure metal surface. This figure is a clear demonstration of electrocatalysis as it shows the rate of the ORR as a function of oxygen adsorption energies, hence an effect in electrochemistry is observed because of the nature of metals like that observed in the field of catalysis. The metal located at the peak of the volcano is associated with the highest activity which in this case belongs to the platinum. This characteristic is the main reason for using platinum as electrode material in fuel cell technology as it meets the biggest challenge of small rate of cathode reaction, i.e., oxygen production, in the field.

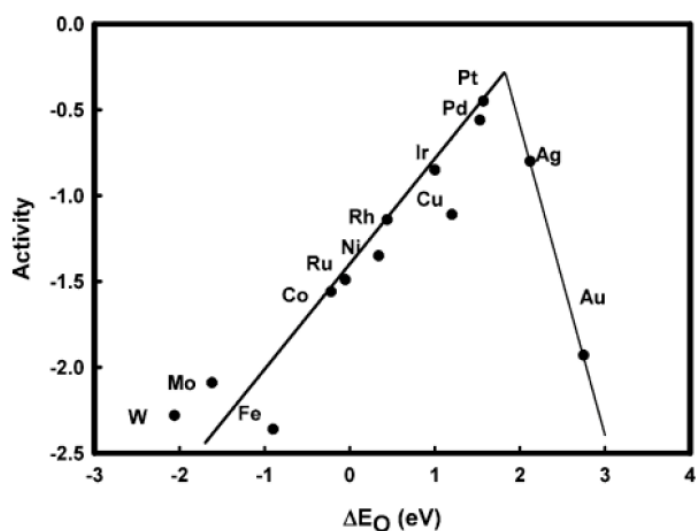


Figure 1-16: Exchange currents for electrolytic hydrogen evolution as a function of strength of intermediate metal-hydrogen bond formed during electrochemical reaction, reprinted with permission from [153], Copyright 2021.

1.5.2 Thermodynamic concepts

1.5.2.1 Oxygen reduction reaction (ORR)

ORR in aqueous solutions can happen by two reaction pathways: (1) a four-electron pathway where molecular oxygen is reduced to form water, which is preferable in fuel cell applications; and (2) a two-electron pathway where molecular oxygen is reduced to produce hydrogen peroxide for distributed hydrogen peroxide production applications. The reaction pathways in acid and alkaline medium occur according to the following equations where E^0 stands for the thermodynamic electrode potential at standard conditions.

In acid electrolytes:

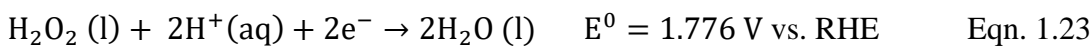
4-electron pathway:



2-electron pathway:



The 2-electron pathway generates hydrogen peroxide that can be further reduced to water in acidic electrolytes:



or can be decomposed by a disproportionation reaction:



In alkaline electrolytes:

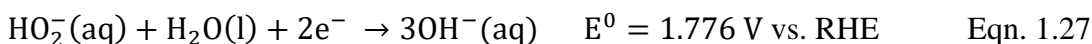
4-electron pathway:



2-electron pathway:



The reduction of hydrogen peroxide can also take place in alkaline media:



Or the hydrogen peroxide can undergo a disproportionation reaction:



The main barrier/limiting factor for the sluggish ORR mechanism is the transfer of the electrons from the surface of the electrocatalyst to the reactant O_2 molecules. The mechanisms are categorized into two main categories. One is known as the inner-sphere electron transfer mechanism which is facilitated through direct adsorption of O_2 molecules on the surface of the catalyst. And the second one is called the outer-sphere mechanism in which an electron is transferred to the solvated molecular O_2 , $\text{O}_2 \cdot (\text{H}_2\text{O})_n$, via hydroxyl species adsorbed on the catalyst surface. In acidic electrolyte, only the first type, the inner-sphere electron transfer is present whilst in the alkaline media, both inner- and outer-sphere electron transfer mechanisms coexist. Therefore, the catalytic activity is limited in acid electrolyte as compared to the alkaline medium since the catalysts are not able to promote

the ORR process without providing adsorption sites for O₂ molecules on inner sphere layer, pertaining to the difficulty of the acid ORR as comparison to the alkaline ORR ¹⁵⁴.

Among the different mechanisms proposed for such multi-electron complex ORR reaction ¹⁵⁵, the most commonly used reaction mechanism in acid media scheme is suggested by Wroblowa et al ¹⁵⁶ by which H₂O₂ is formed as an intermediate product of the ORR in the so called “peroxo mechanism” ^{153,157,158}. On the other hand, the complete 4-electron ORR to H₂O follows either the “dissociative”, “associative” or “peroxide decomposition” mechanism shown in **Table 1-1**. In the “dissociative mechanism” the O₂ reduction and protonation follows the O-O in the bond breaking, in the “associative mechanism” the bond breaking follows a first reaction step, and in the “peroxide decomposition mechanism”, the adsorbed H₂O₂ is dissociated into OH.

Table 1-1: Mechanisms for electrocatalytic Oxygen Reduction Reaction, taken from [85].

| H ₂ O ₂ Formation (“peroxo mechanism”) | O ₂ intermediate dissociation to H ₂ O (“dissociative mechanism”) | Hydroperoxo intermediate dissociation path to H ₂ O (“associative mechanism”) | H ₂ O ₂ decomposition |
|---|---|---|---|
| $O_2(g) \rightarrow O_2^*$ $O_2^* + H^+ + e^- \rightarrow OOH^*$ $OOH^* + H^+ + e^- \rightarrow H_2O_2^*$ $H_2O_2^* \rightarrow H_2O_2(g)$ | $O_2(g) \rightarrow O_2^*$ $O_2^* \rightarrow 2O^*$ $2O^* + 2H^+ + 2e^- \rightarrow 2OH^*$ $2OH^* + 2H^+ + 2e^- \rightarrow 2H_2O^*$ | $O_2(g) \rightarrow O_2^*$ $O_2^* + H^+ + e^- \rightarrow OOH^*$ $OOH^* \rightarrow OH^* + O^*$ $OH^* + O^* + H^+ + e^- \rightarrow 2OH^*$ | $O_2(g) \rightarrow O_2^*$ $O_2^* + H^+ + e^- \rightarrow OOH^*$ $OOH^* + H^+ + e^- \rightarrow H_2O_2^*$ $H_2O_2^* \rightarrow 2OH^*$ |

1.5.2.2 Hydrogen fuel cell electrode reactions

A fuel cell is a type of electrochemical energy converter which relies on the following electrode reactions on its anode and cathode for it to operate.

At the anode, oxidation reaction occurs in which hydrogen loses its electrons to produce protons and electrons.



At the cathode, the reduction of oxygen happens where oxygen gains the electrons and forms water, or it is partially reduces to form hydrogen peroxide as in **equations 1.30** and **1.31**, respectively.



1.5.2.3 Reaction rate, current density and Tafel analysis

The rate of an electrochemical reaction is dictated by the difference between the electrode potential and the reversible potential. The reversible cell potential is the maximum amount of potential that an ideal cell can achieve. The reversible potential is used to calculate the losses at a specific electrode. However, its quantity is not specified as there is no absolute zero value. This challenge is overcome by choosing a specific electrode reaction as a standard to which all other electrode systems can be referred. This standard universal reference electrode is known as the reversible hydrogen electrode shown in the **equation 1.32** ¹⁵⁹.



Another important parameter in electrochemical reactions is the overpotential which is defined as the potential difference between the thermodynamically determined

reduction potential of a half reaction and the experimentally obtained potential at which the redox reaction occurs. Observing an overpotential in an electrochemical cell implies the excess energy required on top of the thermodynamically expected energy to make the reaction happen ¹⁶⁰. The extra/missing energy is lost as activation overpotential. This generally consists of two components: 1. The electrical energy associated with the interaction of the ions and electric field and 2. the activation energy of the charge transfer reaction which is the case for any chemical reaction. This activation potential can be characterized with the important parameter of current density denoted as i or j which is considered more important than the current, I in the electrochemical kinetics. The activation overpotential (η_a) and current density can be quantitatively related to each other via the Butler-Volmer equation (BVE) ¹⁶⁰.

We can apply the Butler-Volmer equations of electron kinetics (**equations 1.34-1.35**) for the anodic and cathodic rate constants of a simple electron transfer anodic and cathodic half reactions represented by **equation 1.33**.



$$K_a = k_0 \exp [\alpha_a nF(E-E^\theta)/RT] \quad \text{Eqn. 1.34}$$

$$K_c = k_0 \exp [\alpha_c nF(E-E^\theta)/RT] \quad \text{Eqn. 1.35}$$

Where k_0 , α_a , α_c and E^θ stand for standard rate constant of the reaction, anodic and cathodic coefficients, and standard electrochemical potential of the system, respectively. The value of α for metals is estimated as 0.5 and, in the rate determining step of the reaction, anodic and cathodic coefficients sum up to 1. The value of the current at equilibrium is zero

hence $I_a = -I_c = I_0$ where I_0 stands for the exchange current and can be used to represent the rate of an electrode reaction as shown in **equation 1.36** for the reduction reaction ^{161,162}.

$$I_0 = -I_c = nFAk_0 [O]_{\infty} \exp [-\alpha_c nF(E_{eq}-E^{\theta})/RT] \quad \text{Eqn. 1.36}$$

If we assume that $[O]^* = [O]_{\infty}$ (* stands for reaction sites close to the surface of the electrode), then O is produced and consumed at the same rate and taking summation of anodic and cathodic coefficients that equal to 1 into account, $[O]_{\infty} = [R]_{\infty} = c_{\infty}$ then $E_{eq} = E^{\theta}$ and we have **equation 1.37** where n is the number of electrons that participate in the half-cell reaction and F is the Faraday's constant.

$$I_0 = nFAk_0 c_{\infty} \quad \text{Eqn. 1.37}$$

Equations 1.34 and **1.35** can be used to find Tafel from a region where potential is close to the equilibrium potential where the current density is exponentially dependant on potential. Considering the reduction half reaction, since $j_c/nF = -k_c[O]^*$,

$$\ln|j_c| = \ln|j_0| - \frac{\alpha_c nFE}{RT} \quad \text{Eqn. 1.38}$$

Tafel slope can be found from the Tafel plot of $\ln|j_c|$ vs E as shown in **Figure 1-17**. The slope is given by $\alpha_c n$ or $\alpha_a n$ and the y-intercept at $E=E_{eq}$ gives $\ln|j_0|$, where j_0 represents the exchange current density which was shown earlier in **equation 1.36** that can be related to the standard rate constant ^{161,162}.

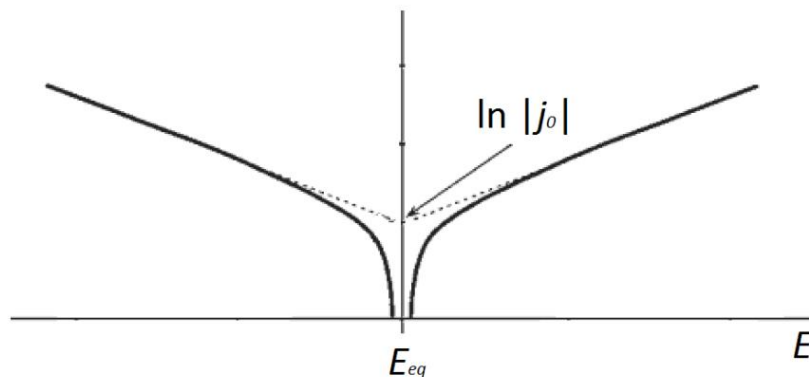


Figure 1-17: Tafel plot, taken from [21].

1.5.2.4 Mass transfer

Transport processes becomes an important factor whenever passing of a current is involved in a cell. This is because the participating ions and neutral species that participate in electrode reactions happening at the anode and cathode, must be transferred to the respective electrode surface for the reaction to take place. Mass transfer happens by three different modes- each playing an important role in the electrochemical dynamics. These modes are namely: 1. migration: where charged species travel under the influence of an electrode field or i.e. a gradient of electrical potential, 2. Diffusion, where species travel under the influence of concentration gradient i.e., a gradient in chemical potential and lastly 3. Convection, which basically means stirring or hydrodynamic transport which is divided into two types of natural and forced convection. The first type occurs when the fluid flow occurs when there is a density gradient, and the second type is characterized by laminar flow, turbulent flow as well as the stagnant regions ²¹.

1.6 Thesis outline

- **Chapter 1:** This chapter discusses the importance and applications of hydrogen peroxide in section 1.1 and backgrounds of the conventional large scale and emerging alternatives methods of production of this chemical in an industrial scale in section 1.2. The state-of-the art electrocatalysts as well as the nonprecious Metal-Nitrogen-Carbon electrocatalysts for the oxygen reduction reaction were reviewed in detail in section 1.3 and its subsections with a particular interest on the electrocatalysts discussed in the literature for the electrochemical production of hydrogen peroxide. Section 1.4 covers the cell design and practical devices and the challenges involved in translation of the results obtained from RRDE to practical devices. The chapter ends with a discussion on the essential fundamental electrochemistry concepts including the Sabatier analysis, thermodynamics, and reaction kinetics in section 1.5.
- **Chapter 2:** this chapter discusses the synthesis procedures of the 4 different sets of nanocatalysts along with the materials used. It further discusses the electrochemical method for the evaluation of the activity and selectivity of the electrocatalysts and electrode preparation. Also, in this chapter, various structural characterization techniques for the study of the physicochemical properties of the electrocatalyst are discussed.
- **Chapter 3:** This chapter includes all the results obtained from the extensive characterization imaging performed of nanocatalysts as well as the activity and selectivity results from the electrochemical catalytic performance investigation using the conventional three-electrode electrochemical cell and the rotating ring disk

electrode (RRDE). The major electrochemical results are the polarization curves obtained from the RRDE study on the 4sets of nanocatalysts of different metal concentration in different electrolytes as well as the contribution of Ni₃S₂ to the ORR activity.

- **Chapter 4:** this chapter summarizes the major findings and contribution to this work as well as the suggested future works.

1.7 Thesis objectives and approach

The ultimate objective of the project presented here will be to develop a new inexpensive and earth abundant M-N-C (with the metal being Ni) electrocatalyst that is capable of reducing oxygen to hydrogen peroxide selectively through 2e-ORR based on simplistic synthesis technique and to understand the role of different amount of nickel precursor and the pH of the electrolyte on the activity and selectivity of the catalyst as well as the potential responsible active sites for the ORR performance in each electrolyte. To accomplish this, nanostructured Ni-N-C electrocatalysts were synthesized by pyrolyzing, acid leaching and re-pyrolyzing a mixture of nickel (II) chloride, polyaniline (PANI) and cyanamide (CM) at a range of Ni precursors amount. Detailed physicochemical and electrochemical characterization of these materials were done using extensive characterization techniques as well as the rotating ring disk electrode (RRDE) technique in order to provide further insight and understanding regarding the nature of the materials as well as the ORR performance of the electrocatalysts in terms of activity and selectivity trends towards the production of H₂O₂ in acidic (0.1M HClO₄) and alkaline (0.1M KOH)

electrolytes. We then correlated the results of electrochemical and various microscopy and spectroscopy material characterization techniques, to hypothesize and identify the different active site structures that are at play under acidic and alkaline media.

This work will provide a rigorous investigation and systematic insight into the synthesis-structure-property-performance relationships of Ni-N-C catalysts that will further provide a basis of knowledge for the further investigations in identifying the exact active site structures responsible for the formation of H_2O_2 through the ORR that in turn guides the future design and synthesis of inexpensive catalyst materials that possess high activity and selectivity towards the production H_2O_2 through ORR. A simplified breakdown of the tasks carried out throughout this thesis are shown in **Figure 1-18**.

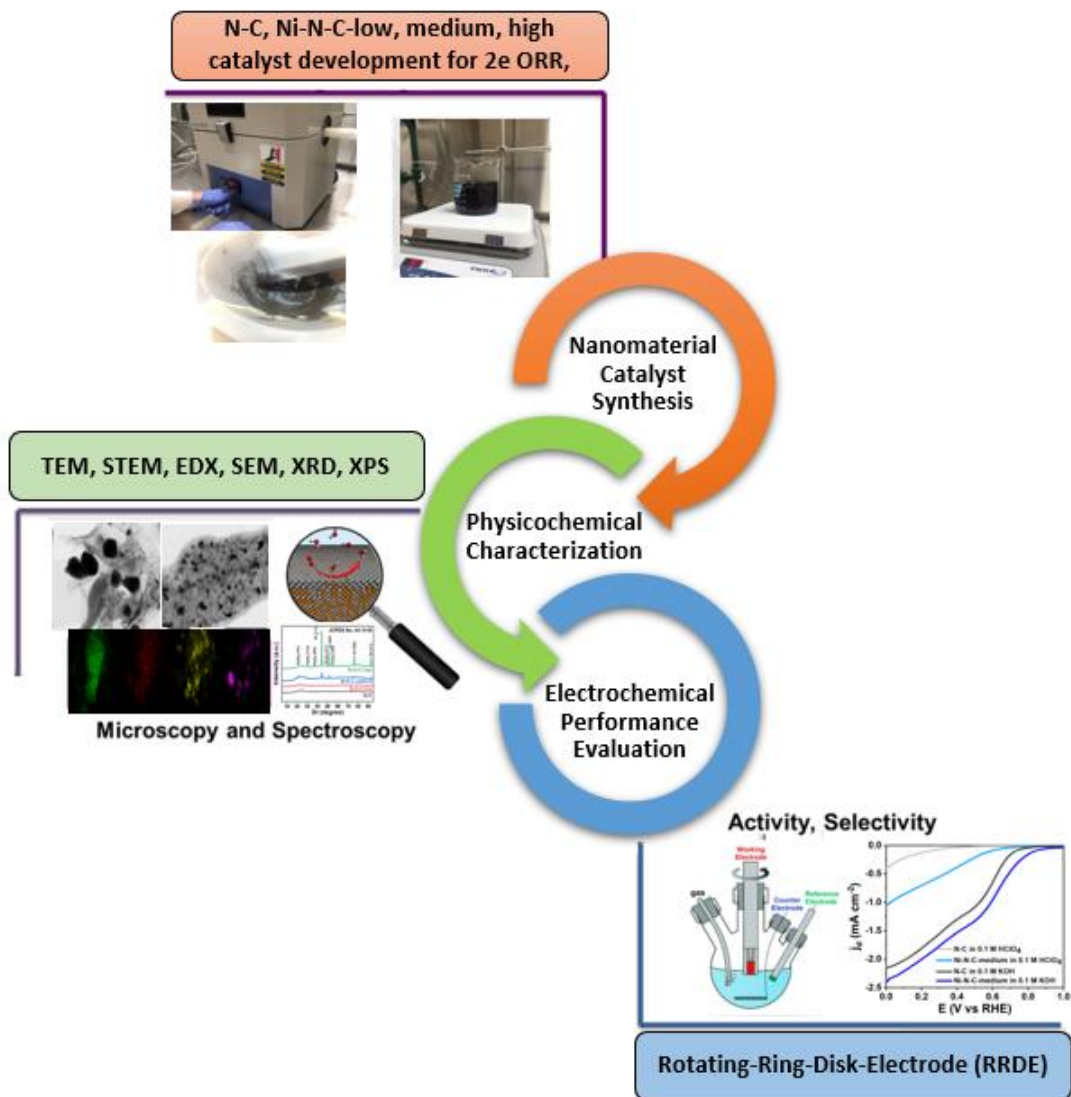


Figure 1-18: Schematic of the project workflow.

Chapter 2

This chapter includes content that has been adapted from:

“Identifying Activity and Selectivity Trends for the Electro-synthesis of Hydrogen Peroxide via Oxygen Reduction on Nickel-Nitrogen-Carbon Catalysts”

Ladan Shahcheraghi, Chunyang Zhang, Hye-Jin Lee, Melissa Cusack-Striepe, Fatma Ismail, Ahmed Abdellah and Drew C. Higgins, 2021 (Submitted).

Methodology

2.1 Materials

This work was carried out at Higgins lab, where all the reagents, the catalyst synthesis as well as the electrochemical measurement equipments were provided. The characterization equipments were made available by the Canadian Centre of Electron Microscopy (CCEM) and McMaster University’s Biointerfaces Institute (BI) and McMaster Analytical X-ray Diffraction Facility (MAX).

2.1.1 Reagents

The list of the reagents used in this work are shown in **Table 2-1** and they are used without additional purifications and/or further treatment.

Table 2-1: Reagents.

| Chemical reagent/material | Supplier |
|------------------------------------|--|
| Aniline | ACS reagent, 99.5% purity, Sigma-Aldrich |
| Nickel (II) chloride hexahydrate | 99.9% trace metal basis, Sigma-Aldrich |
| Ammonium persulfate | ACS reagent, 98% purity, Sigma-Aldrich |
| Cyanamide | 99% purity, Sigma-Aldrich |
| Sulfuric acid | ACS reagent. 95.0-98.0 %, Sigma-Aldrich |
| Hydrochloric acid | ACS reagent, 37 %, Sigma -Aldrich |
| Nickel sulfide | 99.7% trace metals basis, Sigma -Aldrich |
| High surface area Vulcan carbon | Vulcan CX-72R, FuelCellStore |
| Nafion | 5 wt% Nafion in ethanol |
| Isopropanol | ACS reagent, 99.5%, Sigma -Aldrich |
| Perchloric acid | ACS reagent, 70 %, Sigma-Aldrich |
| Potassium hydroxide | ACS reagent, 85%, pellets, Sigma-Aldrich |
| Alumina slurry suspension solution | Pine |
| O ₂ | Ultra High Purity, Praxair |
| N ₂ | Ultra High Purity, Praxair |
| Ar | Ultra High Purity, Praxair |

2.1.2 Equipments

The most important equipments used in this study are listed in **Table 2-2**.

Table 2-2: Principle equipments.

| Equipment | Supplier |
|--|--|
| VSP-300 Multipotentiostat | Bio-Logic |
| Rotating Ring-Disc Electrode | Pine |
| Platinum Ring and Glassy carbon disc electrode | Pine |
| Tube Furnace | Thermo Scientific Lindberg/Blue M TF55030A-1 |
| Oven | VWR Oven F Air 2.3 CF |
| Ag/AgCl Reference Electrode | Pine |

2.2 Conventional 3-electrode electrochemical cell

A Conventional 3-electrode electrochemical cell shown in **Figure 2-1**, is one of the common types of electrochemical cell which can be used to characterize electrochemical reaction. In this type of cell, the working electrode consists of the electrocatalyst that is to be characterized and its potential can be controlled as the current passes through it. A counter electrode which is usually platinum (for platinum catalyst investigations) is added to complete the electrical circuit, however, for non-PGM experiments, a graphite rod is used as the counter electrode as platinum might have the potential of causing contamination to the catalyst. Lastly, a reference electrode in this case an Ag/AgCl electrode is used which

is basically added to control the potential of the working electrode and to minimize the electrolyte effects ¹⁶³.

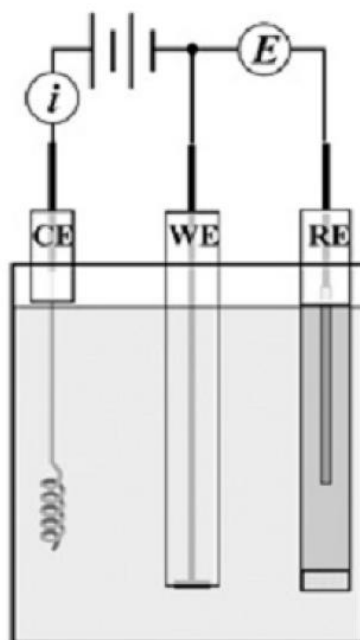


Figure 2-1: A conventional 3-electrode cell, taken from [163].

2.2.1 Preparation of electrode

The RDE and the RRDE both consist of a glassy carbon disk working electrode which is separated from a platinum ring electrode by a thin layer of Teflon. The dimensions of these electrodes are listed in **Table 2-3**. The surface of the GC disk working electrode was polished mechanically using a 0.05 μm alumina slurry suspension solution from Pine Instruments and micro cloth polishing pads by gently polishing the surface of the electrode against the slurry while turning and keeping the electrode surface parallel to the surface of the micro cloth in a figure 8 pattern (**Figure 2-2**) on a glass petri dish, followed by a 20 minute sonication of the polished disks in a solution that contains 40 % Millipore water,

40% isopropanol and 20% acetone which would be equivalent to 8 ml of water and IPA and 4 ml of acetone in a small vial. A second sonication of the same duration was performed, this time only in a Millipore water to get rid of the alumina particles and organics that were remained on the surface of the disks. The nice, flat, clean GC disk electrodes were then collected and rinsed with Millipore water, ready for the deposition of the catalyst's inks ¹⁶⁴.

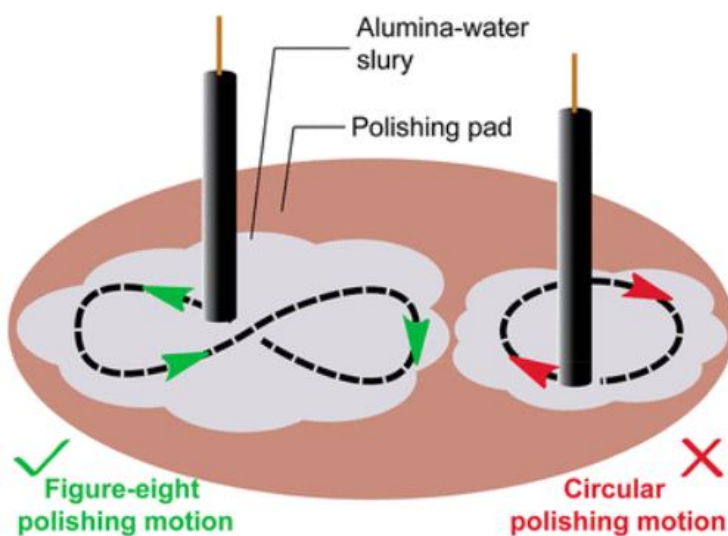
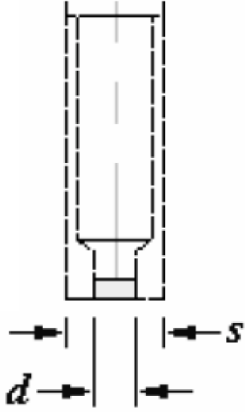
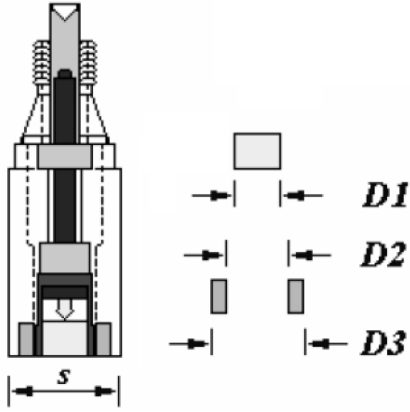


Figure 2-2: Polishing glassy carbon disk electrode, reprinted with permission from [165], Copyright 2017 American Chemical Society.

Table 2-3: RDE and RRDE electrode dimensions, taken from [166].

| RDE | RRDE |
|--|---|
|  |  |
| <p>Shroud diameter (s): 12.0 mm</p> <p>Disk diameter (d): 5.0 mm</p> <p>GC disk electrode geometric area: 0.19635 cm²</p> | <p>Disk diameter (D1): 5.0 mm</p> <p>Ring ID (D2): 6.50 mm</p> <p>Ring OD (D3): 7.50 mm</p> <p>Shroud diameter (s): 15.0 mm</p> <p>Collection efficiency: 22%</p> |

Catalyst-coated electrodes were prepared through an ink-based spin-coating process to achieve uniform electrode coverage. The inks were formulated by mixing synthesized catalysts (3.0 mg) in 750 μL of isopropanol (ACS reagent, 99.5% purity, Sigma-Aldrich), followed by a ultrasonication for 20 minutes to produce homogeneous, uniform, and well-dispersed inks. A 3.27 μL aliquot of the catalyst ink was then drop-casted in three intervals to get a total of 9.8 μL ink deposited onto the tip of a well-polished glassy carbon disk electrode of the RRDE spinning at an initial rate of 150 rpm increased to 400 rpm followed

by the deposition of a 15 μL of dilute Nafion solution prepared from mixing 200 μL of Nafion (Sigma Aldrich, 5 wt% Nafion in ethanol) which acts as a binder in 19 ml of isopropanol, dried at room temperature. The final electrode-catalyst loading was 0.2 mg cm^{-2} .

2.2.2 Set-up

The setup for the electrochemical measurements of H_2O_2 involved using a standard sealed three-electrode cell with a rotating ring disk electrode (RRDE) (Pine Research Instrumentation, Inc.) connected to a Bio-Logic VSP-300 Multipotentiostat system and a Pine rotation controller, using a sample-coated glassy carbon electrode, graphite rod and an Ag/AgCl for working, counter and reference electrode in the cell, respectively as shown in **Figure 2-3**. The electrolytes were prepared by distilled water and concentrated HClO_4 and KOH to give HClO_4 and KOH solutions with the concentration of 0.1 M. Pure O_2 and N_2 gases were used as the inlet gas.

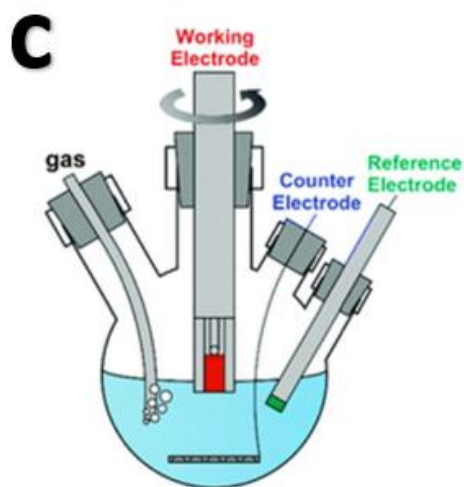
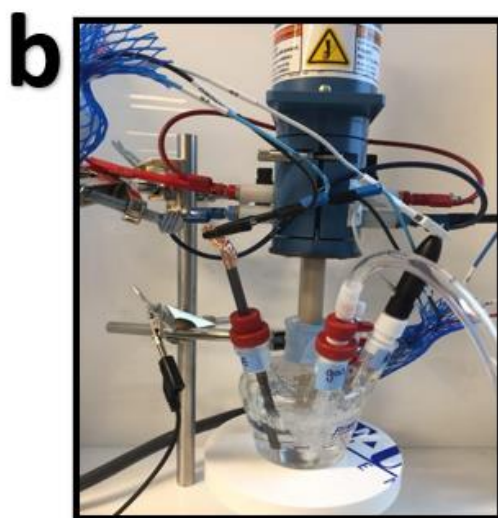
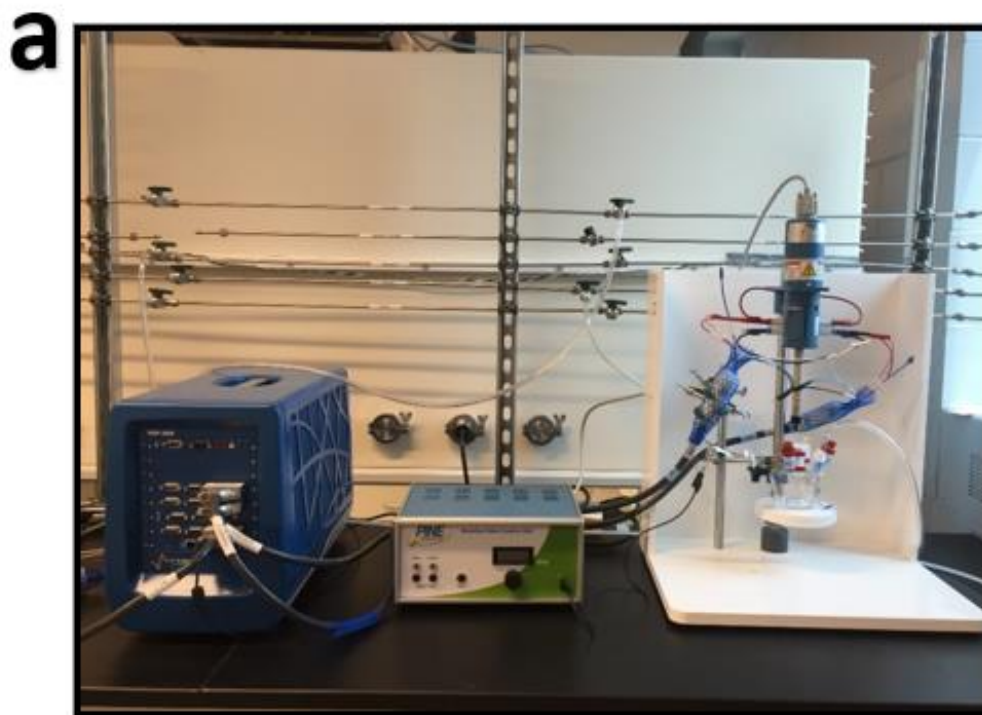


Figure 2-3: Photos of (a) the experimental setup with the RRDE connected to Bio-Logic SP-300 bipotentiostat system, controlled by a computer and Pine rotator, (b) RRDE with conventional three-electrode cell with a O_2/N_2 gas inlet, Ag/AgCl reference electrode and graphite rod as the counter electrode, and (c) schematic diagram of the standard three electrode cell used for RRDE measurements, adapted form [167], with permission from the Royal Society of Chemistry.

2.2.3 Cyclic voltammetry

Cyclic voltammetry is a well-known technique in electrochemistry that is particularly utilized to get a better understanding of new electrochemical systems. Usually it is the main first test that is done in any electrochemical evaluation study as it enables a fast location of electrode potentials of the electroactive species involved in the system as well as convenient evaluation of the way redox processes are impacted by the type of electrolyte/media¹⁶⁸⁻¹⁷⁰ A CV basically is obtained when a current as a function of electrode potential is recorded while the potential is cycled or swept linearly at a scan rate v between two chosen values (low and high (**Figure 2-4**)). A single or multiple cycle can be used depending on the type of information needed. The graph that is resulted from this experiment is called a voltammogram and has the y-axis as current as a function of potential that is plotted in the x-axis.

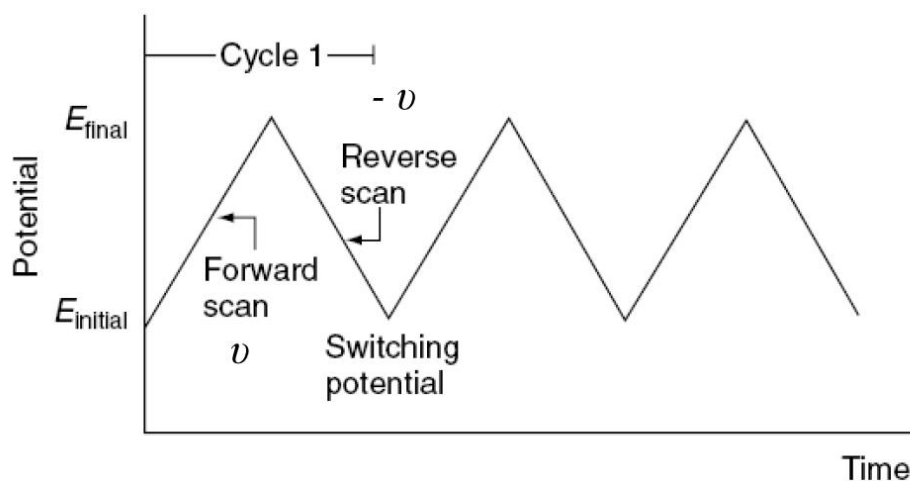


Figure 2-4: Potential–time excitation signal in a cyclic voltametric experiment, taken from [171].

2.2.3.1 Characterization of metal surfaces

The reduction and oxidation processes happen at the working electrode. Oxidation process takes place when the potential is pushed to the upper value while the reduction process happens when the potential is reversed to the lower value. This way cyclic voltammetry can be used for catalyst surface characterization as it is considered a surface sensitive technique. In acid aqueous electrolyte, hydrogen and oxygen are adsorbed on the surface of the noble metals by charge transfer. The potential at which corresponding features of the CV plot appear as well as their shape are specific to each metal and gives us information about their identity ¹⁷². For example, in the case of an electrode that is made up of the platinum metal where some interesting reactions happen at its surface, specific features in acidic electrolyte are identified using a CV where some interesting reactions occur at the surface of the Pt electrode. **Figure 2-5** shows a typical cyclic voltammogram of Pt in acidic electrolyte where three different regions are distinguished. In the region between 0 and 0.4 V (vs RHE), the adsorption and oxidation of hydrogen in the cathodic and anodic sweeps respectively have given rise to two pairs of peaks that are assigned to weakly and strongly bound hydrogen ^{173,174}. **Reaction 2.1** shows the adsorption-desorption of hydrogen.

The second region from 0.4 to 0.8 (vs RHE) is called the double-layer region. The current recorded in this region is raised by the accumulation of charges from the electrolyte at the polarised interface and is not due to any reaction as no electrochemical reaction takes place in this region. The third region which is above 0.8 V (vs RHE), the chemisorption of the oxygen and formation of oxides occur. As the potential is raised above 0.8 V (vs RHE),

the adsorption of oxygen becomes increasingly irreversible due to the rearrangement of the oxygen species layer into a two-dimensional lattice of O species and metal atoms ¹⁷⁵. At the onset of the oxide formation, the O-containing species present in the electrolyte (H₂O, OH⁻) start interacting with the Pt surface and the progress in the process results in the development of a 3-dimensional oxide lattice.

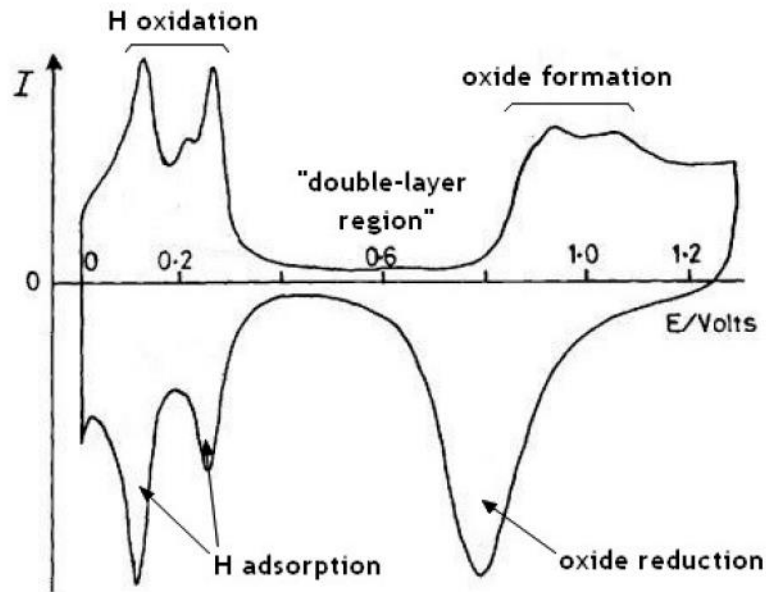
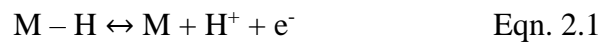


Figure 2-5: Cyclic voltammogram of a Pt electrode in 0.5 M H₂SO₄ at 25 °C and scan rate of 100 mV s⁻¹, taken from [21].

2.2.3.2 Electrochemical active surface area (ECSA)

Cyclic voltammetry (CV) can be applied to determine the electrochemically active surface area (ECSA) of catalyst materials in acidic electrolyte. CV involves cycling the potential of the catalyst coated electrode under nitrogen saturated acid electrolyte. The

ECSA of the catalyst materials were calculated by collecting measurements on the charging currents of the double-layer capacitance. ECSA is considered as a significant parameter for the ORR performance hence when evaluating electrochemical performance of Ni-based materials it is imperative to know the ECSA of the material in order to compare the intrinsic catalytic activity between catalysts. Knowing the ECSA will allow us to quantify the area of the reacting interface and will hence allows for a more accurate performance comparison of the catalyst materials.

For our catalysts that have porous and layered morphology, the intrinsic electrocatalytic ability should take surface area into consideration, as the active sites are extensively exposed. The value of the electrochemical surface area (ECSA) is proportional to the amounts of the active sites involved in electrochemical reactions; therefore, it is generally considered to be a significant parameter for the high ORR performance. Here, ECSA values were determined by conducting the CVs and measuring the charging currents of double-layer capacitance at scan rate of 20 mVs^{-1} in nitrogen saturated electrolyte. Background CVs of each of the four catalyst samples were integrated [getting units of A.V] and divided by scan rate [V/s] to get the charge transferred [Coulombs, or A.s]. The resulting value were then divided by 2 to account for the fact that the integration was done for both the anodic and the cathodic sweep so that the charge transferred is not counted twice. Then the capacitance value [in Farads/g] of our high surface area 3-dimentional material was obtained by dividing this value by the potential window of 1 (as we swept the potential from 0 to 1 V) as well as the mass of the catalyst material.

The capacitance value C_d was then converted to the ECSA using **equation 2.2** in which C_d is capacitance of the double layer and the C_s is the specific capacitance of the working electrode which is the expected amount of capacitance per unit surface area for a carbon material that is empirically measured by measuring the capacitance of a carbon electrode with a known surface area ¹⁷⁶. For estimation of surface area here, we use the literature reported specific capacitance of $C_s = 0.015 \text{ mF cm}^{-2}$ in our calculations ^{176,177}.

$$\text{ECSA} = \frac{C_d}{C_s} \quad \text{Eqn. 2.2}$$

2.2.4 Rotating disk electrode (RDE)

Reactant species are transported to or from the surface of the electrode by two main modes of mass transport known as diffusion and convection. Charged species can also transport through migration under an electrical field ¹⁷⁰. Mass transport rates can be greatly elevated with the introduction of forced convection by which the diffusion layer thickness can be significantly reduced. Forced convection is achieved by externally imposing electrode movement with respect to the electrolyte, for instance by rotating the electrode as in RDE that turns about its vertical axis (**Figure 2-6**) at a typical rotation rate of 400 to 10000 rpm. As **Figure 2-6** shows, RDE consists of a glassy carbon disk that is set into an insulating (PTFE) sheath.

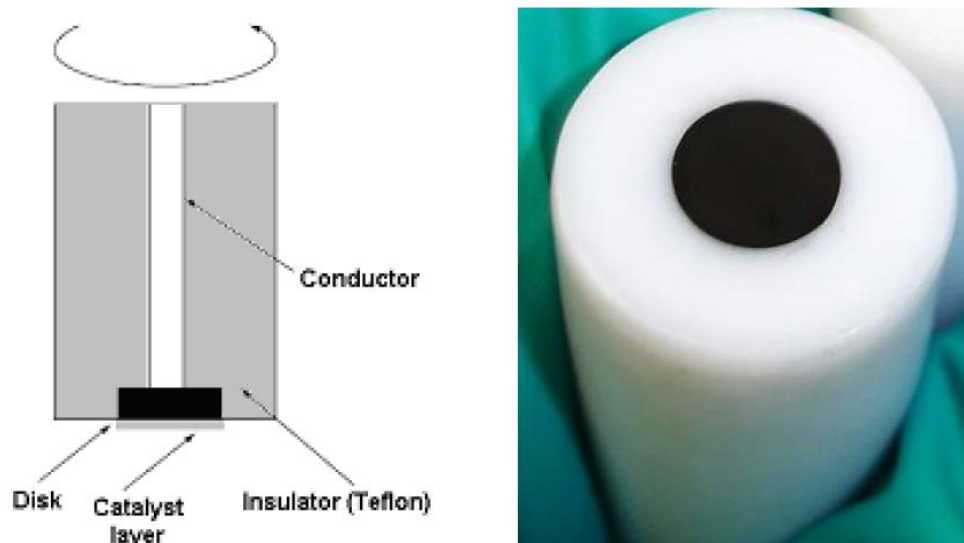


Figure 2-6: Rotating disk electrode, taken from [21].

The rotation of the working electrode results in a forced convection where well-defined convective flow pattern of the electrolyte is induced and pumped up from the bulk towards the surface of the electrode followed by throwing out centrifugally as shown in **Figure 2-7**. The potential of the glassy carbon working disk electrode is also swept back and forth between two potential limits like that happening in CV mentioned earlier.

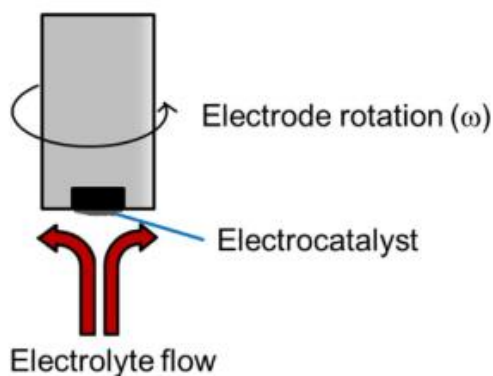


Figure 2-7: Schematic of the convective electrolyte flow induced by the rotation of electrode, taken from [178].

2.2.5 Rotating ring disk electrode (RRDE)

A rotating ring-disk electrode (RRDE) is an elegant in situ technique that makes use of a second working electrode to study multi-electron electrochemical reaction mechanisms or to detect reaction by-products. It is a simple technique for the investigation of a high throughput of catalyst materials in a time efficient manner that makes it an ideal method¹⁷⁸. It consists of a coaxial ring electrode right outside the disk electrode separated from each other by a thin insulating ring (**Figure 2-8a**). In our case, RRDE is used to monitor simultaneously the H₂O₂ production which occurs during the O₂ reduction at the disk of the RRDE. The rotation of the electrode continuously sweeps away the H₂O₂ radially from the disk electrode to the ring electrode where they are detected and oxidized back to oxygen ($\text{H}_2\text{O}_2 \rightarrow \text{O}_2 + 2\text{H}^+ + 2\text{e}^-$) causing a positive current to be generated.

Bio-Logic VSP-300 Multipotentiostat system is connected to the RRDE to measure the two signals coming from the disk and ring electrodes and to maintain the potential of the ring electrode at a specific value (in this case, at +1.2V vs RHE) to cause an immediate conversion of the peroxide coming from the disk electrode to oxygen for the aid of identification and quantification of the product and determination of the yield of the reaction by measuring the fraction of the current at the disk that leads to H₂O₂ as a function of potential (**Figure 2-8b**).

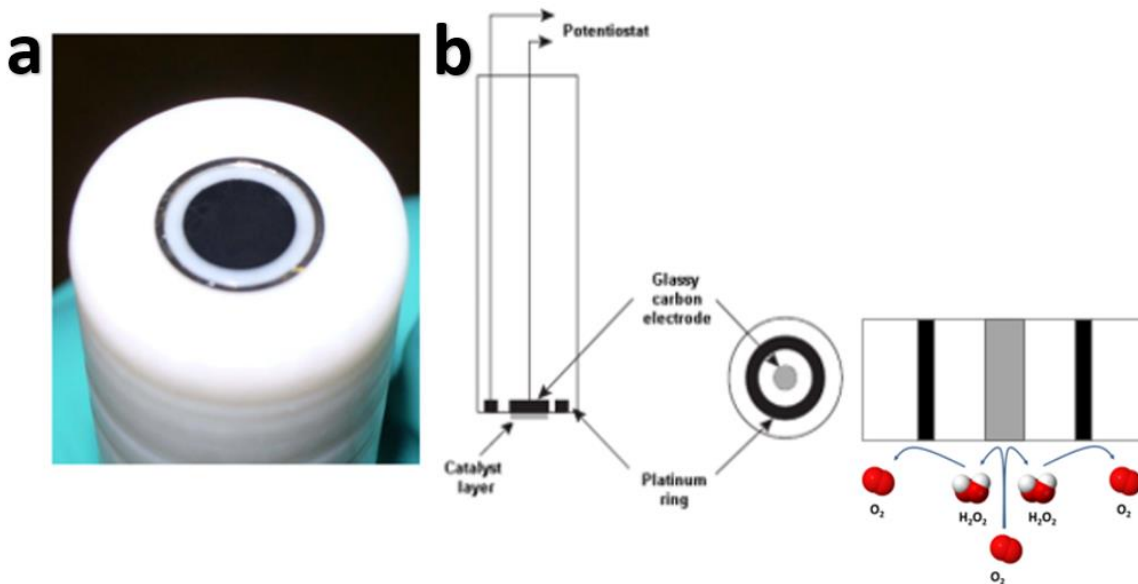


Figure 2-8: (a) photo of RRDE and (b) schematic of the RRDE working principle for the measurement of H_2O_2 . After reduction of O_2 to H_2O_2 at the disk, the H_2O_2 is being collected and oxidized at the ring of the RRDE tip, taken from [163].

An identical flow pattern as that shown in **Figure 2-7** in RDE is produced by the rotation of the RRDE where the forced convection causes the solution to be drawn up to the disk electrode and then being thrown out to the surface of the rotating structure. These would mean that the ring electrode is downstream of the disk electrode and hence the species formed at the disk will only arrive at the ring partially. This convective flow pattern appearing at the surface of the rotating electrode would cause some of the species to bypass the ring and pass into the bulk solution. This fraction of the product species that would travel from the disk to ring depends on three factors: (1) the characteristics of the RRDE, (2) stability of the product in the electrolyte and (3) the rotation rate which determines the amount of time taken by species to transport from the disk to the ring¹⁷⁰. From the O_2 reduction at the disk and the H_2O_2 oxidation at the ring, two currents are detected called as

disk current (I_d) and ring current (I_r) or peroxide current respectively, which are related to each other by the parameter N shown in **equation 2.3**. The collection efficiency, N , is defined as “the fraction of a completely stable species formed at the disk (I_d) that is detected at the ring (I_r)”^{161,170} (**equation 2.3**) and has the theoretical value of 0.22.^{21,179}

$$N = \frac{I_r}{I_d} \quad \text{Eqn. 2.3}$$

From these values, it is possible to derive the number of transferred electrons (n) per molecule of O_2 and also the selectivity for the H_2O_2 formation that is defined as “the percentage of the reduced O_2 molecules that are converted to H_2O_2 ” calculated using **equations 2.4 and 2.5**¹⁸⁰.

$$n = \frac{4I_d}{I_d + I_r/N} \quad \text{Eqn. 2.4}$$

$$\text{Selectivity}_{H_2O_2} = \frac{200 \times I_r}{(N \times |I_d|) + I_r} \quad \text{Eqn. 2.5}$$

2.2.6 Electrochemical measurements

Oxygen reduction reaction (ORR) measurements were performed by rotating ring disk electrode (RRDE) testing at room temperature and ambient pressure in oxygen-saturated conditions. H_2O_2 selectivity were obtained from polarization curves under steady-state conditions in oxygen-saturated electrolyte between 0.0 to 1.0 V at a scan rate of 20 mVs^{-1} at 900 r.p.m. while holding the potential of the platinum ring electrode at 1.2 V. A total of two electrolytes with pH~1 (0.1 M $HClO_4$) and pH~13 (0.1 M KOH) was used. All the potentials were measured versus the $Ag/AgCl$ electrode and then converted to the reversible hydrogen electrode (RHE) scale. 500 activation cycles on the platinum ring

electrode were run initially at a scan rate of 500 mVs⁻¹ and 900 r.p.m. prior to the main ORR measurements to ensure the cleanliness of the electrode, reaching steady-state condition and obtaining reproducible CV. O₂ was continuously purged through the electrolyte during electrochemical measurements ensuring maintained O₂ saturation. The measurements were repeated three rounds in freshly made electrolytes for each of the catalyst that were tested to ensure reproducibility of the results. The ORR current was corrected by removing the background current, i.e., correcting for the non-Faradaic current (capacitance) that arises from the charging/discharging of the double layer. The currents were normalized based on the disk electrode geometric surface area (SA=0.19635 cm²) in order to obtain the net Faradaic disk electrode current densities that arises from the electroreduction of oxygen (**equation 2.6**).

$$i_{\text{Faradaic,geometric}} = \frac{I_{\text{disk-ORR}} - I_{\text{disk-N}_2}}{SA_{\text{geometric}}} \quad \text{Eqn. 2.6}$$

The collection efficiency value of RRDE set-up (N=0.22), was then used to calculate the number of transferred electrons and the H₂O₂ selectivity accordingly using **equations 2.4** and **2.5**.

2.2.7 Calibration of reference electrode

All potentials in this work were measured using an Ag/AgCl reference electrode, and all potential values were converted to the reversible hydrogen electrode (RHE) scale. The calibration of Ag/AgCl reference electrode was performed in a standard three-electrode system with a clean polished Pt wire as the working electrode, graphite rod as the counter

electrode and the Ag/AgCl as the reference electrode. Prior to the calibration, the Pt wire was cleaned with a butane flame until it glows red and was then allowed to cool down before inserting it into the electrolyte solution. 0.1 M KOH and HClO₄ solutions were used as the electrolyte and they were pre-purged and saturated hydrogen (H₂) gas. Cyclic voltammetry was run at a scan rate of 5 mV s⁻¹, and the potential value at which the curve crosses the x-axis, i.e., the current crossed zero, was taken to be the thermodynamic potential for the RHE. For example, in 0.1 M KOH, the zero current point is at -1.032 V, so $E(\text{RHE}) = E(\text{Ag/AgCl}) + 1.032 \text{ V}$; in 0.1 M HClO₄, the zero current point is at -0.320 V, so $E(\text{RHE}) = E(\text{Ag/AgCl}) + 0.320 \text{ V}$. **Figure 2-9** shows the CVs of the calibration of our reference electrode in both alkaline and acid electrolytes.

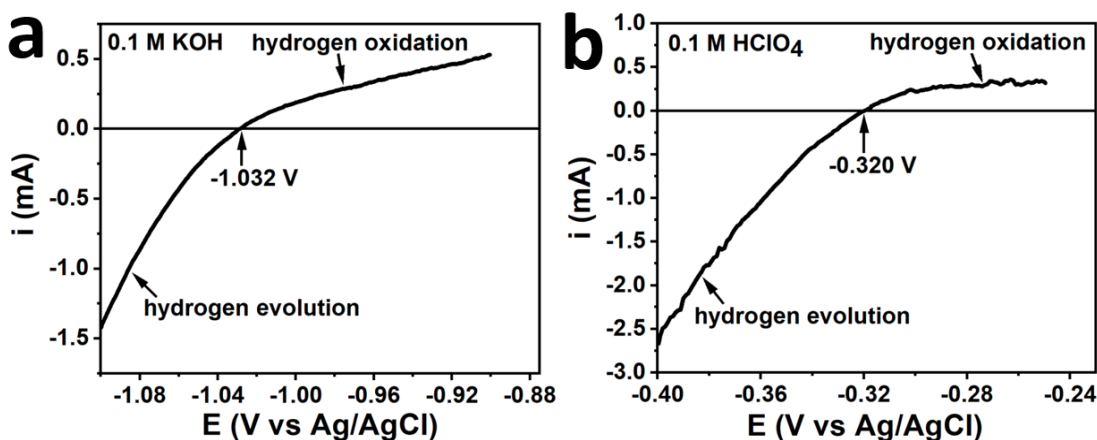


Figure 2-9: Cyclic voltammograms of Ag/AgCl reference electrode calibration versus reversible hydrogen electrode (RHE) in (a) 0.1 M KOH and (b) 0.1 M HClO₄.

2.3 Catalyst synthesis

The catalysts synthesized are categorized into metal free nitrogen doped carbon and metal containing Nickel-Nitrogen-Carbon catalysts of three different concentrations.

Commercial and Pyrolyzed Ni₃S₂/VC were also prepared. Detailed synthesis procedure of all catalysts are as follows.

2.3.1 Nickel-Nitrogen-Carbon catalysts

1 ml of Aniline was added to 200 ml of 1.5 M HCl solution stirred by a magnetic bar at room temperature on a stir plate, followed by the addition 2.0 g of cyanamide and 0.08 g, 0.30 g or 1.20 g of nickel (II) chloride for the synthesis of Ni-N-C-low, Ni-N-C-medium, and Ni-N-C-high catalysts, respectively. Once NiCl₂ was dissolved, 1.5 g of ammonium persulfate was added to the solution as an oxidant to catalyze the oxidative polymerization of aniline. The solution was stirred with a magnetic stir bar at 600 r.p.m. at room temperature for 2 hours to allow full polymerization of aniline, and then the liquid was evaporated by heating the hot plate to 80°C while stirring at 200 r.p.m. until it became tar-like (approximately 12 hours). The collected material was subsequently heat treated at 900 °C in an argon atmosphere for 1 hour inside a tube furnace. The resultant powder was ground and crushed using a mortar and pestle and was then mixed with 100 mL of 0.5 M H₂SO₄ and sonicated for 10 minutes to obtain a well-dispersed solution. This solution was then covered and stirred at 800 r.p.m. on a hot plate set at 90°C for 6 hours to leach out any acid-soluble nanoparticles or residues. The resulting solution was then filtered and washed. The recovered powder was collected and dried in an oven at 90°C for 12 hours. The dried powder was pyrolyzed again at 900 °C in an argon atmosphere for 3 hours to obtain the final catalyst.

2.3.2 Nitrogen doped carbon catalysts

The metal-free N-C catalyst was prepared using the exact same procedure as the Ni-N-C catalysts except that no Ni salt was added during the synthesis and hence the steps after the first pyrolysis was not performed as there was no need for acid leaching, drying and second pyrolysis. Therefore, the final powder was collected right after the first pyrolysis.

2.3.3 Commercial and pyrolyzed Ni₃S₂/VC

Benchmark Ni₃S₂/VC samples were prepared by mixing commercial Ni₃S₂ and high surface area Vulcan XC-72 (VC, FuelCellStore) powders in a ratio of 20 wt.% to 80 wt.%, respectively. A portion of the Ni₃S₂/VC were also subjected to the same pyrolysis and acid wash conditions as the Ni-N-C catalysts (P- Ni₃S₂/ VC). Solubility of Ni₃S₂ in acid was investigated by acid leaching 0.5 g of commercial Ni₃S₂ powder in a mixture of 100 ml of 0.5 M H₂SO₄ and 10 ml Millipore water. The powder was poured into the solution mixture and sonicated for 10 minutes to be well dispersed and then it was stirred for 6 hours with a magnetic bar at 80-0 rpm on a hot plate set at 90°C. The resulting solution was then filtered, and spray washed with Millipore water using a vacuum filtration.

2.4 Physicochemical characterization techniques

The structure and property of the synthesized electrocatalyst materials were studied by extensive characterization that included a variety of physicochemical techniques. The

results were then correlated to ones obtained from the electrochemical performance evaluation in order to elucidate the important factors that governs the electrochemical properties and catalytic activity and hence aid the rational design and synthesis of improved catalysts in the future work.

2.4.1 Scanning electron microscopy (SEM)

All SEM measurements reported in this work have been carried out using a FEI Magellan 400 with sub-nanometer resolution. SEM is considered as a powerful imaging tool that helps us investigate the different features of materials that possess a micro and/or nanostructure in terms of morphology and topology. In the operation of this technique, the sample is usually illuminated with a powerful beam of electrons and as a result an image is created based on collected secondary electrons or those that were backscattered¹⁷⁹. The size of the electron beam used in this process determines the resolution of the final image that can be on a nanometer or micrometer scale. In this project, SEM is used for the investigation of the distinct nanostructures of the synthesized N-C and Ni-N-C materials. The preparation of the samples was done by the spreading the nano powder on a carbon tape secured to a sample holder stub. This was then placed into the SEM machine and the sample chamber was then evacuated in order for the imaging to be done¹⁷⁸.

2.4.2 Transmission electron microscopy (TEM)

Field-emission transmission electron microscopy (TEM), high-resolution image-corrected transmission electron microscopy (HRTEM) and High-angle annular dark-field scanning transmission electron microscopy (HAADF-STEM) images were performed on

FEI Titan 80-300 LB operating at 300 keV in Canadian Centre of Electron Microscopy (CCEM) to allow for high resolution images to be obtained for our electrocatalyst samples on the nanometer and atomic scale. Generally, TEM machines are operated by the illumination of a very small area of interest on sample with an electron beam (produced by a field emission techniques) that passes through several condensers with a constant current density. The scattering of the electrons can be in two forms of elastic or inelastic which are finally collected when they hit the sample. With the processing of these diffracted electrons that are collected based on the electron diffraction theory, an image can be produced. TEM is effective in determining many different structures due to its high resolution. The common structures include the nanostructures, defects within the samples, exposed crystal as well as atomic arrangements ¹⁷⁸.

2.4.3 Energy-dispersive X-ray spectroscopy (EDX)

Energy dispersive x-ray spectroscopy (EDX) is a technique that is usually done in parallel with SEM and TEM imaging. In this work we used FEI Titan 80-300 LB operating at 300 keV in Canadian Centre of Electron Microscopy (CCEM) to conduct the EDX. In EDX imaging, electrons are bombarded onto the surface of the materials which produces x-ray emissions that gets collected by a detector. Energy of emitted x-rays energy along with its corresponding intensity are characteristic of each element and can be used for their identification and quantification within the sample that is under investigation. Elemental mapping is usually paired with EDX imaging and is used to analyze the x-rays emissions from localized positions on the sample. These emissions vary in intensities due to the

different atomic content in each of the specific locations and hence results in the generation of a concentration map of various elements existing in the sample under investigation.

2.4.4 X-ray diffraction (XRD)

X-ray diffraction (XRD) is a one of the widely used characterization techniques in broad fields of engineering and materials science. It helps scientists and engineers to identify materials and crystal arrangements using the big diffraction pattern data base as a point of comparison. In the present study, XRD is used as a tool to identify our catalysts crystal phases. The XRD patterns are obtained with Cu K α radiation ranging from 5 to 95 degree at McMaster Analytical X-Ray Diffraction Facility (MAX). However, in the case of the commercial Ni₃S₂/VC and acid treated/pyrolyzed Ni₃S₂/VC powders, the patterns were obtained using of Co K α radiation as the X-ray source but for comparison with most data that is published using Cu K α radiation we converted it to Cu using **equation 2.7**. XRD operated by the emission of X-ray beams from a source and their interaction with the atoms present in the materials that is under investigation. This produces a diffraction pattern specific for each crystal phase present in the sample. This pattern is considered as a characteristic of the crystal phase because the wavelengths of the x-rays and distance between atoms in samples that have crystalline or polycrystalline structure, are similar ¹⁷⁸.

$$2\theta(\text{Cu}) = 2 \times \arcsin (\sin (2\theta(\text{Co})/2) \times 0.8605) \quad \text{Eqn. 2.7}$$

2.4.5 X-ray photoelectron spectroscopy (XPS)

X-ray photoelectron spectroscopy is a technique used to find the identity and composition of atoms in the top ca. 0.5 to 5 nm of a sample hence it is considered as a

surface specific characterization technique. In this work, XPS was carried out on PHI Quantera II Scanning XPS Microprobe at Biointerfaces Institute at McMaster University. XPS operates by exposing the samples to x-ray photons with a set energy level which then interact with the sample under test and release electrons. The number of these electrons are then counted, and their kinetic energies are measured to be compared with the initial X-ray energies resulting in the determination of the electron binding energy in the sample materials. XPS are commonly used for nitrogen-doped graphitic carbon structures, such as metal-nitrogen-carbon catalysts where different spectra are obtained with the high resolution N1s (i.e., nitrogen) spectra being the most analyzed component in the entire XPS signal as it gives information about the quantity of various nitrogen functionalities such as pyrrolic, pyridinic, graphitic when the N1s spectra is deconvoluted. This same outlook can be applied to various other elements and bonding configurations too ¹⁷⁸.

Chapter 3

This chapter includes content that has been adapted from:

“Identifying Activity and Selectivity Trends for the Electro-synthesis of Hydrogen Peroxide via Oxygen Reduction on Nickel-Nitrogen-Carbon Catalysts”

Ladan Shahcheraghi, Chunyang Zhang, Hye-Jin Lee, Melissa Cusack-Striepe, Fatma Ismail, Ahmed Abdellah and Drew C. Higgins, 2021 (Submitted).

Results and discussion

3.1 Physical characterization

The as-synthesized metal-free N-C, Ni-N-C-low, Ni-N-C-medium, and Ni-N-C-high catalysts were characterized using scanning electron microscopy (SEM) and transmission electron microscopy (TEM). All four catalysts showed similar structures by SEM as depicted in **Figure 3-1**, indicating that the overall nanostructure is relatively insensitive to changes in Ni content. The samples revealed a morphology consisting of hierarchical pore structures that can be considered desirable for catalytic applications due to improved mass transport. Interestingly, fiber-like structures were observed in both Ni-N-C-medium and Ni-N-C-high catalysts (**Figure 3-1c, d**), likely arising due to the ability of Ni to catalyze the formation of carbon nanotubes.

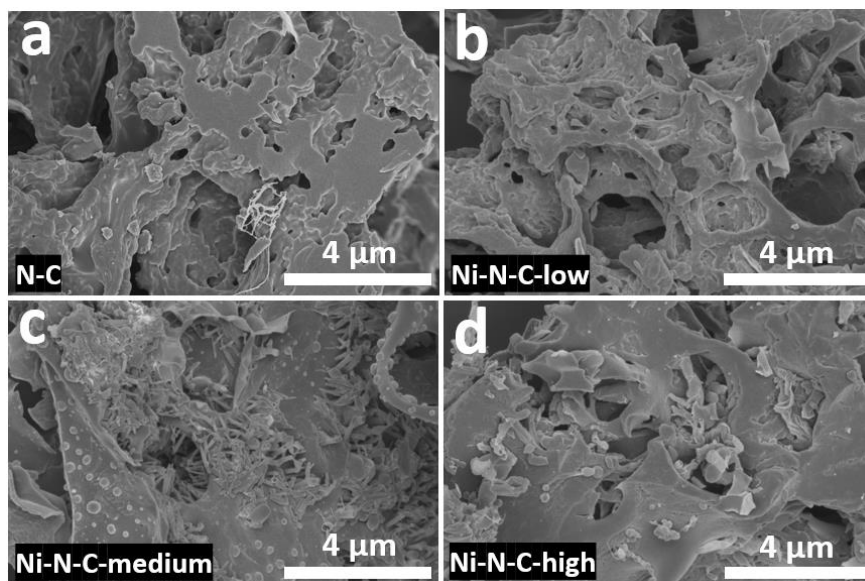


Figure 3-1: SEM images of (a) N-C, (b) Ni-N-C-low, (c) Ni-N-C medium, and (d) Ni-N-C-high catalysts

To further investigate the effect of Ni loading on catalyst structures, high-resolution transmission electron microscopy (HRTEM) was conducted. **Figures 3-2** and **3-3** show TEM images at different resolutions where the overall morphology of the main structures including fibrous carbon particles (primary phase) and layers of porous carbon sheets (secondary phase) are observed in the nickel containing samples. For the Ni-N-C catalysts, a uniform dispersion of small dark spots was observed over the entire surface, indicating the formation of nickel-based particles during materials synthesis.

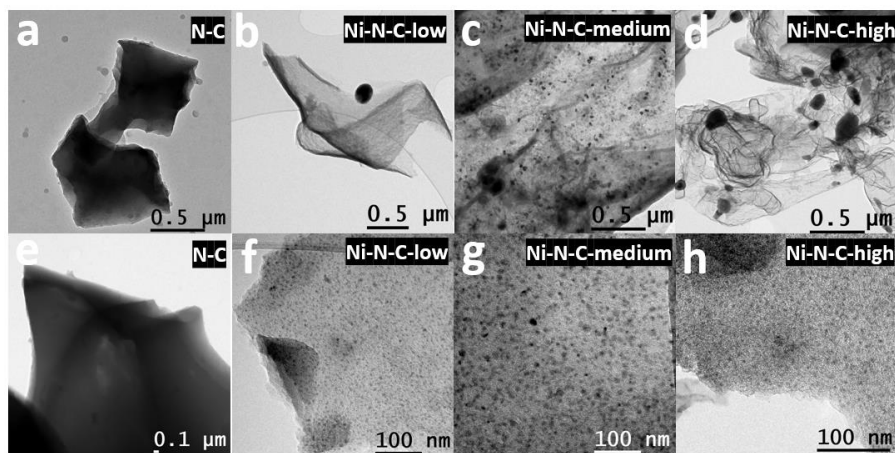


Figure 3-2: Low and high magnification HRTEM results of (a,e) N-C, (b,f) Ni-N-C-low, (c,g) medium, and (d,h) high catalysts

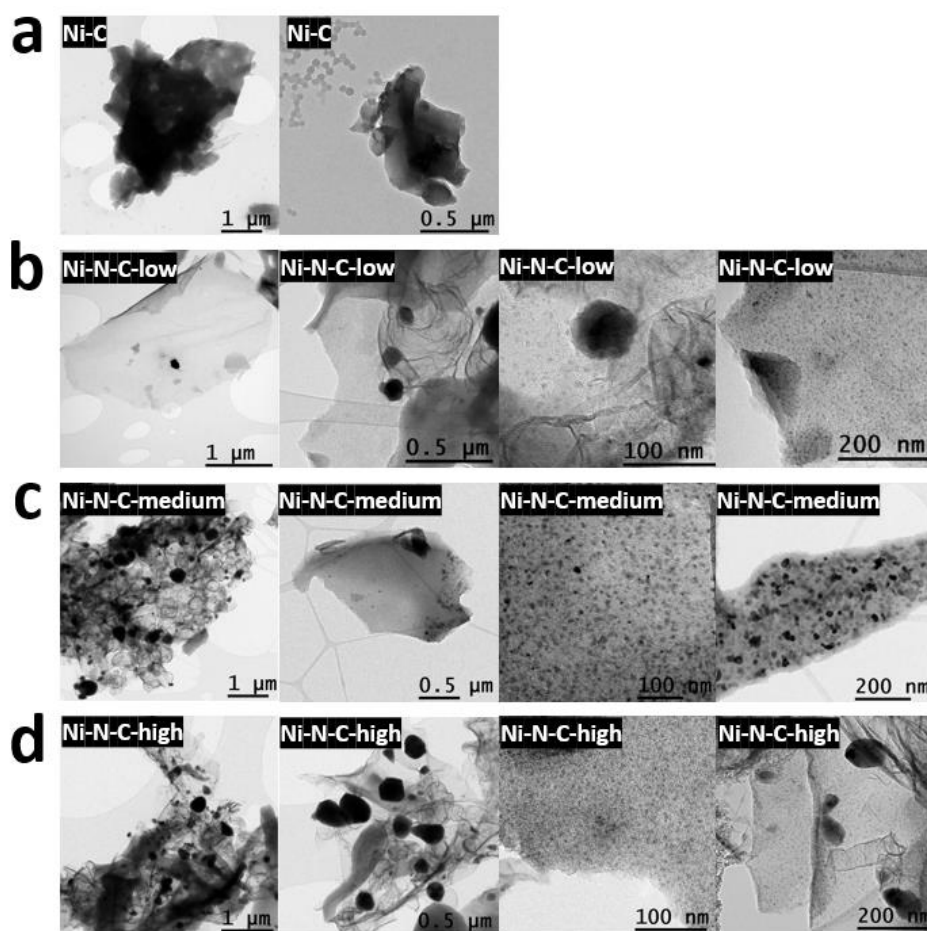


Figure 3-3: Low and high magnification HRTEM results of N-C, Ni-N-C-low, medium, and high catalysts.

Aberration-corrected high-angle annular dark-field scanning transmission electron microscopy (HAADF-STEM) and energy-dispersive X-ray spectroscopy (EDS) elemental mapping was conducted (**Figure 3-4**). The results of EDS mapping show bright regions in all three Ni-containing catalysts, confirming the presence of Ni-based particles that are bright due to their high Z-contrast as compared to their neighboring light elements such as C or O. It should also be noted that Ni signal was observed distributed throughout all regions of the catalyst structure, potentially indicating the formation of atomically dispersed Ni-N-C sites within the carbon framework.

It is worth to note that sulfur was found in all materials, due to the presence of ammonium persulfate during the synthesis procedure. In all materials, EDS maps show a homogeneous distribution of carbon, oxygen, and sulfur, with the elemental compositions from highest to lowest in Ni-N-C samples being carbon, oxygen, nickel, and sulfur. The exact elemental compositions of all catalyst samples are presented in **Table 3-1**. Nitrogen was not detected by EDS owing to the limitations of this technique; however, a more detailed analysis on the near-surface elemental compositions of the samples is presented later in the paper using XPS analysis which includes interrogation of the nitrogen species present in the materials.

Table 3-1: Elemental compositions of Ni-N-C-low, Ni-N-C-medium, Ni-N-C-high and metal-free N-C catalyst samples from STEM-HAADF and EDS analysis

| | Ni-N-C-low | Ni-N-C-medium | Ni-N-C-high |
|---------|------------|---------------|-------------|
| Element | At. % | At. % | At. % |
| C | 95.43 | 90.85 | 83.48 |
| O | 1.51 | 2.67 | 1.61 |
| S | 0.69 | 1.12 | 4.81 |
| Ni | 2.37 | 5.36 | 10.10 |

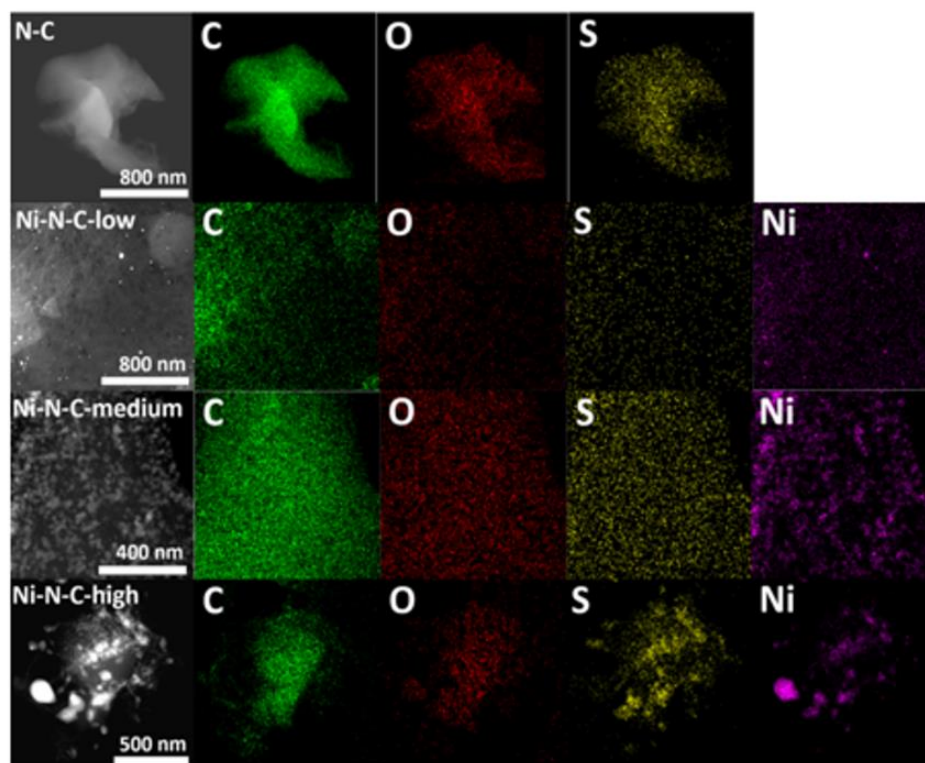


Figure 3-4: STEM-HAADF and EDS maps for C, O, S, Ni.

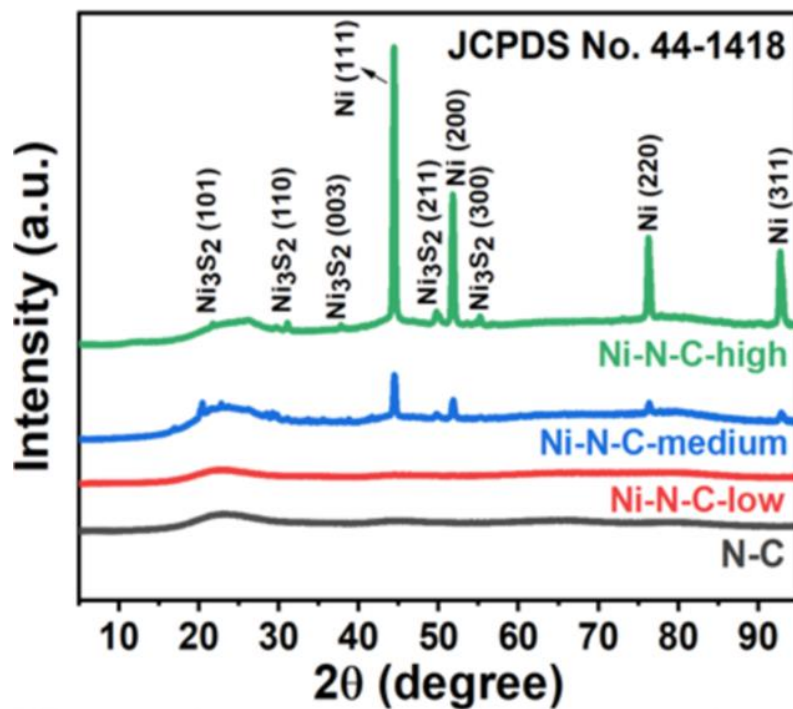


Figure 3-5: X-ray diffraction pattern of N-C, Ni-N-C-low, Ni-N-C-medium, and Ni-N-C-high catalysts.

Having observed and confirmed the presence of nanoparticles by the aid of electron microscopy, powder X-ray diffraction (XRD) was then performed to probe the crystalline structures present in the samples (**Figure 3-5**). The XRD pattern of the N-C catalyst shows a broad carbon peak centered at ca. 22° that is attributed to graphitic carbon, with its broadness resulting from the amorphous nature of its structure. All three Ni-containing samples exhibit a similar broad diffraction peak at 26° , which can be assigned to the (002) plane of a graphitic carbon, indicating that 900°C was sufficient to form some degree of graphitization in our materials.

In addition, intense diffraction peaks were exhibited in all three Ni-containing catalysts corresponding to metallic Ni and Ni_3S_2 (JCPDS no. 44-1418), although the peaks

for Ni_3S_2 were relatively small compared to those of metallic Ni indicating smaller crystallite sizes. It is interesting to observe metallic nickel in the samples, as its removal would be expected during the acid leach process employed during catalyst synthesis. Therefore, it is expected that these metallic Ni particles embedded within a protective graphitic shell that prevents their dissolution^{140,181}. Because they are protected, these preserved Ni nanoparticles are not likely to contribute to the activity and selectivity of the catalysts as the protective shell around them hinder electrolyte/reactant access during electrochemical O_2 reduction testing.

As the presence of Ni_3S_2 phase species were also revealed by XRD (**Figure 3-5**), we wanted to investigate the acid stability of these species to determine whether they may have survived the acid leach procedure or were protected by a graphitic carbon shell similar to the Ni metal nanoparticles. We evaluated the solubility of Ni_3S_2 in acid using commercial Ni_3S_2 powders and they were found to survive an acid washing procedure. These results indicate that the Ni_3S_2 species in our catalyst materials may be exposed to the electrolyte/reactants during electrochemical testing, and therefore we need to consider their contributions during ORR measurements (vide infra). XRD (**Figure 3-6**) was also performed on both commercial $\text{Ni}_3\text{S}_2/\text{VC}$ and acid treated/pyrolyzed $\text{Ni}_3\text{S}_2/\text{VC}$ powders to ensure similar structures were present in the commercial Ni_3S_2 samples as in our Ni-N-C catalyst materials. There is a sharp peak observed at 61° for the pyrolyzed $\text{Ni}_3\text{S}_2/\text{VC}$ sample which is from the single crystal Si wafer that the samples were mounted on, so it can be ignored.

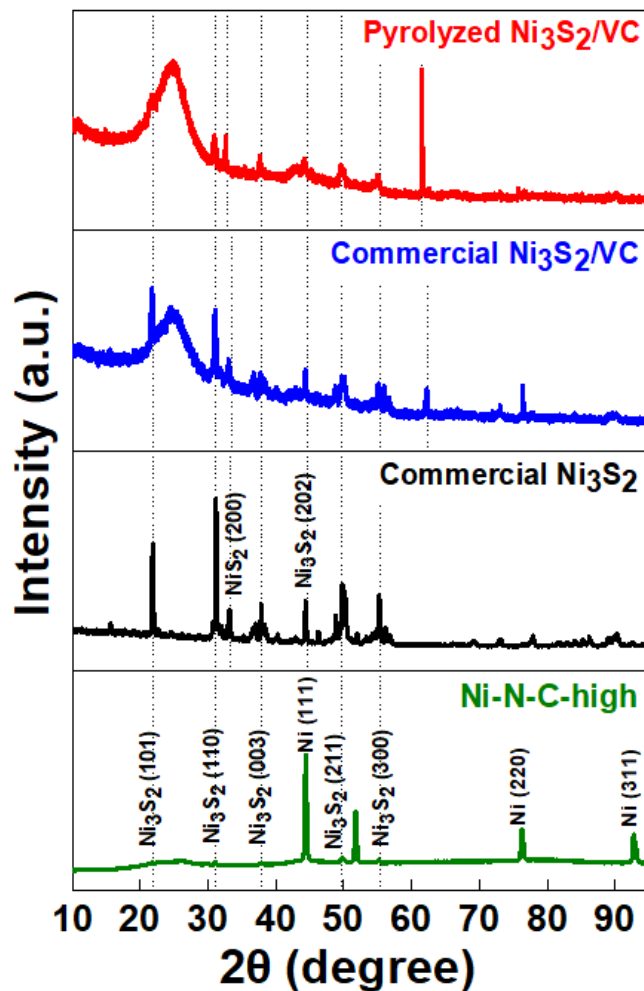


Figure 3-6: X-ray diffraction pattern of Ni-N-C-high catalyst, commercial Ni₃S₂, commercial Ni₃S₂ mixed with Vulcan Carbon and pyrolyzed Ni₃S₂/Vulcan Carbon nano-powders.

X-ray photoelectron spectroscopy (XPS) was used to identify near-surface elemental compositions and chemical structures present in the synthesized catalysts. The chemical compositions of the N-C, Ni-N-C-low, medium, and high catalysts determined from the survey spectra (**Figure 3-7a**) are summarized in **Table 3-3**. High-resolution XPS spectra of Ni 2p₃, C 1s, N 1s, O 1s and the S 2p of N-C, Ni-N-C-low, medium, and high catalysts are shown in **Figure 3-8**.

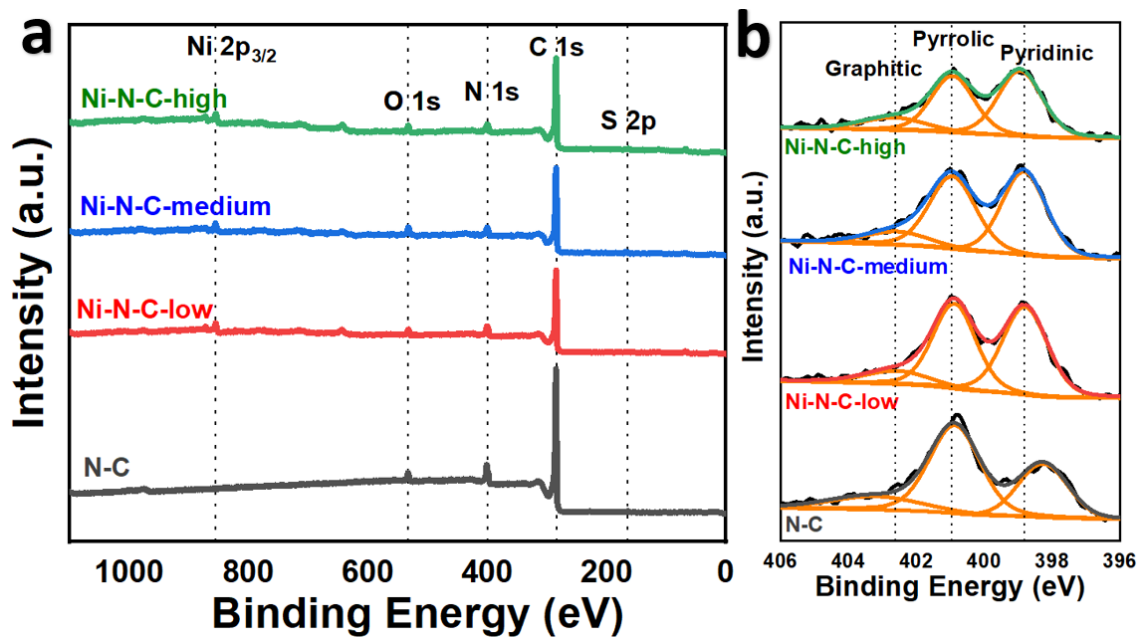


Figure 3-7: (a) XPS spectrum of N-C, Ni-N-C-low, medium, high catalysts (b) deconvolution of the high-resolution XPS spectra of N 1s of N-C, Ni-N-C-low, medium, high catalysts

Table 3-2: Elemental compositions of Ni-N-C-low, Ni-N-C-medium, Ni-N-C-high and metal-free N-C catalyst samples from XPS analysis

| Element | N-C | | Ni-N-C-low | | Ni-N-C-medium | | Ni-N-C-high | |
|----------|--------------------|-------|--------------------|-------|--------------------|-------|--------------------|-------|
| | Peak position (eV) | At. % | Peak position (eV) | At. % | Peak position (eV) | At. % | Peak position (eV) | At. % |
| Carbon | 284.7 | 85.0 | 284.7 | 85.7 | 284.7 | 83.9 | 284.8 | 84.8 |
| Nitrogen | | 11.6 | | 9.5 | | 8.3 | | 8.2 |
| Oxygen | 532.6 | 3.0 | 532.2 | 3.0 | 532.1 | 5.3 | 532.5 | 4.3 |
| Nickel | - | 0.0 | 854.6 | 1.2 | 854.6 | 1.3 | 854.7 | 1.5 |
| Sulfur | | 0.4 | | 0.6 | | 1.3 | | 1.1 |

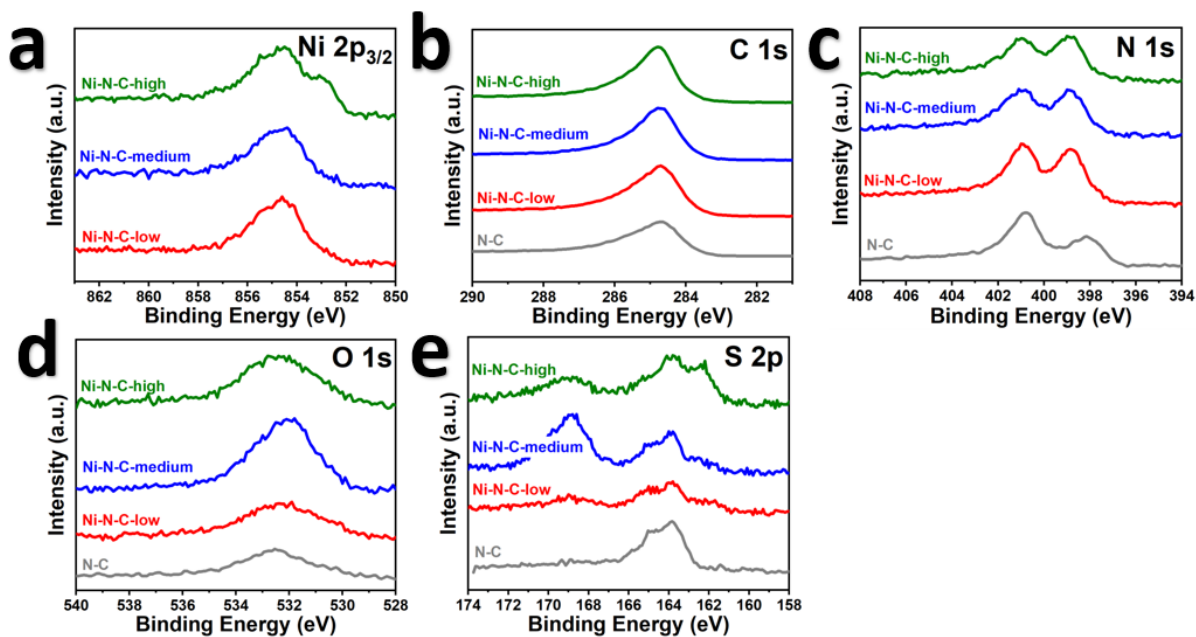


Figure 3-8: High-resolution XPS of N-C, Ni-N-C-low, medium, and high catalysts. (a) Ni 2p_{3/2} spectra, (b) the C 1s spectra, (c) N 1s spectra, (d) the O 1s spectra and (e) the S 2p spectra.

Based on the XPS quantification, the content of Ni increased with increase in Ni concentration present during synthesis from 1.2 at % for Ni-N-C-low to 1.5 at% for Ni-N-C-high. All four catalysts exhibited a near surface nitrogen concentration of >8 at %. Particularly, the metal-free catalyst exhibited the highest concentration of nitrogen of ca. 11.6 at % as compared to that of the Ni containing catalysts (9.5 at%, 8.3 at%, and 8.3 at% for Ni-N-C-low, Ni-N-C-medium, and Ni-N-C-high, respectively). To gain further insight into the chemical structure of the nitrogen species, high resolution XPS analysis of the N 1s region was performed (**Figure 3-7b**).

The N 1s spectra of the N-C and Ni-N-C catalysts were deconvoluted into three peaks: 398.2-398.9 eV, 400.8-400.9 eV and 402.5-403.1 eV which are attributed to pyridinic, pyrrolic/quaternary and graphitic nitrogen, respectively^{140,182}. A summary of the

different types of nitrogen groups at the near-surface is summarized in **Table 3-3**. The fraction of pyridinic nitrogen relative to the total nitrogen content increased with increasing addition of Ni, from 41% for Ni-N-C-low into 44% for Ni-N-C-high. This result suggests that Ni dopant atoms facilitates the formation of pyridinic nitrogen sites which can potentially coordinate Ni in a Ni-N-C configuration. This shift in the distribution of various nitrogen species distribution highlights the role nickel plays in tuning the type of nitrogen present, which is likely due to the formation of nitrogen-coordinated Ni species, whereby theoretical calculations have indicated that the binding energy between Ni atoms and four-fold pyridinic sites can be as high as 8 eV ¹⁸³.

Table 3-3: Detail breakdown of N1s signal showing the peak position and relative composition of different near-surface nitrogen groups.

| Functional group | N-C | | Ni-N-C-low | | Ni-N-C-medium | | Ni-N-C-high | |
|-------------------------|--------------------|-------|--------------------|-------|--------------------|-------|--------------------|-------|
| | Peak position (eV) | At. % | Peak position (eV) | At. % | Peak position (eV) | At. % | Peak position (eV) | At. % |
| Pyridinic | 398.2 | 30 | 398.8 | 41 | 398.8 | 43 | 398.9 | 44 |
| Pyrrolic/ Quaternary | 400.8 | 53 | 400.9 | 44 | 400.9 | 43 | 400.9 | 40 |
| Graphitic | 403.1 | 18 | 402.5 | 15 | 402.6 | 14 | 402.7 | 16 |

3.2 Electrochemical performance

3.2.1 Activity and selectivity of Ni-N-C catalysts in acidic electrolyte

RRDE voltammetry was used to evaluate the electrocatalytic performance of N-C and Ni-N-C catalysts. **Figure 3-9** shows the CV curves of all four catalysts obtained in oxygen and nitrogen saturated 0.1 M HClO₄ electrolyte.

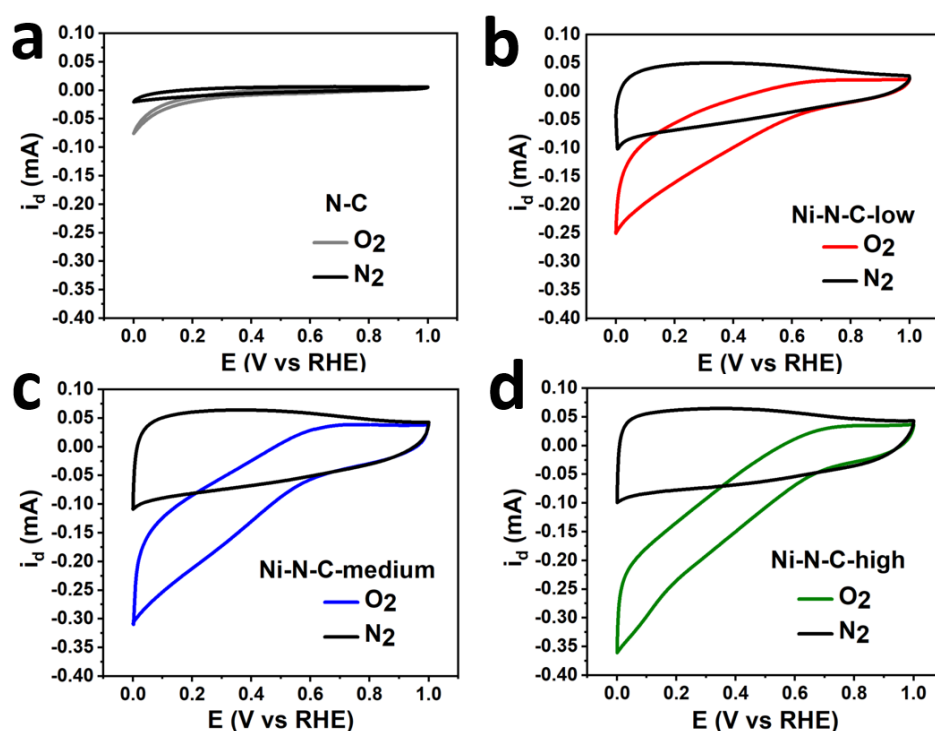


Figure 3-9: Cyclic voltammograms of N-C and Ni-N-C cast glassy carbon electrode in 0.1 M HClO₄ saturated with N₂ and O₂, respectively. Catalyst loading: 0.2 mg cm⁻², scan rates: 20 mV s⁻¹ (a) N-C (b) Ni-N-C-low, (c) Ni-N-C-medium, (d) Ni-N-C-high catalyst.

The normalized (to geometric electrode surface area) and background corrected linear sweep voltammograms of N-C, Ni-N-C-low, medium, high catalysts obtained in oxygen saturated 0.1 M HClO₄ electrolyte at a scan rate of 20 mVs⁻¹ are shown in **Figure**

3-10 a. For the disk current density, the onset potential (the potential at which a current density of 0.1 mA cm^{-2} is achieved) of N-C catalyst was 0.23 V vs RHE . Meanwhile, Ni-N-C-low, medium and high exhibited a much higher onset potential at 0.58 , 0.59 and 0.64 V vs RHE , respectively, indicating Ni plays an important role in improving the activity of the catalyst for the ORR. Furthermore, the same onset potentials observed for Ni-N-C-low, medium and high catalysts suggest the presence of similarly structured active sites within the catalysts. The current density and thereby catalytic activity towards the ORR increased with an increase in contents of Ni from -0.18 mA cm^{-2} for Ni-N-C-low to -0.21 mA cm^{-2} for Ni-N-C-medium and -0.31 mA cm^{-2} for Ni-N-C-high at 0.5 V vs RHE (**Figure 3-10a**). At this potential the N-C catalyst did not produce any Faradaic ORR current, which is consistent with previous reports on the important role of metal in providing catalytic activity for nitrogen-doped carbon catalysts in acidic medium ¹⁸⁴.

The electrochemical accessible surface area (ECSA) is an important parameter as it is generally proportional to the number of active sites available for the ORR. Background CVs were used to determine the ECSA of the materials by calculating the double-layer capacitance. The ECSA of each sample was ultimately calculated by dividing the capacitance obtained from the integration of the background electrical double layer current by literature-established specific capacitance values of carbon-based materials (0.015 mF cm^{-2}) ^{176,177} according to **equation 2.2**. ECSA values of the catalysts increased with the presence of Ni during synthesis, from $35.4 \text{ m}^2 \text{ g}^{-1}$ for N-C to $352 \text{ m}^2 \text{ g}^{-1}$ for Ni-N-C-low. Further increases in ECSA were observed at higher Ni contents, with a ECSA of $459 \text{ m}^2 \text{ g}^{-1}$ for Ni-N-C-medium and $464 \text{ m}^2 \text{ g}^{-1}$ for Ni-N-C-high measured.

Ring currents collected on the platinum ring electrode at a constant potential of 1.2 V vs RHE along with their calculated corresponding yields of H₂O₂ based on **equation 2.5** are shown **Figure 3-10 b** and **c**, respectively, which provides information about the selectivity of these catalyst materials towards the 2e⁻ ORR. As a rule of thumb, all selectivity data in this paper are reported for disk potential values where the disk current density and ring current are greater than 0.1 mA cm⁻² and 0.4 μA, respectively. Anything below these threshold values is not reported as the data is impacted by noise and capacitance. The number of electrons transferred was also calculated using **equation 2.4** and shown in **Figure 3-11**. As **Figure 3-10c** demonstrates, the selectivity towards the 2e-ORR increased with Ni content, with Ni-N-C-high showing the highest selectivity of 43% H₂O₂ at a potential of 0.5 V vs RHE (i.e., at a low overpotential) which meets one of the important challenges faced by the M-N-C catalysts since the promotion of the ORR commonly only happens at high overpotentials in acid media. While this is not as high as the 93% H₂O₂ selectivity obtained by Co-N-C at a similar potential of 0.59 V vs RHE and catalyst loading 25 μg cm_{disk}⁻² or 80% H₂O₂ selectivity for Mn-N-C (25 μg cm_{disk}⁻²) or 82% H₂O₂ selectivity for other Ni-N-C (25 μg cm_{disk}⁻²) catalysts at much lower electrode potentials of ca. 0.2 V vs RHE reported in the literature^{137,185}, it shows promise as our Ni-N-C catalysts employ an inexpensive transition metal (Ni) that is much cheaper than cobalt and utilize a simple preparation process, thereby warranting further investigation and optimization.

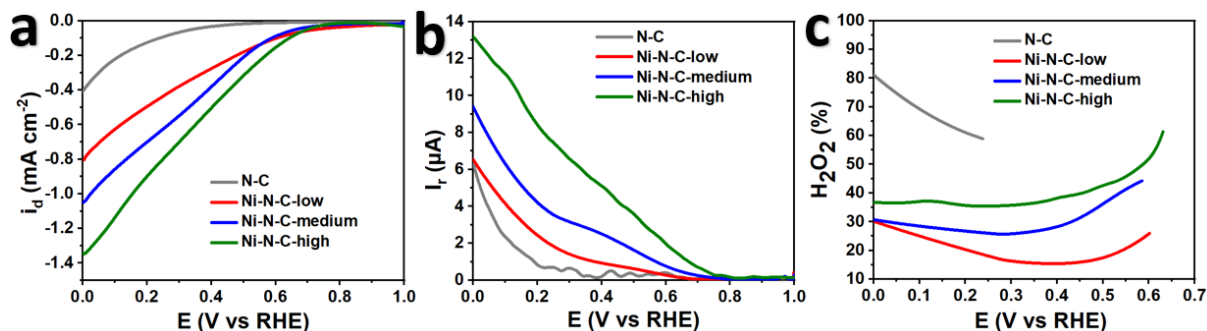


Figure 3-10: RRDE results for ORR on N-C and Ni-N-C catalysts containing different Ni concentrations. (a) O₂ reduction current densities obtained from the disk electrode, (b) ring currents collected on the Pt ring at a constant potential of 1.2 V_{RHE} (c) calculated selectivity of catalysts for reduction of O₂ to H₂O₂. The experiments were performed at a scan rate of 20 mV s⁻¹, using a catalyst loading of 0.2 mg cm⁻² on the RRDE tip, 0.1 M HClO₄ electrolyte, at room temperature and ambient pressure.

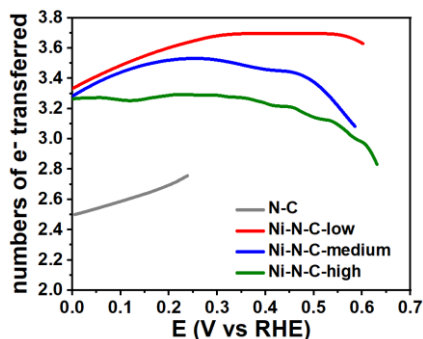


Figure 3-11: Number of transferred electrons (n) as a function of electrode potential in ORR performed in 0.1 M HClO₄ using a catalyst loading of 0.2 mg cm⁻² on the RRDE tip, at room temperature and ambient pressure.

Collectively, the obtained results indicate that the active sites in acidic electrolyte (0.1 M HClO₄) contributing to the increase in activity of Ni-N-C catalysts compared to N-C catalysts arise due the presence of Ni during catalyst synthesis. We postulate the active site species are in the form of atomically dispersed nickel ions coordinated with nitrogen that are embedded throughout the Ni-N-C structure as reported previously for materials prepared by pyrolyzing a mixture of nickel, nitrogen and carbon precursors^{140,186–188}; or due to the Ni₃S₂ particles present in the catalyst that have been previously shown capable

of facilitating the ORR in neutral media ¹⁸⁹. We were able to experimentally rule out significant contributions from Ni₃S₂ to the activity of the Ni-N-C catalysts (vide infra), and therefore speculate that atomically dispersed Ni-N-C sites are responsible for the activity and selectivity observed. With higher Ni contents present during synthesis, a higher number of these active site structures could be formed due to both the higher surface area supported by ECSA measurements and the higher amount of Ni available for coordination.

3.2.2 Active sites of Ni-N-C catalysts in different pH electrolytes

Although the performance of electrocatalysts in acidic electrolyte is more critical as compared to that in alkaline electrolyte for practical implications due to instability of HO₂⁻ in alkaline conditions, the alkaline study was also conducted to gain insight into the active site structures present in these materials. We investigated the ORR activity and selectivity in an alkaline electrolyte (0.1 M KOH) and compared the results with that in acidic electrolyte (0.1 M HClO₄) for N-C and Ni-N-C-medium catalysts shown in **Figure 3-12** as the identity of active site structures for the ORR can vary depending on the pH of the electrolyte.

Ni-N-C-medium shows a higher disk current density and ring current than N-C in alkaline medium. Ni-N-C-medium shows a higher disk current density and ring current than N-C in alkaline medium. Overall, both N-C and Ni-N-C-medium catalysts showed significantly higher disk current densities (-1.1 mA cm⁻² and -1.3 mA cm⁻² for N-C and Ni-N-C-medium catalysts at 0.5 V vs RHE, respectively) than those in the acidic electrolyte,

where Ni-N-C-medium shows a current density of -0.2 mA cm^{-2} whereas the N-C catalyst show no appreciable activity at 0.5 V vs RHE . In addition, the ring current as well as the % H_2O_2 were also higher in alkaline having a % H_2O_2 of 87% and 76% for N-C and Ni-N-C medium catalysts, respectively, in alkaline electrolyte at 0.58 V vs RHE , which was relatively constant over the entire potential range investigated. This is in contrast to acidic electrolyte where Ni-N-C-medium catalysts showed a selectivity of 36% at 0.5 V vs RHE which decreased at lower electrode potentials, whereas N-C showed no appreciable ORR activity until 0.23 V vs RHE and no H_2O_2 production until 0.20 V vs RHE . These results show much higher ORR performance of the catalysts in alkaline electrolyte as compared to that in acidic electrolyte in terms of both activity and selectivity towards H_2O_2 . This is likely due to the more facile ORR kinetics in alkaline media in comparison to acidic media

190,191

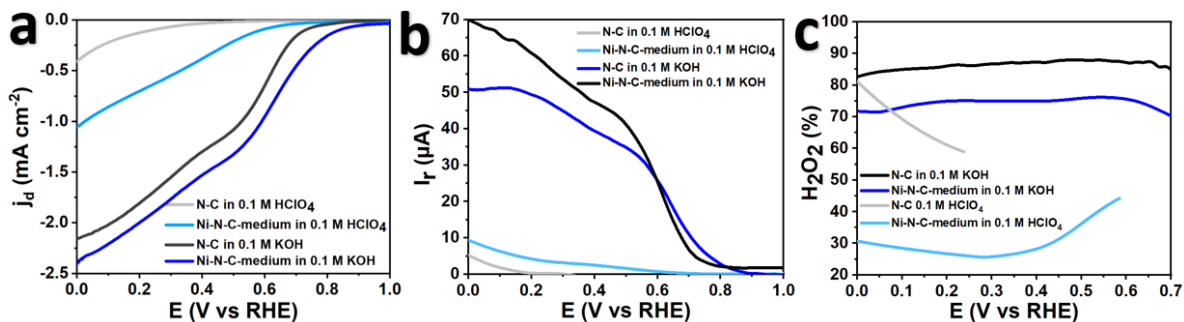


Figure 3-12: RRDE results for ORR on N-C and Ni-N-C-medium catalysts in two different electrolytes of 0.1 M HClO₄ and 0.1 M KOH (a) O₂ reduction current densities obtained from the disk electrode, (b) ring currents collected on the Pt ring at a constant potential of $1.2 \text{ V}_{\text{RHE}}$ (c) calculated selectivity of catalysts for reduction of O₂ to H₂O₂. The experiments were performed at a scan rate of 20 mV s^{-1} , using a catalyst loading of 0.2 mg cm^{-2} on the RRDE tip at room temperature and ambient pressure.

It is noteworthy that the ORR performance of N-C and Ni-N-C-medium catalysts in alkaline electrolyte exhibited only minor differences in contrast to those observed in

acidic electrolyte (**Figure 3-12**). In addition, the ORR results of N-C and Ni-N-C low, medium, and high catalysts obtained in alkaline electrolyte also showed marginally differences (**Figure 3-13**). These results indicates that different active site structures are likely at play in alkaline electrolytes, potentially consisting of nitrogen-doped carbon sites that have been shown capable of facilitating the ORR in alkaline media but not in acidic media ¹⁹².

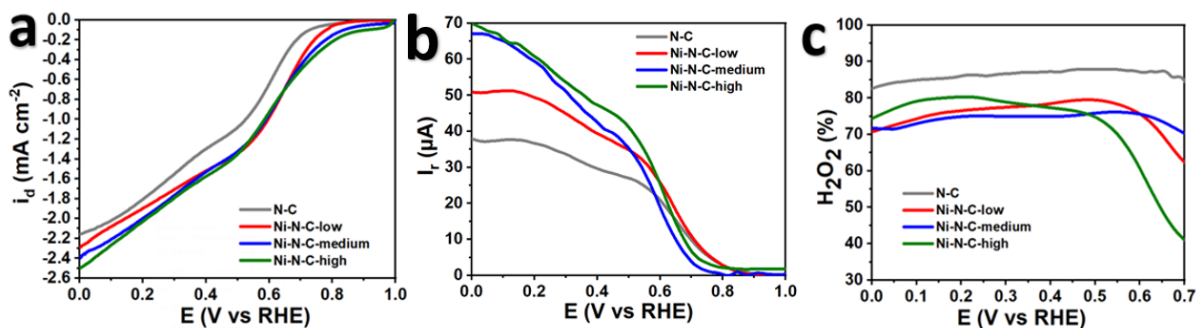


Figure 3-13: RRDE results for ORR on N-C and Ni-N-C catalysts containing different Ni concentrations in 0.1 M KOH electrolyte. (a) O₂ reduction current densities obtained from the disk electrode, (b) ring currents collected on the Pt ring at a constant potential of 1.2 V_{RHE} (c) calculated selectivity of catalysts for reduction of O₂ to H₂O₂. The experiments were performed at a scan rate of 20 mV s⁻¹, using a catalyst loading of 0.2 mg cm⁻² on the RRDE tip at room temperature and ambient pressure.

3.3.3 Ni₃S₂ contribution to the ORR activity

To investigate the potential contributions of Ni₃S₂ species that are present in our catalyst on ORR performance, we conducted ORR measurements in both acidic (**Figure 3-14 a-c**) and alkaline electrolyte (**Figure 3-14 d-f**) on commercial Ni₃S₂ particles that were mixed with Vulcan XC-72 carbon black (Ni₃S₂/VS). To subject the Ni₃S₂ to the same procedures used in Ni-N-C catalyst synthesis, we also acid treated and pyrolyzed the Ni₃S₂/VC materials (P-Ni₃S₂/VC) and tested their ORR activity. Additionally, ORR

measurements on pure Vulcan XC-72 powder (VC) are also shown. In acidic electrolyte (Figure 3-14 a-c) the commercial Ni_3S_2 containing samples showed no appreciable activity at potentials above ca. 0.3 V vs RHE, suggesting that these species are not providing significant contributions to the activity of Ni-N-C catalysts in acidic electrolytes. However, in alkaline electrolyte (Figure 3-14 d-f), the commercial Ni_3S_2 samples in addition to the pure VC show considerable activity for the ORR and selectivity towards H_2O_2 , indicating they likely provide contributions to the alkaline based ORR performance of Ni-N-C, and further providing evidence for the more facile ORR kinetics in alkaline media that can occur on a variety of different (including metal free) active site structures.

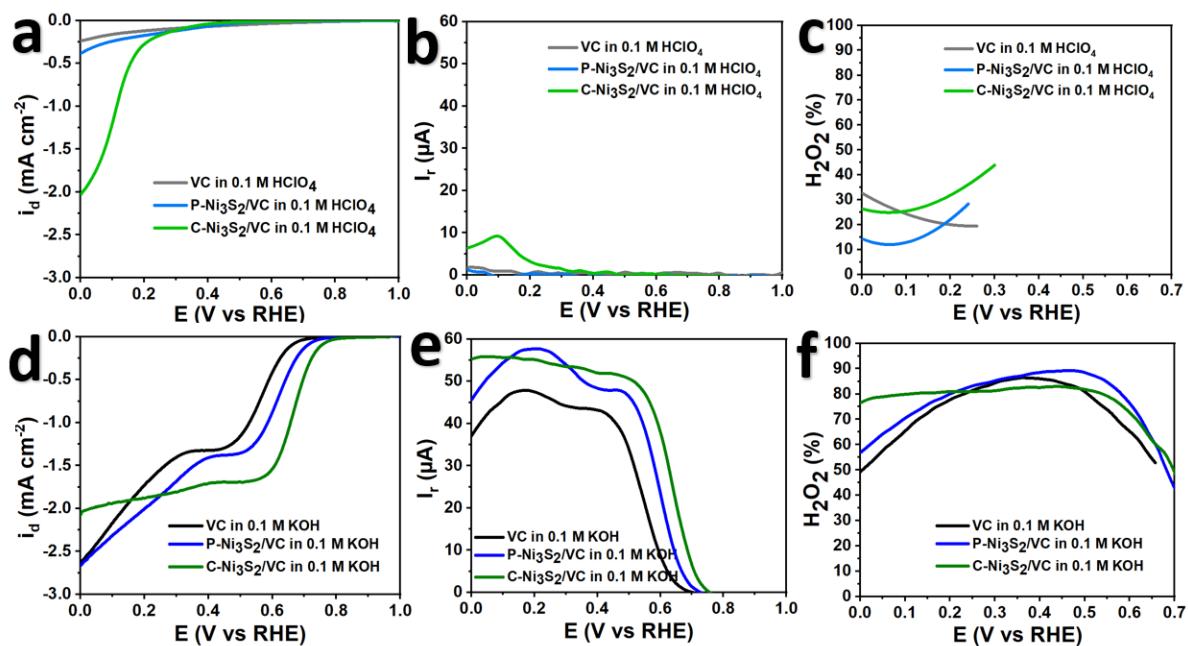


Figure 3-14: RRDE results for ORR on Vulcan Carbon (VC), Pyrolyzed $\text{Ni}_3\text{S}_2/\text{VC}$ and Commercial $\text{Ni}_3\text{S}_2/\text{VC}$ nano-powders in two different electrolytes of 0.1 M HClO_4 (a-c) and 0.1 M KOH (d-f) (a,d) O_2 reduction current densities obtained from the disk electrode, (b,e) ring currents collected on the Pt ring at a constant potential of 1.2 V_{RHE} (c,f) calculated selectivity of catalysts for reduction of O_2 to H_2O_2 . The experiments were performed at a scan rate of 20 mV s^{-1} , using a loading of 0.2 mg cm^{-2} on the RRDE tip at room temperature and ambient pressure.

Chapter 4

Conclusions and suggested future work

Hydrogen peroxide (H_2O_2) is among the top 100 most important industrial chemicals used for a variety of applications, including pulp and textile bleaching, chemical synthesis, detoxification, and water treatment. Synthesis of H_2O_2 by the decentralized electrochemical method through the 2e ORR is promising alternative to the energy intensive batch multistep industrial anthraquinone process. However, this route has important challenge of finding cost-effective electrocatalysts that possess high activity, stability, and selectivity towards H_2O_2 . Metal-nitrogen-carbon catalysts (M-N-C) are an exciting class of materials that are promising replacements for expensive state-of-the-art noble-metal catalysts used for electrocatalytic production of H_2O_2 through the 2-electron oxygen reduction reaction (ORR) due to their high activity as well as low cost of their abundant precursor materials. The type of metal, the metal-precursor as well as their relative content used in the pyrolyzed M-N-C catalyst materials are found to directly impact their ORR performance in terms of activity and selectivity. However, the outstanding challenge faced by this class of catalysts is to employ an inexpensive transition metal.

In this work, we synthesized inexpensive and earth abundant nickel-nitrogen-carbon (Ni-N-C) electrocatalysts by pyrolyzing, acid leaching and re-pyrolyzing a mixture of nickel (II) chloride, polyaniline (PANI) and cyanamide (CM) at a range of Ni precursors amounts. We reported the electrocatalytic activity and selectivity of these materials towards H₂O₂ production in acidic (0.1M HClO₄) and alkaline (0.1M KOH) electrolytes using the rotating ring disk electrode (RRDE) technique. We found that the activity and selectivity of the catalysts depended on the amount of nickel added during synthesis as well as the pH of the electrolyte.

We employed various physicochemical characterization techniques to study the structure of these materials and to correlate them with the electrochemical study in order to identify different active site structures that are at play under acidic and alkaline media. We identified that the materials were found to be heterogeneous in nature. In acidic media, we postulate that the presence of Ni precursors during catalyst synthesis results in the formation of atomically dispersed Ni-N_x active site structures that are capable of facilitating the ORR. In alkaline media, whereby the ORR is a more facile process, various active site structures are likely at play including Ni-centered active sites, Ni₃S₂ particles formed during catalyst synthesis, and nitrogen-doped carbon sites present in the carbon matrix of the catalyst structure. For the ORR activity and selectivity in acidic media can be advantageous for the distributed production of H₂O₂, the best Ni-N-C catalyst in this work was able to achieve a selectivity of 43% H₂O₂ at a potential of 0.5 V vs RHE (i.e., only 200 mV of overpotential).

this work highlights the potential of Ni-N-C catalysts for the ORR and generates scientific insight for the electrochemical synthesis of H₂O₂. This work provides a rigorous systematic investigation and insight into the synthesis-structure-property-performance relationships of Ni-N-C catalysts that can be used to guide further investigations towards the identification of the exact active site structures responsible for the formation of H₂O₂ using advanced in situ characterization techniques, and also provide valuable design criteria for developing catalyst materials with high activity and selectivity for the reduction of oxygen into H₂O₂ using inexpensive precursors and simplistic synthesis techniques

Furthermore, identifying the mechanisms that dictate activity and selectivity, such as whether different active site structures on these Ni-N-C catalysts are leading to an indirect 4e⁻ ORR process or H₂O₂ disproportionation in the electrode structures can provide valuable insight in terms of future catalyst designs. As a future direction, theoretical calculations (molecular/electronic level modeling) can be combined with the experimental approaches to study the ORR mechanism involved in both the acid and alkaline medias and their relationship with catalyst active site structures and composition to tailer new catalyst structures with better activity and selectivity. Density functional theory (DFT) calculations and modelling software can be used to study these materials and compare the results with the experimental results. Further electrocatalyst optimization would also be worth investigating to find better designs of experiments that can enhance our understanding of the parameters involved in the preparation of the electrocatalysts that would allow for development of well controlled Ni-N-C nanoparticles. Also, durability studies can be done on the developed catalysts as durability is another important factor in selecting a good

catalyst for decentralized production of H_2O_2 through ORR and finally as a more long-term future goal, the synthesized catalysts can be integrated into an electrochemical device such as a fuel cell.

Bibliography

1. Division, C. and M. S. D. R. AD819081 Hydrogen Peroxide Manual. 1–488 (1967).
2. Campos-Martin, J. M., Blanco-Brieva, G. & Fierro, J. L. G. Hydrogen Peroxide Synthesis: An Outlook beyond the Anthraquinone Process. *Angew. Chem., Int. Ed.* **45**, 6962 (2006).
3. Richard, L. The 100 most important chemical compounds: a reference guide. *Choice Rev. Online* **45**, 45-3798-45–3798 (2008).
4. Pesterfield, L. The 100 Most Important Chemical Compounds: A Reference Guide (by Richard L. Myers). *J. Chem. Educ.* **86**, 1182 (2009).
5. Cook, B. An Introduction to Fuel Cells and Hydrogen Technology. *Eng. Sci. Educ. J.* **11**, 205–216 (2003).
6. Samanta, C. Direct synthesis of hydrogen peroxide from hydrogen and oxygen: An overview of recent developments in the process. *Appl. Catal. A Gen.* **350**, 133–149 (2008).
7. Campos-Martin, J. M., Blanco-Brieva, G. & Fierro, J. L. G. Hydrogen peroxide synthesis: An outlook beyond the anthraquinone process. *Angewandte Chemie - International Edition* vol. 45 6962–6984 (2006).

8. Kroschwitz, J. I. & Seidel, A. *Kirk-Othmer encyclopedia of chemical technology*. (2004).
9. Grades, E. & Pizzutilo, E. Towards On-Site Production of Hydrogen Peroxide with Gold- Palladium catalysts in Electrocatalysis and Heterogeneous Catalysis. (2017).
10. Li, W. HYDROGEN PEROXIDE ELECTROSYNTHESIS IN SOLID POLYMER ELECTROLYTE (SPE) REACTORS WITH AND WITHOUT POWER CO-GENERATION by M . A . Sc ., The University of British Columbia , 2010 A THESIS SUBMITTED IN PARTIAL FULFILLMENT OF THE REQUIREMENTS FOR THE DEGREE O. 207 (2017).
11. Ciriminna, R., Albanese, L., Meneguzzo, F., Pagliaro, M. & Hydrogen Peroxide. A Key Chemical for Today's Sustainable Development. *ChemSusChem* **9**, 3374 (2016).
12. Yi, Y., Wang, L., Li, G. & Guo, H. A Review on Research Progress in the Direct Synthesis of Hydrogen Peroxide from Hydrogen and Oxygen: Noble-Metal Catalytic Method, Fuel-Cell Method and Plasma Method. *Catal. Sci. Technol.* **6**, 1593 (2016).
13. Yang, S. *et al.* Toward the Decentralized Electrochemical Production of H₂O₂: A Focus on the Catalysis. *ACS Catal.* **8**, 4064–4081 (2018).
14. Jones, C. W. *Applications of Hydrogen Peroxide and Derivatives*. (The Royal Society of Chemistry, 1999). doi:10.1039/9781847550132.

15. Gopal. Electrochemical Synthesis of Hydrogen Peroxide. *US Pat.* (2004).
16. Foller, P. C. & Bombard, R. T. Processes for the Production of Mixtures of Caustic Soda and Hydrogen-Peroxide Via the Reduction of Oxygen. *J. Appl. Electrochem.* **25**, 613 (1995).
17. Production of hydrogen peroxide. *United States Pat. Off.* (1939)
doi:10.1016/s0958-2118(02)80183-5.
18. Oor, G. U. G., Ag, D., Lenneberg, R. G. & Ag, D. Hydrogen Peroxide. *Ullmann's Encycl. Ind. Chem.* **1**, 131–139 (2007).
19. Eul, W.; Moeller, A.; Steiner, N. Hydrogen Peroxide. *Kirk-Othmer Encycl. Chem. Technol.* (2001) doi:10.2165/00128415-201214070-00096.
20. Yang, S. *et al.* Toward the Decentralized Electrochemical Production of H₂O₂: A Focus on the Catalysis. *ACS Catal.* **8**, 4064–4081 (2018).
21. Campos, M. I. Q. R. Investigations into the Electrochemical Synthesis of Hydrogen Peroxide. **2**, (2010).
22. Stoll, P. E. L. & Langel, A. E. A. United States Patent. (1989).
23. Cassidy, K. D. Electrosynthesis of Hydrogen Peroxide in an Acidic Environment with RuO₂ as a Water Oxidation Catalyst & Silver Nanoparticles in Zeolite Y: Surface Enhanced Raman Spectroscopic (SERS) Studies. *Thesis* (2011).
24. McIntyre, J. A. METHOD FOR ELECTROLYTIC PRODUCTION OF ALKALINE PEROXIDE SOLUTIONS. *United States Pat.* (1984).

25. C. OLOMAN, A. P. W. Hydrogen peroxide production in trickle-bed electrochemical reactors. *J. Electrochem. Appl. Eng. Chem. Columbia, Br.* **9**, 1–7 (1979).
26. Guillet, N. *et al.* Electrogeneration of Hydrogen Peroxide in Acid Medium Using Pyrolyzed Cobalt-Based Catalysts: Influence of the Cobalt Content on the Electrode Performance. *J. Appl. Electrochem.* **36**, 863–870 (2006).
27. Edwards, J. K. *et al.* Switching Off Hydrogen Peroxide Hydrogenation in the Direct Synthesis Process. *Sci. (Washington, DC, U. S.)* **323**, 1037 (2009).
28. Centi, G., Dittmeyer, R., Perathoner, S. & Reif, M. Tubular Inorganic catalytic membrane reactors: advantages and performance in multiphase hydrogenation reactions. *Catal. Today* **79–80**, 139–149 (2003).
29. Viswanathan, V. & Hansen, H. A. Selective Electrochemical Generation of Hydrogen Peroxide from Water Oxidation. *J. Phys. Chem. Lett.* **6**, 4224–4228 (2015).
30. Fujishima, A., Rao, T. N. & Tryk, D. A. Titanium dioxide photocatalysis. *J. Photochem. Photobiol. C Photochem. Rev.* **1**, 1–21 (2000).
31. Cai, R., Hashimoto, K., Fujishima, A. & Kubota, Y. Conversion of photogenerated superoxide anion into hydrogen peroxide in TiO₂ suspension system. *J. Electroanal. Chem.* **326**, 345–350 (1992).
32. Kormann, C., Bahnemann, D. W. & Hoffmann, M. R. Photocatalytic Production of

- H₂O₂ and Organic Peroxides in Aqueous Suspensions of TiO₂, ZnO, and Desert Sand. *Environ. Sci. Technol.* **22**, 798–806 (1988).
33. Cai, R., Kubota, Y. & Fujishima, A. Effect of copper ions on the formation of hydrogen peroxide from photocatalytic titanium dioxide particles. *J. Catal.* **219**, 214–218 (2003).
34. Goto, H., Hanada, Y., Ohno, T. & Matsumura, M. Quantitative analysis of superoxide ion and hydrogen peroxide produced from molecular oxygen on photoirradiated TiO₂ particles. *J. Catal.* **225**, 223–229 (2004).
35. Jakob, H. A. J. *et al.* Peroxo Compounds, Inorganic. *Ullmann's Encycl. Ind. Chem.* (2000) doi:10.1002/14356007.a19.
36. Sanderson, W. R. Cleaner industrial processes using hydrogen peroxide. *Pure Appl. Chem.* **72**, 1289–1304 (2000).
37. Venugopalan, M., Jones, R. A. & Stage, C. C. T. CHEMISTRY OF DISSOCIATED WATER VAPOR AND RELATED SYSTEMS. (1965).
38. Synthesis, H. O., Edwards, J. K. & Hutchings, G. J. Palladium and Gold – Palladium Catalysts for the Direct Synthesis of Hydrogen Peroxide **. 9192–9198 (2008) doi:10.1002/anie.200802818.
39. Edwards, J. K., Freakley, S. J., Lewis, R. J., Pritchard, J. C. & Hutchings, G. J. Advances in the Direct Synthesis of Hydrogen Peroxide from Hydrogen and Oxygen. *Catal. Today* **248**, 3 (2015).

40. Yamanaka, I. & Murayama, T. Neutral H₂O₂ Synthesis by Electrolysis of Water and O₂. *Angew. Chem.* **120**, 1926–1928 (2008).
41. Siahrostami, S. *et al.* Enabling Direct H₂O₂ Production through Rational Electrocatalyst Design. *Nat. Mater.* **12**, 1137 (2013).
42. Abate, S. *et al.* Performances of Pd-Me (Me=Ag, Pt) catalysts in the direct synthesis of H₂O₂ on catalytic membranes. *Catal. Today* **117**, 193–198 (2006).
43. Wulff, G. *et al.* Nonhazardous Direct Oxidation of Hydrogen to Hydrogen Peroxide Using a Novel Membrane Catalyst. **411008**, 1826–1829 (2001).
44. Weber, W. & Dusseldorf, O. F. Manufacture of Hydrogen Peroxide. *Henkel, H.; Weber, W. Henkel CIE. U.S. Pat. 1,108,752, 1914* (1914).
45. Edwards, J. K. *et al.* Switching Off Hydrogen Peroxide Hydrogenation in the Direct Synthesis Process. *Science (80-.)*. **323**, 1037–1042 (2009).
46. Choudhary, V. R., Gaikwad, A. G. & Sansare, S. D. Activation of supported Pd metal catalysts for selective oxidation of hydrogen to hydrogen peroxide. *Catal. Letters* **83**, 235–239 (2002).
47. Catalysts, A. T. *et al.* Solvent-Free Oxidation of Primary Alcohols to Aldehydes Using. *Science (80-.)*. **311**, 362–366 (2006).
48. Burch, R. & Ellis, P. R. An Investigation of Alternative Catalytic Approaches for the Direct Synthesis of Hydrogen Peroxide from Hydrogen and Oxygen. *Appl. Catal., B* **42**, 203 (2003).

49. Choudhary, V. R., Sansare, S. D. & Gaikwad, A. G. Direct Oxidation of H₂ to H₂O₂ and Decomposition of H₂O₂ Over Oxidized and Reduced Pd-Containing Zeolite Catalysts in Acidic Medium. *Catal. Letters* **84**, 81–87 (2002).
50. Muthukrishnan, A., Nabaie, Y., Okajima, T. & Ohsaka, T. Kinetic Approach to Investigate the Mechanistic Pathways of Oxygen Reduction Reaction on Fe-Containing N-Doped Carbon Catalysts. *ACS Catal.* **5**, 5194 (2015).
51. Lunsford, J. H. The Direct Formation of H₂O₂ from H₂ and O₂ over Palladium Catalysts. *J. Catal.* **216**, 455 (2003).
52. Vulpescu, G. D. *et al.* One-step selective oxidation over a Pd-based catalytic membrane; evaluation of the oxidation of benzene to phenol as a model reaction. *Catal. Commun.* **5**, 347–351 (2004).
53. Abate, S. *et al.* Preparation, performances and reaction mechanism for the synthesis of H₂O₂ from H₂ and O₂ based on palladium membranes. *Catal. Today* **104**, 323–328 (2005).
54. Melada, S., Pinna, F., Strukul, G., Perathoner, S. & Centi, G. Palladium-modified catalytic membranes for the direct synthesis of H₂O₂: preparation and performance in aqueous solution. *J. Catal.* **235**, 241–248 (2005).
55. Melada, S., Pinna, F., Strukul, G., Perathoner, S. & Centi, G. Direct synthesis of H₂O₂ on monometallic and bimetallic catalytic membranes using methanol as reaction medium. *J. Catal.* **237**, 213–219 (2006).

56. Liu, Q. & Lunsford, J. H. The roles of chloride ions in the direct formation of H₂O₂ from H₂ and O₂ over a Pd/SiO₂ catalyst in a H₂SO₄/ethanol system. *J. Catal.* **239**, 237–243 (2006).
57. Yamanaka, I., Hashimoto, T., Ichihashi, R. & Otsuka, K. Direct Synthesis of H₂O₂ Acid Solutions on Carbon Cathode Prepared from Activated Carbon and Vapor-Growing-Carbon-Fiber by a H₂/O₂ Fuel Cell. *Electrochim. Acta* **53**, 4824 (2008).
58. Sudoh, M., Kitaguchi, H. & Koide, K. Electrochemical Production of Hydrogen Peroxide by Reduction of Oxygen. *J. Chem. Eng. Japan* **18**, 409–414 (1985).
59. Wang, K. H., Choi M. H., Koo, C. M., Choi, Y. S. & Chung I. J. Synthesis and characterization of maleated polyethylene/clay nanocomposites. *Polymer (Guildf)*. **42**, 9819–9826 (2001).
60. Gyenge, E. L. & Oloman, C. W. Electrosynthesis of Hydrogen Peroxide in Acidic Solutions by Mediated Oxygen Reduction in a Three-Phase (Aqueous/organic/gaseous) System Part I: Emulsion Structure, Electrode Kinetics and Batch Electrolysis. *J. Appl. Electrochem.* **33**, 655 (2003).
61. Kastening, B. Herstellung von Wasserstoffperoxid durch kathodische Reduktion von Sauerstoff. *Chemie Ing. Tech.* **49**, 1333–1339 (1972).
62. Alvarez-Gallegos, A. & Pletcher, D. The removal of low level organics via hydrogen peroxide formed in a reticulated vitreous carbon cathode cell, Part 1. The electrosynthesis of hydrogen peroxide in aqueous acidic solutions. *Electrochim.*

- Acta* **44**, 853–861 (1998).
63. Oloman, C. & Watkinson, A. P. The electroreduction of oxygen to hydrogen peroxide on fixed bed cathodes. *Can. J. Chem. Eng.* **54**, 312–318 (1976).
 64. Kuehn, C. G. THREE COMPARTMENT ELECTROLYTIC HYDROGEN, CELL METHOD FOR PRODUCING. *United States Pat.* (1982).
 65. Da Pozzo, A., Di Palma, L., Merli, C. & Petrucci, E. An experimental comparison of a graphite electrode and a gas diffusion electrode for the cathodic production of hydrogen peroxide. *J. Appl. Electrochem.* **35**, 413–419 (2005).
 66. Qiang, Z. M., Chang, J. H. & Huang, C. P. Electrochemical Generation of Hydrogen Peroxide from Dissolved Oxygen in Acidic Solutions. *Water Res.* **36**, 85 (2002).
 67. Yamada, N., Yaguchi, T., Otsuka, H. & Sudoh, M. Development of Trickle-Bed Electrolyzer for On-Site Electrochemical Production of Hydrogen Peroxide. *J. Electrochem. Soc.* **146**, 2587–2591 (1999).
 68. Ando, Y. & Tanaka, T. Proposal for a new system for simultaneous production of hydrogen and hydrogen peroxide by water electrolysis. *Int. J. Hydrogen Energy* **29**, 1349–1354 (2004).
 69. Drogui, P., Elmaleh, S., Rumeau, M., Bernard, C. & Rambaud, A. Oxidising and disinfecting by hydrogen peroxide produced in a two-electrode cell. *Water Res.* **35**, 3235–3241 (2001).

70. Drogui, P., Elmaleh, S., Rumeau, M., Bernard, C. & Rambaud, A. Hydrogen peroxide production by water electrolysis: Application to disinfection. *J. Appl. Electrochem.* **31**, 877–882 (2001).
71. Raymond J. Jasinski. METHOD FOR THE ELECTROLYTHIC PRODUCTION OF HYDROGEN PEROXDE. *United States Pat.* 1–7 (1983).
72. Alcaide, F., Brillas, E., Cabot, P. & Casado, J. Electrogeneration of Hydroperoxide Ion Using an Alkaline Fuel Cell. *J. Electrochem. Soc.* **145**, 3444–3449 (1998).
73. Brillas, E., Alcaide, F. & Cabot, P.-L. A small-scale flow alkaline fuel cell for on-site production of hydrogen peroxide. *Electrochim. Acta* **48**, 331–340 (2002).
74. Sethuraman, V. A., Weidner, J. W., Haug, A. T., Pemberton, M. & Protsailo, L. V. Importance of catalyst stability vis-à-vis hydrogen peroxide formation rates in PEM fuel cell electrodes. *Electrochim. Acta* **54**, 5571–5582 (2009).
75. XU, F. *et al.* A new cathode using CeO₂/MWNT for hydrogen peroxide synthesis through a fuel cell. *J. Rare Earths* **27**, 128–133 (2009).
76. Lobytseva, E., Kallio, T., Alexeyeva, N., Tammeveski, K. & Kontturi, K. Electrochemical synthesis of hydrogen peroxide: Rotating disk electrode and fuel cell studies. *Electrochim. Acta* **52**, 7262–7269 (2007).
77. Otsuka, K. & Yamanaka, I. One Step Synthesis of Hydrogen Peroxide Through Fuel Cell Reaction. *Electrochim. Acta* **35**, 319 (1990).
78. Yamanaka, I., Onisawa, T., Hashimoto, T. & Murayama, T. A fuel-cell reactor for

the direct synthesis of hydrogen peroxide alkaline solutions from H₂ and O₂.

ChemSusChem **4**, 494–501 (2011).

79. Yamanaka, I., Onizawa, A. T., Suzuki, H., Hanaizumi, N. & Otsuka, K. Electrocatalysis of Heat-treated Mn – Porphyrin / Carbon Cathode for Synthesis of H₂ O₂ Acid Solutions by H₂ / O₂ Fuel Cell Method. **35**, 116–117 (2006).
80. Yamanaka, I., Onizawa, T., Takenaka, S. & Otsuka, K. Direct and Continuous Production of Hydrogen Peroxide with 93 % Selectivity Using a Fuel-Cell System. *Angew. Chemie* **115**, 3781–3783 (2003).
81. Murayama, T., Tazawa, S., Takenaka, S. & Yamanaka, I. Catalytic neutral hydrogen peroxide synthesis from O₂ and H₂ by PEMFC fuel. *Catal. Today* **164**, 163–168 (2011).
82. Yamanaka, I., Tazawa, S., Murayama, T., Iwasaki, T. & Takenaka, S. Catalytic Synthesis of Neutral Hydrogen Peroxide at a CoN₂C_x Cathode of a Polymer Electrolyte Membrane Fuel Cell (PEMFC). *ChemSusChem* **3**, 59 (2010).
83. LLC, C. R. C. P. *FUEL CELL TECHNOLOGY TECHNOLOGY HANDBOOK*. New York (2003).
84. Katsounaros, I., Cherevko, S., Zeradjanin, A. R. & Mayrhofer, K. J. J. Oxygen electrochemistry as a cornerstone for sustainable energy conversion. *Angew. Chemie - Int. Ed.* **53**, 102–121 (2014).
85. Katsounaros, I. *et al.* Hydrogen peroxide electrochemistry on platinum: towards

- understanding the oxygen reduction reaction mechanism. *Phys. Chem. Chem. Phys.* **14**, 7384–7391 (2012).
86. T. R. Ralph. Catalysis for Low Temperature Fuel Cells. 117–135 (2002).
87. Sarapuu, A., Vaik, K., Schiffrin, D. J. & Tammeveski, K. Electrochemical reduction of oxygen on anthraquinone-modified glassy carbon electrodes in alkaline solution. *J. Electroanal. Chem.* **541**, 23–29 (2003).
88. Steele, B. C. H. & Heinzl, A. Materials for fuel-cell technologies. *Nature* **414**, 345–352 (2001).
89. Duke, F. R. & Haas, T. W. THE HOMOGENEOUS BASE-CATALYZED DECOMPOSITION OF HYDROGEN PEROXIDE¹. *J. Phys. Chem.* **65**, 304–306 (1961).
90. Jiang, Y. *et al.* Selective Electrochemical H₂O₂ Production through Two-Electron Oxygen Electrochemistry. **1801909**, 17–19 (2018).
91. Siahrostami, S. *et al.* Enabling direct H₂O₂ production through rational electrocatalyst design. *Nat. Mater.* **12**, 1137–1143 (2013).
92. Kulkarni, A., Siahrostami, S., Patel, A. & Nørskov, J. K. Understanding Catalytic Activity Trends in the Oxygen Reduction Reaction. *Chem. Rev.* **118**, 2302–2312 (2018).
93. Jung, E., Shin, H., Hooch Antink, W., Sung, Y.-E. & Hyeon, T. Recent Advances in Electrochemical Oxygen Reduction to H₂O₂: Catalyst and Cell Design. *ACS*

- Energy Lett.* **5**, 1881–1892 (2020).
94. Perry, S. C. *et al.* Electrochemical synthesis of hydrogen peroxide from water and oxygen. *Nat. Rev. Chem.* **3**, 442–458 (2019).
 95. Verdaguer-Casadevall, A. *et al.* Trends in the Electrochemical Synthesis of H₂O₂: Enhancing Activity and Selectivity by Electrocatalytic Site Engineering. *Nano Lett.* **14**, 1603–1608 (2014).
 96. Verdaguer-casadevall, A. *et al.* Trends in the Electrochemical Synthesis of H₂O₂ : Enhancing Activity and Selectivity by Electrocatalytic Site Engineering Trends in the Electrochemical Synthesis of H₂O₂ : Enhancing Activity and Selectivity by Electrocatalytic Site Engineering. *Nano Lett.* **14**, 1603 (2014).
 97. Wu, J. & Yang, H. Platinum-Based Oxygen Reduction Electrocatalysts. *Acc. Chem. Res.* **46**, 1848–1857 (2013).
 98. Sun, Y. *et al.* Activity-Selectivity Trends in the Electrochemical Production of Hydrogen Peroxide over Single-Site Metal-Nitrogen-Carbon Catalysts. *J. Am. Chem. Soc.* **141**, 12372–12381 (2019).
 99. Strasser, P., Gliech, M., Kuehl, S. & Moeller, T. Electrochemical processes on solid shaped nanoparticles with defined facets. *Chem. Soc. Rev.* **47**, 715–735 (2018).
 100. Beermann, V. *et al.* Tuning the Electrocatalytic Oxygen Reduction Reaction Activity and Stability of Shape-Controlled Pt–Ni Nanoparticles by Thermal

Annealing – Elucidating the Surface Atomic Structural and Compositional Changes. *J. Am. Chem. Soc.* **139**, 16536–16547 (2017).

101. Zhang, C., Shen, X., Pan, Y. & Peng, Z. A review of Pt-based electrocatalysts for oxygen reduction reaction. *Front. Energy* **11**, 268–285 (2017).
102. Alonso, E. *et al.* Conductive bacterial cellulose-polyaniline blends: Influence of the matrix and synthesis conditions. *Carbohydr. Polym.* **183**, 254–262 (2018).
103. Zuo, G. *et al.* Journal of Solid State Chemistry Fabrication of Ni , Co and N co-doped carbon composites and use its as electrocatalysts for oxygen reduction reaction. *J. Solid State Chem.* **276**, 128–132 (2019).
104. Han, L. *et al.* In-Plane Carbon Lattice-Defect Regulating Electrochemical Oxygen Reduction to Hydrogen Peroxide Production over Nitrogen-Doped Graphene. *ACS Catal.* **9**, 1283–1288 (2019).
105. Han, L. *et al.* In-Plane Carbon Lattice-Defect Regulating Electrochemical Oxygen Reduction to Hydrogen Peroxide Production over Nitrogen-Doped Graphene. *ACS Catal.* **9**, 1283–1288 (2019).
106. Yasin, S. *et al.* Optimization of Mechanical and Thermal Properties of iPP and LMPP Blend Fibres by Surface Response Methodology. *Polymers (Basel)*. **10**, 1135 (2018).
107. Shi, X., Zhang, Y., Siahrostami, S. & Zheng, X. Light-Driven BiVO₄ – C Fuel Cell with Simultaneous Production of H₂ O₂. **1801158**, 1–9 (2018).

108. Article, R. A review of Pt-based electrocatalysts for oxygen reduction reaction. **11**, 268–285 (2020).
109. Li, J. *et al.* Atomically dispersed manganese catalysts for oxygen reduction in proton-exchange membrane fuel cells. *Nat. Catal.* **1**, 935–945 (2018).
110. Wang, X. X. *et al.* Nitrogen-Coordinated Single Cobalt Atom Catalysts for Oxygen Reduction in Proton Exchange Membrane Fuel Cells. **1706758**, 1–11 (2018).
111. Li, J. & Jaouen, F. Structure and activity of metal-centered coordination sites in pyrolyzed metal–nitrogen–carbon catalysts for the electrochemical reduction of O₂. *Current Opinion in Electrochemistry* vol. 9 198–206 (2018).
112. Osmieri, L. Transition metal–nitrogen–carbon (M–N–C) catalysts for oxygen reduction reaction. Insights on synthesis and performance in polymer electrolyte fuel cells. *ChemEngineering* vol. 3 1–32 (2019).
113. Chung, H. T. *et al.* Direct atomic-level insight into the active sites of a high-performance PGM-free ORR catalyst. *Science (80-.)*. **357**, 479–484 (2017).
114. Hossen, M. M., Artyushkova, K., Atanassov, P. & Serov, A. Synthesis and characterization of high performing Fe-N-C catalyst for oxygen reduction reaction (ORR) in Alkaline Exchange Membrane Fuel Cells. *J. Power Sources* **375**, 214–221 (2018).
115. Gao, L. *et al.* Correlating Fe source with Fe-N-C active site construction: Guidance for rational design of high-performance ORR catalyst. *J. Energy Chem.* **27**, 1668–

- 1673 (2018).
116. Martinaiou, I. *et al.* Activity and degradation study of an Fe-N-C catalyst for ORR in Direct Methanol Fuel Cell (DMFC). *Appl. Catal. B Environ.* **262**, 118217 (2020).
117. Mamtani, K. *et al.* Evolution of N-Coordinated Iron–Carbon (FeNC) Catalysts and Their Oxygen Reduction (ORR) Performance in Acidic Media at Various Stages of Catalyst Synthesis: An Attempt at Benchmarking. *Catal. Letters* **146**, 1749–1770 (2016).
118. Wu, G., More, K. L., Johnston, C. M. & Zelenay, P. High-performance electrocatalysts for oxygen reduction derived from polyaniline, iron, and cobalt. *Science (80-.)*. **332**, 443–447 (2011).
119. Zhu, Z. *et al.* Porous Co-N-C ORR catalysts of high performance synthesized with ZIF-67 templates. *Mater. Res. Bull.* **114**, 161–169 (2019).
120. Chen, L. *et al.* Insights into the role of active site density in the fuel cell performance of Co-N-C catalysts. *Appl. Catal. B Environ.* **256**, 117849 (2019).
121. Wang, R. *et al.* ZIF-derived Co–N–C ORR catalyst with high performance in proton exchange membrane fuel cells. *Prog. Nat. Sci. Mater. Int.* (2020)
doi:<https://doi.org/10.1016/j.pnsc.2020.09.010>.
122. Hyo-Young, K. & Young-Wan, J. Fabrication of Mn-N-C Catalyst for Oxygen Reduction Reactions Using Mn-Embedded Carbon Nanofiber. *Energies* **13**, 2561

(2020).

123. Liu, K. *et al.* Mn- and N- doped carbon as promising catalysts for oxygen reduction reaction: Theoretical prediction and experimental validation. *Appl. Catal. B Environ.* **243**, 195–203 (2019).
124. Li, J. *et al.* Atomically dispersed manganese catalysts for oxygen reduction in proton-exchange membrane fuel cells. *Nat. Catal.* **1**, 935–945 (2018).
125. ZHANG, R., ZHANG, J., MA, F., WANG, W. & LI, R. Preparation of Mn-N-C catalyst and its electrocatalytic activity for the oxygen reduction reaction in alkaline medium. *J. Fuel Chem. Technol.* **42**, 467–475 (2014).
126. Higgins, D. *et al.* Manganese-Based Non-Precious Metal Catalyst for Oxygen Reduction in Acidic Media. *{ECS} Trans.* **61**, 35–42 (2014).
127. Wang, Y. *et al.* Rational Design and Synthesis of Hierarchical Porous Mn–N–C Nanoparticles with Atomically Dispersed MnN_x Moieties for Highly Efficient Oxygen Reduction Reaction. *ACS Sustain. Chem. Eng.* **8**, 9367–9376 (2020).
128. Xiao, L., Yang, J.-M., Huang, G.-Y., Zhao, Y. & Zhu, H.-B. Construction of efficient Mn-N-C oxygen reduction electrocatalyst from a Mn(II)-based MOF with N-rich organic linker. *Inorg. Chem. Commun.* **118**, 107982 (2020).
129. Lin, L., Zhu, Q. & Xu, A.-W. Noble-Metal-Free Fe–N/C Catalyst for Highly Efficient Oxygen Reduction Reaction under Both Alkaline and Acidic Conditions. *J. Am. Chem. Soc.* **136**, 11027–11033 (2014).

130. Wang, M.-Q. *et al.* Pyrolyzed Fe–N–C Composite as an Efficient Non-precious Metal Catalyst for Oxygen Reduction Reaction in Acidic Medium. *ACS Catal.* **4**, 3928–3936 (2014).
131. Yin, P. *et al.* Single Cobalt Atoms with Precise N-Coordination as Superior Oxygen Reduction Reaction Catalysts. *Angew. Chem. Int. Ed. Engl.* **55**, 10800–10805 (2016).
132. Nugraha, M., Tsai, M.-C., Su, W.-N., Chou, H.-L. & Hwang, B. J. Descriptor study by density functional theory analysis for the direct synthesis of hydrogen peroxide using palladium–gold and palladium–mercury alloy catalysts. *Mol. Syst. Des. Eng.* **3**, 896–907 (2018).
133. Iglesias, D. *et al.* N-Doped Graphitized Carbon Nanohorns as a Forefront Electrocatalyst in Highly Selective O₂ Reduction to H₂O₂. *Chem* **4**, 106–123 (2018).
134. Zitolo, A. *et al.* Identification of Catalytic Sites for Oxygen Reduction in Iron- and Nitrogen-Doped Graphene Materials. *Nat. Mater.* **14**, 937 (2015).
135. Li, G., Edwards, J., Carley, A. F. & Hutchings, G. J. Direct synthesis of hydrogen peroxide from H₂ and O₂ and in situ oxidation using zeolite-supported catalysts. *Catal. Commun.* **8**, 247–250 (2007).
136. Yamanaka, I. *et al.* Electrocatalysis of Heat-Treated Cobalt-Porphyrin/carbon for Hydrogen Peroxide Formation. *Electrochim. Acta* **108**, 321–329 (2013).

137. Gao, J. *et al.* Enabling Direct H₂O₂ Production in Acidic Media through Rational Design of Transition Metal Single Atom Catalyst. *Chem* **6**, 658–674 (2020).
138. Gao, J. *et al.* Enabling Direct H₂O₂ Production in Acidic Media through Rational Design of Transition Metal Single Atom Catalyst Enabling Direct H₂O₂ Production in Acidic Media through Rational Design of Transition Metal Single Atom Catalyst. *CHEMPR* 1–17 (2019) doi:10.1016/j.chempr.2019.12.008.
139. Zheng, T. *et al.* Large-Scale and Highly Selective CO₂ Electrocatalytic Reduction on Nickel Single-Atom Catalyst. *Joule* **3**, 265–278 (2019).
140. Koshy, D. M. *et al.* Understanding the Origin of Highly Selective CO₂ Electroreduction to CO on Ni,N-doped Carbon Catalysts. *Angew. Chemie* **132**, 4072–4079 (2020).
141. Weekes, D. M., Salvatore, D. A., Reyes, A., Huang, A. & Berlinguette, C. P. Electrolytic CO₂ Reduction in a Flow Cell. *Acc. Chem. Res.* **51**, 910–918 (2018).
142. Burdyny, T. & Smith, W. A. CO₂ reduction on gas-diffusion electrodes and why catalytic performance must be assessed at commercially-relevant conditions. *Energy Environ. Sci.* **12**, 1442–1453 (2019).
143. Ren, S. *et al.* Molecular electrocatalysts can mediate fast, selective CO₂ reduction in a flow cell. *Science* (80-.). **365**, 367–369 (2019).
144. Kim, H. W. *et al.* Efficient hydrogen peroxide generation using reduced graphene oxide-based oxygen reduction electrocatalysts. *Nat. Catal.* **1**, 282–290 (2018).

145. Lu, Z. *et al.* High-efficiency oxygen reduction to hydrogen peroxide catalysed by oxidized carbon materials. *Nat. Catal.* **1**, 156–162 (2018).
146. Yamanaka, I., Tazawa, S., Murayama, T., Ichihashi, R. & Hanaizumi, N. Catalytic Synthesis of Neutral H₂O₂ Solutions from O₂ and H₂ by a Fuel Cell Reaction. *ChemSusChem* **1**, 988 (2008).
147. Li, W., Bonakdarpour, A., Gyenge, E. & Wilkinson, D. P. Drinking Water Purification by Electrosynthesis of Hydrogen Peroxide in a Power-Producing PEM Fuel Cell. *ChemSusChem* **6**, 2137 (2013).
148. Chen, Z. *et al.* Development of a reactor with carbon catalysts for modular-scale, low-cost electrochemical generation of H₂O₂. *React. Chem. Eng.* **2**, 239–245 (2017).
149. Xia, C., Xia, Y., Zhu, P., Fan, L. & Wang, H. Direct electrosynthesis of pure aqueous H₂O₂ solutions up to 20% by weight using a solid electrolyte. *Science* (80-.). **366**, 226–231 (2019).
150. Jayashree, R. S. *et al.* On the performance of membraneless laminar flow-based fuel cells. *J. Power Sources* **195**, 3569–3578 (2010).
151. Jayashree, R. S. *et al.* Air-Breathing Laminar Flow-Based Microfluidic Fuel Cell. *J. Am. Chem. Soc.* **127**, 16758–16759 (2005).
152. Xia, C. *et al.* Confined local oxygen gas promotes electrochemical water oxidation to hydrogen peroxide. *Nat. Catal.* **3**, 125–134 (2020).

153. Nørskov, J. K. *et al.* Origin of the Overpotential for Oxygen Reduction at a Fuel-Cell Cathode. *J. Phys. Chem. B* **108**, 17886 (2004).
154. Ramaswamy, N. & Mukerjee, S. Influence of Inner- and Outer-Sphere Electron Transfer Mechanisms during Electrocatalysis of Oxygen Reduction in Alkaline Media. *J. Phys. Chem. C* **115**, 18015–18026 (2011).
155. Gnanamuthu, D. S. & Petrocelli, J. V. A Generalized Expression for the Tafel Slope and the Kinetics of Oxygen Reduction on Noble Metals and Alloys. *J. Electrochem. Soc.* **114**, 1036 (1967).
156. Wroblowa, H. S., Yen-Chi-Pan & Razumney, G. Electroreduction of oxygen: A new mechanistic criterion. *J. Electroanal. Chem. Interfacial Electrochem.* **69**, 195–201 (1976).
157. Walch, S., Dhanda, A., Aryanpour, M. & Pitsch, H. Mechanism of Molecular Oxygen Reduction at the Cathode of a PEM Fuel Cell: Non-Electrochemical Reactions on Catalytic Pt Particles. *J. Phys. Chem. C* **112**, 8464–8475 (2008).
158. Jacob, T. & Goddard III, W. A. Water Formation on Pt and Pt-based Alloys: A Theoretical Description of a Catalytic Reaction. *ChemPhysChem* **7**, 992–1005 (2006).
159. Prentice, G. *Encyclopedia of Physical Science and Technology*. (2003).
160. Bard, A. J., Faulkner, L. R., Swain, E. & Robey, C. *Electrochemical Methods Fundamentals and Applications*. (2001).

161. Brett, C. . M. . & Oliveira-Brett, A. M. *Electroanalysis. Oxford Chemistry Primers* (1998). doi:10.1515/bmte.1999.44.s2.11.
162. Brett, C. *Electrochemistry. Principles, Methods and Applications.* (Oxford University Press, 1993).
163. Zoski, C. *Handbook of electrochemistry.* (2007).
164. Kit, P. & Overview, C. Pine Research Electrode Polishing Guide. **10013**, 3–6 (2016).
165. Elgrishi, N. *et al.* A Practical Beginner’s Guide to Cyclic Voltammetry. *J. Chem. Educ.* **95**, 197–206 (2018).
166. E6R1 ChangeDisk Series. *Pine Res.* **005**, 6–8 (2016).
167. Hong, W. T. *et al.* Toward the rational design of non-precious transition metal oxides for oxygen electrocatalysis. *Energy Environ. Sci.* **8**, 1404–1427 (2015).
168. Wang, J. *Analytical electrochemistry.* (Wiley-VCH, 2006). doi:10.1016/s0165-9936(96)90116-8.
169. Harvey, D. (DePauw U. *Modern analytical chemistry. McGraw-Hill Higher Education* (2000).
170. Pletcher, D. *A First Course in Electrode Processes.* (The Royal Society of Chemistry, 2009).
171. Pletcher, D. *Industrial electrochemistry.* Kluwer (1989).

doi:10.1179/bcj.1983.18.2.70.

172. Tessuer, B. preparation, Characterisation and Evaluation of Core-Shell Electrocatalyst for PEMFCs. *PhD Thesis* (2009).
173. Will, F. G. Hydrogen Adsorption on Platinum Single Crystal Electrodes. *J. Electrochem. Soc.* **112**, 451 (1965).
174. Jüttner, K. Technical Scale of Electrochemistry. *Encycl. Electrochem.* **5**, (2007).
175. Lowde, D. R., Williams, J. O. & McNicol, B. D. The characterisation of catalyst surfaces by cyclic voltammetry. *Appl. Surf. Sci.* **1**, 215–240 (1978).
176. Centeno, T. A. & Stoeckli, F. On the specific double-layer capacitance of activated carbons, in relation to their structural and chemical properties. *J. Power Sources* **154**, 314–320 (2006).
177. McCrory, C. C. L., Jung, S., Peters, J. C. & Jaramillo, T. F. Benchmarking Heterogeneous Electrocatalysts for the Oxygen Evolution Reaction. *J. Am. Chem. Soc.* **135**, 16977–16987 (2013).
178. Higgins, D. Nanostructured oxygen reduction catalyst designs to reduce the platinum dependency of polymer electrolyte fuel cells by. *PhD Thesis* (2015).
179. Goldstein, J. *et al.* *Scanning electron microscopy and X-ray microanalysis*. (Springer USA, 2003).
180. Shao, M. H. *et al.* Palladium Monolayer and Palladium Alloy Electrocatalysts for Oxygen Reduction. *Langmuir* **22**, 10409–10415 (2006).

181. Huang, L. F., Hutchison, M. J., Santucci, R. J., Scully, J. R. & Rondinelli, J. M. Improved Electrochemical Phase Diagrams from Theory and Experiment: The Ni-Water System and Its Complex Compounds. *J. Phys. Chem. C* **121**, 9782–9789 (2017).
182. Sun, Y. *et al.* Efficient Electrochemical Hydrogen Peroxide Production from Molecular Oxygen on Nitrogen-Doped Mesoporous Carbon Catalysts. *ACS Catal.* **8**, 2844–2856 (2018).
183. Yang, M., Wang, L., Li, M., Hou, T. & Li, Y. Structural stability and O₂ dissociation on nitrogen-doped graphene with transition metal atoms embedded: A first-principles study. *AIP Adv.* **5**, (2015).
184. Marcotte, S., Villers, D., Guillet, N., Roué, L. & Dodelet, J. P. Electroreduction of oxygen on Co-based catalysts: Determination of the parameters affecting the two-electron transfer reaction in an acid medium. *Electrochim. Acta* **50**, 179–188 (2004).
185. Gao, J. & Liu, B. Progress of Electrochemical Hydrogen Peroxide Synthesis over Single Atom Catalysts. *ACS Mater. Lett.* **2**, 1008–1024 (2020).
186. Koshy, D. M. *et al.* Direct Characterization of Atomically Dispersed Catalysts: Nitrogen-Coordinated Ni Sites in Carbon-Based Materials for CO₂ Electroreduction. *Adv. Energy Mater.* **10**, 2001836 (2020).
187. Li, X. *et al.* Exclusive Ni–N₄ Sites Realize Near-Unity CO Selectivity for

- Electrochemical CO₂ Reduction. *J. Am. Chem. Soc.* **139**, 14889–14892 (2017).
188. Pan, F. *et al.* Atomic-level active sites of efficient imidazolate framework-derived nickel catalysts for CO₂ reduction. *J. Mater. Chem. A* **7**, 26231–26237 (2019).
189. Falkowski, J. M., Concannon, N. M., Yan, B. & Surendranath, Y. Heazlewoodite, Ni₃S₂: A Potent Catalyst for Oxygen Reduction to Water under Benign Conditions. *J. Am. Chem. Soc.* **137**, 7978–7981 (2015).
190. Shen, H. *et al.* Selective and Continuous Electrosynthesis of Hydrogen Peroxide on Nitrogen-doped Carbon Supported Nickel. *Cell Reports Phys. Sci.* **1**, 100255 (2020).
191. Sgarbi, R. *et al.* Oxygen reduction reaction mechanism and kinetics on M-N_xC_y and M@N-C active sites present in model M-N-C catalysts under alkaline and acidic conditions. *J. Solid State Electrochem.* **25**, 45–56 (2021).
192. Zhang, B., Xu, W., Lu, Z. & Sun, J. Recent Progress on Carbonaceous Material Engineering for Electrochemical Hydrogen Peroxide Generation. *Trans. Tianjin Univ.* **26**, 188–196 (2020).